High Voltage Laboratory Development

An in-depth Description and Report on the Process of Fabricating a Faraday Cage

by
Daniel Asle Vingen Endal

Master's Thesis in Energy
Specialization in Electronic Power Systems
Electrical Power Engineering

GEOPHYSICAL INSTITUTE
UNIVERSITY OF BERGEN
Norway

December 16, 2022

Til minne om mine besteforeldre Aslaug †2020 og Kåre †2013

Acknowledgements

This thesis concludes my time as a master's student at the University of Bergen (UiB).

I want to thank my supervisor Lasse H. Sivertsen of the Department of Computer science, Electrical engineering and Mathematical sciences at Western Norway University of Applied Sciences for the resources and time he has put aside for me. The openness and straightforward dialogue we have had through this process, and the opportunity for us to both speak directly during counselling has been greatly appreciated.

I would like to thank Espen C. Brantzeg from EB Consulting AS for his expertise and enthusiasm surrounding the Faraday cage, related theory and practices. Thank you for letting me partake in quality control of the Faraday cage and field strength measurements during HV testing and for the free use of reports and data sets in my thesis.

Thank you to everyone who has given me technical and grammatical feedback.

To my friends and past and present fellow students at sal 363, thank you for creating a fun and respectful environment these past years. It would not be the same without your company during late hours and early mornings. And long lunch breaks. Sometimes way too long. Our many discussions and peer reviews of each other are what have made these long days worth it.

Lastly, I would like to thank my parents, Hans Peter Endal and Jorid Laura Vingen Endal, and my fiancé, Solfrid Bryn, for being my "pit crew". Thank you for providing me with a safe place, always being interested in my work, being understanding when times have been intense and demanding back my focus when I have been carefree.
Mom and dad; always awake and present, pointing out things I have forgotten or brushed off as "not that important" - you have driven me towards self-realisation.
Solfrid; thank you for talking me back to earth and for being the great support you continue to be.

Daniel Asle Vingen Endal

Bergen, December 2022

Abstract

This thesis examines the quality of protection a Faraday cage provides against electromagnetic fields. The necessary theory to examine and calculate the shielding effectiveness of a Faraday cage, discuss obtained results and conclude the study is collected by researching scientific articles, master theses, books and formula collections published by various antenna manufacturers. The elements of projecting and fabricating a shielded enclosure are detailed from theory, practices and regulations, while the circuit method is used to calculate theoretical shielding effectiveness based on chosen components and materials. Requirement for shielding effectiveness is met across all frequencies on all surfaces, while the requirement for an analogue observation capability have trumped attenuation requirements for windows and the resulting lowered attenuation has been accepted as a compromise. Highest recorded value for leaked electromagnetic radiation with value of -80 dBm at frequency 117MHz is estimated to a value of approximately 350 pW/m^2 which is within the ICNIRP international guidelines for general public exposure to electromagnetic fields.

Contents

List of Figures

List of Tables

Nomenclature

List of Abbreviations

AC	Alternating current
AF	Antenna factor
AH	Access hatch
$avg.$	Average
BFx	Wave trap, 1 through 5
$Bilog$	Bilogarithmic antenna
BV	Private limited company, Dutch
$Corr.$	Correction factor
CW	Continous wave
DC	Direct current
Dx	IEEE measuring point, door
$e.g.$	Exempli gratia - for example
EBC	EB Consulting AS
EM	Electromagnetic
EMC	Electromagnetic compatibility
emf	Electromotive force
EMI	Electromagnetic interference
$EMMA$	Electromagnetic environment handbook
EMP	Electromagnetic pulse
ESD	Electrostatic discharge

FEF	Forskrift om Elektriske Forsyningsanlegg
FMV	The Swedish Defence Materiel Administration
$Freq.$	Frequency
Gx	IEEE measuring point, floor
HF	High frequency
HSE	Health, safety and environment
$Hsp-lab$	High-voltage laboratory
HV	High voltage
HVL	Western Norway University of Applied Sciences (Høgskulen på Vestlandet)
$ICNIRP$	International Commission on Non-Ionizing Radiation Protection
$IEEE$	The Institute of Electrical and Electronics Engineers
INT	International
$Isotrop$	Isotropic antenna
$K1$	Building at HVL campus Bergen
kVA	kilo Volt Ampere
$kVAC$	kilo Volt Alternating Current
$kVDC$	kilo Volt Direct Current
LED	Light emitting diode
LF	Low frequency
$M6$	Measuring point 6
mA	milli Ampere
$Max.$	Maximum
$Min.$	Minimum
$MVin$	Measuring point window
NE	North-east
NEK	Norsk Elektrotekniske komite
OPI	Openings per inch
PLC	Programmable logic controller
ppm	Parts per million

QC	Quality control
$Req.$	Requirement
$RFID$	Radio Frequency Identification
RMS	Root Mean Square
RR	Resonant range
SE	Shielding effectiveness
SE	Single entry frame
$SE1$	Single entry frame 1
$SE2$	Single entry frame 2
SW	South-west
Tx	IEEE measuring point, roof
UiB	University of Bergen
USD	U.S. Dollar
$vs.$	Versus
Vx	IEEE measuring point, wall
WT	Wave trap

Numenclature

α	Sommerfeld constant / fine-structure constant	[−]
δ	Skin depth	[m]
$\frac{d\lambda}{dt}$	Change in magnetic flux	[Wb]
$\hat{r}$	Unit vector of $\vec{r}$	
$\hbar$	Reduced Planck's constant / Dirac constant	Js
λ	Wavelength	[m]
μ_0	Permeability constant of free space	[Hm^{-1}]
μ_r	Relative permeability	
$\nabla\cdot$	Divergence	
$\nabla\mathbf{S}$	Poynting vector	[Wm^{-2}]

$\nabla\times$	Curl	
∇	Gradient	
ω	Angular frequency	[rads^{-1}]
ϕ	Angle from dl to location of q	[rad]
Ψ	Total electric flux enclosed by a surface	[C]
ρ	Specific resistance	[Ωm]
ρ_E	Soil resistivity	[Ωm]
ρ_v	Volume charge density	[Cm^{-3}]
σ	Conductivity	[Sm^{-1}]
τ	Screen thickness	[m]
$\mathbf{A}$	Vector field of a surface	[$-$]
$\mathbf{B}$	Magnetic flux density	[Wbm^{-}2]
$\mathbf{D}$	Electric flux density	[Cm^{-2}]
$\mathbf{E}$	Electric field intensity	[Vm^{-1}]
$\mathbf{H}$	Magnetic field intensity	[Am^{-1}]
$\mathbf{J}$	Conduction current density	[Am^{-2}]
$\mathbf{J}_d$	Displacement current density	[Am^{-2}]
ε_0	Permittivity constant of free space	[Fm^{-1}]
A	Area	[m^2]
a	Distance between Wenner-method electrodes	[m]
A_{cr}	Cross-section	[m^2]
b	Depth Wenner-method electrodes are driven to	[m]
c	Speed of light	[ms^{-1}]
c_0	Speed of light in a vacuum	[ms^{-1}]
dB	Decibel	[dB]
$diagonal$	Adjustment for triangular area of floor in test room	[m^2]
DL	Distance to live parts	[m]
e	Electron charge	[C]
E_e	Electric field strength outside sphere	[Vm^{-1}]

E_m	Dielectric strength of air	$[\mathrm{MVm^{-1}}]$
$E_{(log,V)}$	Electric field strength, numeric	$[\mathrm{dB}\mu\mathrm{Vm^{-1}}]$
$E_{(num)}$	Electric field strength, numeric	$[\mu\mathrm{Vm^{-1}}]$
$E_{[dB\mu V/m]}$	Electric field strength, logarithmic	$[\mathrm{dB}\mu\mathrm{Vm^{-1}}]$
F	Force between two point charges	[N]
f	Frequency	[Hz]
f_1	Frequency where SE has value 3 dB	[Hz]
f_2	Frequency where skin depth is equal to thickness of screen material	[Hz]
f_3	Frequency where SE has value 120 dB	[Hz]
f_4	Frequency where resonance will start to diminish SE	[Hz]
$Floorarea$	Floor area of HV test room	$[\mathrm{m^2}]$
G_n	Antenna gain, numeric	$[\mathrm{m^{-1}}]$
G_{dBi}	Antenna gain, logarithmic	[dBi]
h	Planck's constant	$[\mathrm{m^2kgs^{-1}}]$
H_e	Absolute value of magnetic field without shielding	$[\mathrm{Am^{-2}}]$
H_i	Absolute value of magnetic field with shielding	$[\mathrm{Am^{-2}}]$
$i_T(t)$	Transient current	[A]
I_{enc}	Current enclosed by path	[A]
J_{ind}	Inductive current density	$[\mathrm{Am^{-2}}]$
J_{kap}	Capacitive current density	$[\mathrm{Am^{-2}}]$
k	SI-unit proportionality constant	[–]
K_a	Numeric antenna factor	$[\mathrm{m^{-1}}]$
$K_{a(dB)}$	Logarithmic antenna factor	$[\mathrm{m^{-1}}]$
kV	kilo volt	$[\mathrm{V} \cdot 10^3]$
L	Equivalent inductance	[Hm]
L_{gr}	Grounding inductance	[H]
P_W	Power received in watts	[W]
P_{dBm}	Power received in decibel-milliwatts	[dBm]
Q	Total electric charge enclosed in a volume	[C]

q	Charge	[C]
Q_n	Point charge	[C]
R	Equivalent resistance	[Ωm]
R_1	Region with less than 3 db SE	[−]
R_2	Region with good SE for large rooms	[−]
R_3	Region where the skin effect will be a big factor	[−]
R_4	Region with max. 120 dB SE	[−]
R_5	Region where SE will diminish because of resonance	[−]
r_c	Radius of cylinder	[m]
R_D	Distance	[m]
R_m	Earth resistance	[Ω]
r_{sf}	Radius of a sphere	[m]
r_{sphere}	Radius of sphere with volume equal to HV test room	[m]
S	Measured/estimated power flux density	[Wm^{-2}]
$SE_{H//mag}$	Shielding effectiveness, magnetic fields	[dB]
SE_{sf}	Shielding effectiveness of equivalent sphere	[dB]
SS_A	Shell protection class A	
SS_B	Shell protection class B	
SS_C	Shell protection class C	
SS_D	Shell protection class D	
U_r	Spectrum analyzer received voltage	[V]
V	Electric potential	[V]
v	Frequency	[Hz]
$v_L(t)$	Transient inductive voltage losses	[V]
V_m	Electric potential capable of corona discharge	[V]
$V_{[dB\mu V]}$	Antenna received voltage, logarithmic	[dBμV]
V_{AB}	Potential difference	[V]
v_{dr}	Drift velocity	[ms^{-1}]
V_{emf}	Induced voltage	[V]

V_{ep}	Standard electrode potential	[V]
V_{fa}	Volume of HV test room up to height of niche	[m^3]
V_{niche}	Volume of HV test room above the niche	[m^3]
V_{sphere}	Volume of HV test room converted to sphere	[m^3]
V_{tot}	Volume of entire HV test room	[m^3]
W	Work done on charge	[J]
Z_0	Impedance of vacuum	[Ω]
Z_i	Antenna impedance	[Ω]

Subscript

c	Cylinder
d	Divergence
emf	Electromotive force
enc	Enclosed
ind	Inductive
kap	Capacitive
$mag(cyl)$	Magnetic shielding effectiveness for cylinder
$mag(sf)$	Magnetic shielding effectiveness for sphere
$niche$	Floor area of the niche in test room
nor	Area of HV test room that is inside the niche
ON	Cross-section of test room at height above the niche in the test room
sf	Sphere
sou	Area of HV test room that is "below" maximum width of test room on blueprints

Chapter 1

Introduction

To ensure that the electrical power engineers of tomorrow can acquire knowledge, it is important with a varied educational situation where both theory and practice meet. A possible way to make this happen is with laboratory exercises within small electronics, strong currents and high voltages. It is desirable that students are in a safe environment when they participate in the teaching, and in order to protect against high voltages during laboratory exercises using high voltage, it will be relevant with a Faraday cage present. At Western Norway University of Applied Sciences, campus Kronstad, a former group of bachelor students has constructed a Faraday cage in the high voltage test room. During previous use of the high-voltage laboratory, the card reader system for the nearby doors seized to function properly due to electromagnetic radiation from the laboratory. The University has afterwards been instructed by Statsbygg to design and install a professionally designed Faraday cage.

1.1 Background

Institutions that train electrical power engineers need high-voltage laboratories. The authorities have requirements for how Faraday cages are to be developed and dimensioned when the installation is to protect critical infrastructure against possible threats. These same requirements are imposed on educational institutions, even if the areas of use could not be more different. A Faraday cage in a laboratory has the purpose of delimiting and containing charges and radiation that occur, while cages mentioned for previous situations have the purpose of protecting the contents from outside threats. Is it really necessary for the same requirements to be made?

1.2 Objective

This paper is written with the objective to examine the need for protection in conjunction with high-voltage laboratories at educational institutions. Mandatory governmental

requirements in Norway are based on the protection of critical infrastructure and equipment from foreign threats, i.e. from the outside. The situation in a college or university laboratory is the opposite. Surrounding equipment and infrastructure must be protected against radiation, interference and electrical arcing taking place inside the Faraday cage. The Faraday cage construction also functions as a means of protection for people against experiments being conducted, as well as the aforementioned radiation etc., inside the high-voltage laboratory.

Hypothesis:
There will always be a need for safety measures in today's modern world with regard to high-voltage equipment. Regulations are imposed on the shielded enclosure in order to maintain safety for the laboratory. But is it really necessary to project and install a full-fledged Faraday cage in a college or university high voltage laboratory with peak voltages only reaching as high as 380kVAC RMS/420kVDC? It is conceivable that the solution mandated by the authorities is over-engineered in many cases, and that parts of the funding will be better utilized in other areas. Furthermore, we look at what goes into the process of fabricating a Faraday cage.

1.3 Methods

This thesis follows the process surrounding the new Faraday cage projected and built by EB Consulting AS with a focus on a qualitative approach. Theory, standard commercial practices, and calculations have been researched through a literature review encompassing master theses, articles and books, scientific articles, regulatory standards, quality control test reports, personal messages and discussions with industry professionals, and formulas and equations published by measuring equipment manufacturers.

The research has been conducted with an engineering perspective, with a broad overview and deeper investigations into what is perceived as key information for the problem.
Especially the thesis "Design of the Ohio State University High Voltage Laboratory" [1] in conjunction with the scientific article "An update on the circuit approach to calculate shielding effectiveness" [2] has been essential for the study on theoretical dampening and design theory of the Faraday cage.

Measurement shielding effectiveness is compared to the required dampening, while measured electromagnetic fields are compared to international guidelines to indicate the amount of leakage escaping the shielded enclosure.

Chapter 2

Theory

2.1 Electromagnetism

Electromagnetic phenomena can be summarized using Maxwell's four equations: Gauss's law for electrostatics:

$$\nabla \cdot \mathbf{D} = \rho_v \tag{2.1}$$

Gauss's law for magnetostatics:

$$\nabla \cdot \mathbf{B} = 0 \tag{2.2}$$

Maxwell-Faraday law (Faraday's induction law):

$$\nabla \times \mathbf{E} = -\frac{\partial \mathbf{B}}{\partial t} \tag{2.3}$$

Ampere's circuital law:

$$\nabla \times \mathbf{H} = \mathbf{J} + \frac{\partial \mathbf{D}}{\partial t} \tag{2.4}$$

∇ = vector differential operator; $\mathbf{D}$ = electric flux density; $\mathbf{B}$ = magnetic flux density; $\mathbf{E}$ = electric field intensity; $\mathbf{H}$ = magnetic field intensity; ρ_v = volume charge density and $\mathbf{J}$ = current density.

Maxwell's equations, together with Lenz's law, form the foundation for classical electromagnetics and electric circuits. The equations are based on previously known results from theoretical work, as well as experimental work [3]. Each of these equations describes how electromagnetic phenomena interact with each other, including flux densities, currents and fields, as well as during dynamic and static scenarios.

Each of the equations can be represented as the equations listed above, but also in terms of integral form by applying Stoke's theorem to them.

Stoke's theorem, also called the Kelvin-Stokes theorem and curl theorem, "states that the circulation of a vector field $\mathbf{A}$ around a (closed) path L is equal to the surface integral of the curl of $\mathbf{A}$ over the open surface S bounded by L provided that $\mathbf{A}$ and $\nabla \times \mathbf{A}$ are continuous on S" [3, p. 79].

$$\oint_L \mathbf{A} \cdot d\mathbf{l} = \int_S (\nabla \times \mathbf{A}) \cdot d\mathbf{S} \tag{2.5}$$

Maxwell's first equation is based on Gauss's law for electrostatics, which states that the "*total electric flux* Ψ *through any closed surface is equal to the total charge enclosed by said surface*" [3, p. 124].

$$\Psi = Q_{enc} \tag{2.6}$$

Another way to formulate the electric flux is by using the product of the surface integral over the closed surface and the electric flux density

$$\Psi = \oint d\Psi = \oint_S \mathbf{D} \cdot d\mathbf{S} \tag{2.7a}$$

and since $\Psi = Q$ and Q is the total charge enclosed in a volume we can substitute the last term of equation (2.7a) into equation (2.6)

$$Q = \oint_S \mathbf{D} \cdot d\mathbf{S} = \int \rho_v dv \tag{2.7b}$$

The closed system can have more than one surface, but it can only have one volume, so we take the divergence of the closed-surface integral in (2.7b) and rewrite it as a volume integral

$$\oint_S \mathbf{D} \cdot d\mathbf{S} = \int_v \nabla \cdot \mathbf{D} \; dv \tag{2.8a}$$

Then we substitute last term of (2.7b) for the closed surface integral and get

$$\implies \int_v \rho_v dv = \int_v \nabla \cdot \mathbf{D} \; dv \tag{2.8b}$$

We cancel the volume integrals on each side and are left with the expression for Maxwell's first equation;

$$\rho_v = \nabla \cdot \mathbf{D} \tag{2.9}$$

The equation states that *"the volume charge density is equal to the divergence of the electric flux density* [3, p. 125] *."*

Maxwell's second equation [3] Gauss's law for magnetostatics states that the existence of magnetic monopoles is not possible. This is because the magnetic flux through a surface S is given by

$$\Psi = \int_S \mathbf{B} \cdot d\mathbf{S} \tag{2.10}$$

Where Ψ is the magnetic flux [Wb] and B is the magnetic flux density [Wb/m^2(= T)]. The magnetic flux line is the line formed by the tangent of $\mathbf{B}$ at any point in a magnetic field. The tangent, if its direction is followed, will guide itself back to its origin, showing that magnetic flux lines have no beginning or end. This also means that it is not possible to have a magnetic charge, or a magnetic monopole [3, p. 283]. Because magnetic charges do not exist, the total flux through a closed surface must be zero.

$$\oint \mathbf{B} \cdot d\mathbf{S} = 0 \tag{2.11}$$

The divergence theorem lets us replace the surface integral of $\mathbf{B}$ for the closed surface S with a volume integral of the divergence of $\mathbf{B}$

$$\oint_S \mathbf{B} \cdot d\mathbf{S} = \int_v \nabla \cdot \mathbf{B} dv = 0 \tag{2.12}$$

which gives us the differential form given in equation 2.2 [3, p. 281-284]

$$\nabla \cdot \mathbf{B} = 0$$

Maxwell's third equation Is based on Faraday's law of electromagnetic induction. The law came about during Michael Faraday's experiments[1] on time-varying magnetic fields which showed to produce an electric current. There will be no current flow when a conductor forming a closed loop is exposed to a static magnetic field, but if the field is a time-varying magnetic field, the same conductor will experience "an induced voltage called *electromotive force*"(abb.: emf) produced by the varying magnetic field. The induced voltage will cause an electric current to flow, and the induced voltage can be expressed as

$$V_{emf} = -\frac{d\lambda}{dt} = -N\frac{d\Psi}{dt} \tag{2.13}$$

and is called *Faraday's law*. The induced voltage is negative because it is trying to counter and neutralize the flux forced upon it by the changes in the magnetic field. The factor N is the number of turns in the circuit that passes through the magnetic field, and Ψ is the

[1]Both Michael Faraday and Joseph Henry are credited with the discovery that "a time-varying magnetic field would produce an electric current", as they both experimented and discovered this in the year 1831. M. Faraday made his discovery in London, while J. Henry did his discovery in New York [3, p. 370].

flux in each turn. The induced voltage trying to neutralize the flux producing it is called *Lenz's law*.

Electric fields are generally described as fields caused by electric charges, the flux lines of these fields originate and terminated at the electric charges. Other electric fields exist as well. These fields are produced by electromotive forces and therefore termed *emf-produced fields*. Emf-produced fields can originate from a variety of sources.

A generator with a permanent magnet rotor will produce an alternating emf-produced field, now if we say that the stator coil only has one turn and is connected to a transformer, forming a closed loop, the emf v_{emf} induced in a coil is

$$v_{emf} = -\frac{d\Psi}{dt} \tag{2.14}$$

Where Ψ is the flux passing through the surface S of the conductor as given in eq. (2.10), which we substitute in and get a partial differential equation

$$v_{emf} = -\int_S \frac{\partial \mathbf{B}}{\partial t} \cdot d\mathbf{S} \tag{2.15}$$

The alternating electromotive force is induced in the circuit, which is a closed loop L, meaning

$$v_{emf} = \oint_L \mathbf{E} \cdot d\mathbf{l} \tag{2.16}$$

Comparing and combining equations (2.15) and (2.16) we are left with

$$v_{emf} = \oint_L \mathbf{E} \cdot d\mathbf{l} = -\int_S \frac{\partial \mathbf{B}}{\partial t} \cdot d\mathbf{S} \tag{2.17}$$

by using Stokes theorem on the middle term of eq.2.17 yields

$$\int_S (\nabla \times \mathbf{E}) \cdot d\mathbf{S} = - - \int_S \frac{\partial \mathbf{B}}{\partial t} \cdot d\mathbf{S} \tag{2.18}$$

Cancelling the integrals on both sides of eq. (2.18) brings us the final form of Maxwell's third equation

$$\nabla \times \mathbf{E} = -\frac{\partial \mathbf{B}}{\partial t} \tag{2.19}$$

which shows that a time-varying magnetic field will always create an (opposing) electric field [3, p. 373].

Maxwell's fourth equation Is based on Ampere's circuit law, which states that *"the line integral of the component of **H** around a closed path is the same as the net current I_{enc} enclosed by the path"* [3, p. 273]. This means that the current in a wire, also known as the scalar of an electric field in a path of any shape, is equal to the magnetic field vector. This means that the circulation of the magnetic field intensity **H** can be written as

$$\oint \mathbf{H} \cdot d\mathbf{l} = I_{enc} \tag{2.20}$$

Equation (2.20) is true for both symmetrical and non-symmetrical current distribution, but **H** can only be determined during the presence of symmetrical current distribution.

For equation (2.20) we can apply Stoke's theorem on the left side of the equation which yields

$$I_{enc} = \oint \mathbf{H} \cdot d\mathbf{l} = \int_S (\nabla \times \mathbf{H}) \cdot d\mathbf{S} \tag{2.21}$$

Sadiku writes [3, p. 163] that

$$I_{enc} = \int_S \mathbf{J} \cdot d\mathbf{S} \tag{2.22}$$

That means when the two equations (2.21) and (2.22) are compared we end up with

$$\nabla \times \mathbf{H} = \mathbf{J} \tag{2.23}$$

Maxwell also adds the $\frac{\partial \mathbf{D}}{\partial t}$-term to the current density/right side of eq. (2.23) to represent displacement currents that are not accounted for when taking the divergence of each side of equation (2.23). Displacement currents are not accounted for because the divergence ($\nabla\cdot$) of the curl ($\nabla\times$) of any vector field is equal to zero. But in order for the divergence of **J** to satisfy the continuity of current, as shown in eq. (2.24) (see eq. 5.43 [3, p. 181]), the divergence of **J** cannot be equal to zero ($\nabla \cdot \mathbf{J} \neq 0$).

$$\nabla \cdot \mathbf{J} = -\frac{\partial \rho_v}{\partial t} \tag{2.24}$$

To achieve a correct relation for Maxwell's fourth equation during time-varying conditions, we add the term $\mathbf{J}_d$ to eq. (2.23)

$$\nabla \times \mathbf{H} = \mathbf{J} + \mathbf{J}_d \tag{2.25}$$

Since the job of the term $\mathbf{J}_d$ is to adjust for the term **J** so that the divergence of the left side of eq. (2.23) can become 0, the divergence of term $\mathbf{J}_d$ must cancel the divergence of term **J**; keeping in mind that the divergence of any vector's curl must still be equal to zero.

$$\begin{aligned}\nabla \cdot (\nabla \times \mathbf{H}) = 0 =& \nabla \cdot \mathbf{J} + \nabla \cdot \mathbf{J}_d \\ \implies \nabla \cdot \mathbf{J}_d = -\nabla \cdot \mathbf{J} = \frac{\partial \rho_v}{\partial t} &= \frac{\partial}{\partial t}(\nabla \cdot \mathbf{D}) = \nabla \cdot \frac{\partial \mathbf{D}}{\partial t}\end{aligned} \tag{2.26}$$

Which in short comes down to

$$\nabla \cdot \mathbf{J}_d = \nabla \cdot \frac{\partial \mathbf{D}}{\partial t}$$

By removing the divergence on both sides of this equation, we get the definition for displacement currents [3, p. 381]

$$\mathbf{J}_d = \frac{\partial \mathbf{D}}{\partial t} \tag{2.27}$$

The addition of the term for displacement currents is one of Maxwell's big contributions, which enabled electromagnetic wave propagation. This was later confirmed by Hertz since the equipment needed to test Maxwell's mathematical equation did not exist at the time.

2.1.1 Electrical fields

Electrically charged bodies are surrounded by electric fields. The electric field goes radially out from or in towards the charge, and the direction is given by the polarity of the charged body. The relationship between the charge of several stationary charged bodies', the distance between bodies, and the force between bodies is given by Coulomb's law.

Coulomb's lov is an experimental law developed by French colonel Charles Augustin de Coulomb in 1785. The law derives the force a point charge exerts on another point charge. A point charge refers to a charge that is located on a body with dimensions much smaller than other relevant values. Incidentally, the law only applies to stationary particles, and only to point charges or spherical bodies with a uniform charge. A charge is preferably measured in coulombs, where one coulomb is equal to 6×10^{18} electrons. The size of the number of electrons is due to the fact that one electron charge is only $e = -1.6019 \times 10^{-19}$ C

Coulomb's law states that the force F between two point charges Q_1 and Q_2 is:

1. Along the line between the charges
2. Directly proportional to the product of $Q_1 Q_2$ for the charges
3. Inversely proportional to the square of the distance between the charges

The mathematical representation of Coulomb's law is expressed as

$$F = \frac{kQ_1Q_2}{R_D^2} \tag{2.28}$$

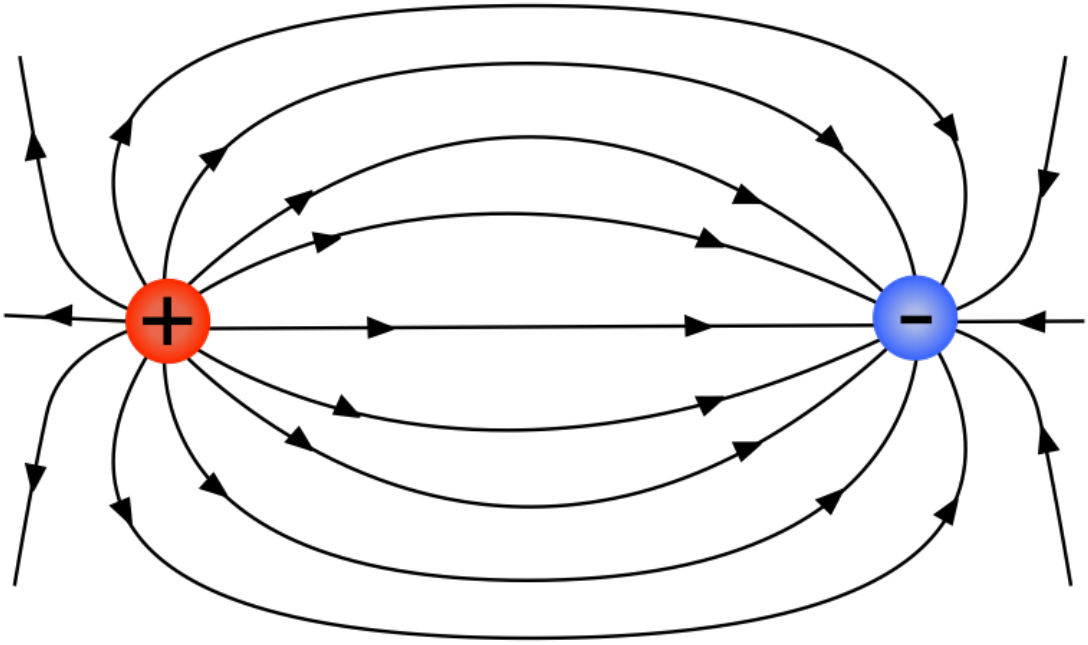

Figure 2.1: Representation of fieldlines between a positively charged body and a negatively charged body. Photo: Daniel Asle Vingen Endal.

[3, p. 104]

The constant k is a proportionality constant that adjusts for which units are used in the formula. When using SI units, the designation for the charges Q_1 and Q_2 is coulomb [C] and the distance R_D has the designation meter [m]. The force F has a denomination in newtons [N]; the proportionality constant with SI units is $k = 1/4\pi\varepsilon_0$. ε_0 is known as the *permittivity constant of free space* (in Farad per meter), and has the value $\varepsilon_0 = 8.854 \times 10^{12} \simeq \frac{10^{-9}}{36\pi}[F/m]$.

Equation 2.28 is thus defined using SI units as

$$F = \frac{Q_1 Q_2}{4\pi\varepsilon_0 R_D^2} \tag{2.29}$$

[3, p. 105]

The magnitude of an electric field is given by the ratio of the electric force exerted on a charged particle divided by the charge of the charged particle. For a charge at a point, this is given by the equation (2.30)

$$\vec{E} = \frac{\vec{F_0}}{q_0} \tag{2.30}$$

$\vec{F_0}$ is the electric force on a charged body q_0 at the point. When the charge of the body is positive, the direction of the electric field $\vec{E}$ is equal to the direction of the force $\vec{F_0}$. If the charge of the body is negative, the direction is opposite.

Electrical potential - V is the electric scalar potential and one of the factors that can be used to find the electric field intensity **E**. According to Sadiku, using the electric potential to find the electric field intensity **E** is easier than using Coulomb's law.

In order to move a charge in an electric field from one point to another point via a distance **l**, the force needed is found by the equation (2.30) from Coulomb's law

$$\vec{\mathbf{F}} = \vec{\mathbf{E}}q \tag{2.31}$$

The work done on the charge q is done by the electric field **E**, the work on the charge thus comes from outside, so the sign of **F** must be negative and we can say that

$$dW = -\vec{\mathbf{F}} \cdot d\mathbf{l} = -q\vec{\mathbf{E}} \cdot d\mathbf{l} \tag{2.32}$$

It means that the work W required to move charge q from A to B is

$$W = -q \int_A^B \mathbf{E} \cdot d\mathbf{l} \tag{2.33}$$

Work required to move a charge is the increase in *electric potential* of charge q at the new point relative to the starting point. The difference in electric potential between the two points is the potential difference (*potential difference*) and is given by work per charge

$$V_{AB} = \frac{W}{q} = -\int_A^B \mathbf{E} \cdot d\mathbf{l} \tag{2.34}$$

As a final note, the electric potential for an arbitrary point is the potential difference in a given point in relation to a chosen reference point ground, defined as zero for the system [3, p. 134].

2.1.2 Magnetic fields

Static magnetic fields are characterized by magnetic field intensity **H** or magnetic flux density **B**. There are both similarities and differences between electric fields and magnetic fields. In the same way that the electric flux density **D** is a function of the product of the electric permittivity in a vacuum and the electric field intensity **E**, the magnetic flux density **B** is a function of the product of the magnetic permeability in a vacuum and the magnetic field intensity **H** [3].

Most current equations for electric fields can easily be reformulated to apply to magnetic fields, provided that the right analogue substitutes for the factors are used.

Historically, H. C. Oersted established a definitive link between electric fields and magnetic fields in the year 1820, after 13 years of trial and error in his experiments [3, p. 261].

Electric fields come from static, also referred to as stationary, charges. Electric charges moving at a constant speed in a constant direction will emit a static magnetic field. This means that a constant flow of electric DC current in a conductor will result in a magnetic field. Other sources that can produce a static magnetic field are magnetization currents (from a permanent magnet), "electron-beam currents" from vacuum tubes, or conductive currents in current-carrying wires, as mentioned above.

Table 2.1: Comparison of the different laws for both electric and magnetic fields [3, p. 262]

Term	**Electric**	**Magnetic**
Basic laws	$\mathbf{F} = \frac{Q_1 Q_2}{4\pi\varepsilon_r^2}\mathbf{a}_r$ $\oint \mathbf{D} \cdot d\mathbf{S} = Q_{enc}$	$d\mathbf{B} = \frac{\mu_0 I d\mathbf{l} \times \mathbf{a}_r}{4\pi R^2}$ $\oint \mathbf{H} \cdot d\mathbf{l} = I_{enc}$
Force law	$\mathbf{F} = Q\mathbf{E}$	$\mathbf{F} = Q\mathbf{u} \times \mathbf{B}$
Source element	dQ	$Q\mathbf{u} = Id\mathbf{l}$
Field intensity	$E = \frac{V}{\ell}(\mathrm{V/m})$	$H = \frac{I}{\ell}(\mathrm{A/m})$
Flux density	$\mathbf{D} = \frac{\Psi}{S}(C/\mathrm{m}^2$	$\mathbf{B} = \frac{\Psi}{S}(\mathrm{Wb/m}^2)$
Relationship between fields	$\mathbf{D} = \varepsilon\mathbf{E}$	$\mathbf{B} = \mu\mathbf{H}$
Potentials	$\mathbf{E} = -\nabla V$ $V = \int \frac{\rho_L dl}{4\pi\varepsilon r}$	$\mathbf{H} = -\nabla V_m(\mathbf{J}{=}0)$ $\mathbf{A} = \int \frac{\mu I d\mathbf{I}}{4\pi R}$
Flux	$\Psi = \int \mathbf{D} \cdot d\mathbf{S}$ $\Psi = Q = CV$ $I = C\frac{dV}{dt}$	$\Psi = \int \mathbf{B} \cdot d\mathbf{S}$ $\Psi = LI$ $V = L\frac{dI}{dt}$
Energy density	$w_E = \frac{1}{2}\mathbf{D} \cdot \mathbf{E}$	$w_m = \frac{1}{2}\mathbf{B} \cdot \mathbf{H}$
Poisson's equation	$\nabla^2 V = -\frac{\rho_v}{\varepsilon}$	$\nabla^2 \mathbf{A} = -\mu\mathbf{J}$

For magnetic fields, there are 2 laws that apply:

· Biot-Savart's law

· Ampere's circuit law

Biot-Savart's law is to magnetostatics what Coulomb's law is to electromagnetism, so Biot-Savart's law is a general law for magnetostatics. Ampere's law is a special case of Biot-Savart's law, in the same way, Gauss's law is a special case of Coulomb's law. Ampere's law is easy to use for symmetrical current sharing problems.

Biot-Savart's Law considers both **B** and **H** for a magnetic field and its intensity. The magnetic field intensity d**H** produced at a point P by the current in a small portion of a conductor designated I dl is proportional to the product of the current I through the conductor segment dl and the angle α between the element l and the line connecting the point P with the element, further it is inversely proportional to the square of the distance R between the element and the point P.

Young & Freedman describe Biot-Savart's law as how we can describe the flux density or field intensity at a point based on the magnetic field from a bounded part of a conductor dl (or a surface or a volume) [4, p. 925]. The current in the conductor is based on the charges moving in the conductor based on the volume of the segment dl given by the cross-section A_{cr} and the length dl. In the conductor, there are n number of charged particles per unit volume that add up the charges to the total charge dQ

$$dQ = n \cdot q \cdot A_{cr} \cdot dl \tag{2.35}$$

The field at an arbitrary point P is given by

$$d\mathbf{B} = \frac{\mu_0}{4\pi} \frac{|dQ| v_{dr} \sin\phi}{r^2} = \frac{\mu_0}{4\pi} \frac{n \cdot |q| \cdot v_{dr} \cdot A_{cr} \cdot dl \cdot \sin\phi}{r^2} \tag{2.36}$$

The current in the conductor is given by the number of charged particles in the volume (n), magnitude charge ($|q|$,[C]), the speed of movement of the charges/drift velocity (v_{dr}, [m/s]), the angle (ϕ, [rad]) from dl to the location of q, and the cross-section (A_{cr}, [m^2]) of the leader segment.

Designation for the current I = A = C/s and is based on the charges located in the volume $A_{cr} \cdot dl$ [m^3]; $I = \int_V n|q| v_{dr} A_{cr} dV = n|q| \int_V v_{dr} A_{cr} dV$

Puts the current I passing through the wire segment dl for $|dQ|v_{dr}$ in dB:

$$dB = \frac{\mu_0}{4\pi} \cdot \frac{Idl \sin \phi}{r^2} \tag{2.37}$$

Convert equation (2.37) to vector-based

$$dB = \frac{\mu_0}{4\pi} \cdot \frac{Id\vec{l} \times \hat{r}}{r^2} \tag{2.38}$$

$d\vec{l}$ is a vector with the length of the current in the segment dl in the same direction as the current I. $\hat{r}$ is the unit vector pointing from the conductor segment in the direction of the measurement point and is $\frac{\vec{r}}{|r|}$.

From Sadiku it is defined that magnetic flux density depends on the product between the magnetic permeability in a vacuum and the magnetic field intensity ($\mathbf{B} = \mu_0\mathbf{H}$).

$$d\mathbf{B} = \frac{\mu_0}{4\pi} \frac{Id\vec{l} \times \hat{r}}{r^2} \tag{2.39a}$$

Takes the integral of both sides

$$\implies \mathbf{B} = \frac{\mu_0}{4\pi} \int \frac{Id\vec{l} \times \hat{r}}{r^2} \tag{2.39b}$$

Because we have already established that $\mathbf{B} = \mu_0\mathbf{H}$ (see relation between fields, table 2.1) we can apply this to the equation from (2.39a) to apply to both $\mathbf{B}$ and $\mathbf{H}$:

$$d\mathbf{H}\mu_0 = \frac{\mu_0}{4\pi} \frac{Id\vec{l} \times \hat{r}}{r^2} \tag{2.40a}$$

Stripping μ_0 from both sides of (2.40a):

$$d\mathbf{H} = \frac{1}{4\pi} \frac{Id\vec{l} \times \hat{r}}{r^2} \tag{2.40b}$$

And taking the integral on both sides to get $\mathbf{H}$

$$\mathbf{H} = \frac{1}{4\pi} \int \frac{Id\vec{l} \times \hat{r}}{r^2} \tag{2.40c}$$

Biot-Savart's law describes the magnetic field, in terms of the flux density and the field intensity, at an arbitrary point in a magnetic field $\mathbf{B}$. The direction for dH and dB is

given by the right-hand rule, where the right thumb points in the same direction as the current I, and dH & dB is in the direction of the fingers when they are placed around the conductor (possibly right-handed screw rule) [3, p. 263].

Ampere's law is derived in Maxwell's fourth equation earlier in this chapter.

2.1.3 Radiation

Electromagnetic charges are the source of electromagnetic fields. Radiation is explained as electromagnetic waves that propagate away from a time-varying source [3, p. 588]. Radiation is a way of transferring energy using antennas. Theoretically, any conductive structure can act as an antenna, but for an effective transmission to happen, a specialized antenna is needed as it increases the transmission efficiency. An antenna can act as both transmitter and receiver. For the best possible transmission of information, an antenna for the transmitter and an antenna for the receiver are necessary. Antennas are needed for two reasons: (1) efficient radiation and (2) minimizing reflections of radiation by matching the antenna impedance with the wave impedance [3, p. 588].

Young and Freedman refers to radiation as the transfer of heat using electromagnetic waves and can be experienced as the heat from the sun, the intense heat radiating from a charcoal grill, or from glowing coals in a fireplace. This heat is not the result of either conduction, because there is no conductive matter in between, or convection through the air because the heat is experienced when there is no wind, but it is a result of radiation. All electromagnetic waves are radiation, from 1 Hz to 10^{28} Hz, and higher. That is, radio, infrared waves, visible light, ultraviolet, microwaves and gamma radiation are all radiation [4, p. 569]. The radiation occurs even without any medium to propagate in, so even in a vacuum radiation will be present.

In classical physics, electromagnetic radiation is the flow of energy that moves at the speed of light in the form of electric and magnetic fields. An electromagnetic wave is characterized by its intensity and frequency. This means the time variation for electric and magnetic fields.

For modern quantum theory, electromagnetic radiation is the flow of photons, also known as "light quanta", through space. Furthermore, photons are energy packets that are defined by the product hv, where h is Planck's constant and v is the frequency. All photons with the same product hv have the same amount of energy and are thus equal. The common denominator for electromagnetic radiation is the dependence on frequency:

- Creation of electromagnetic fields
- How natural radiation occurs

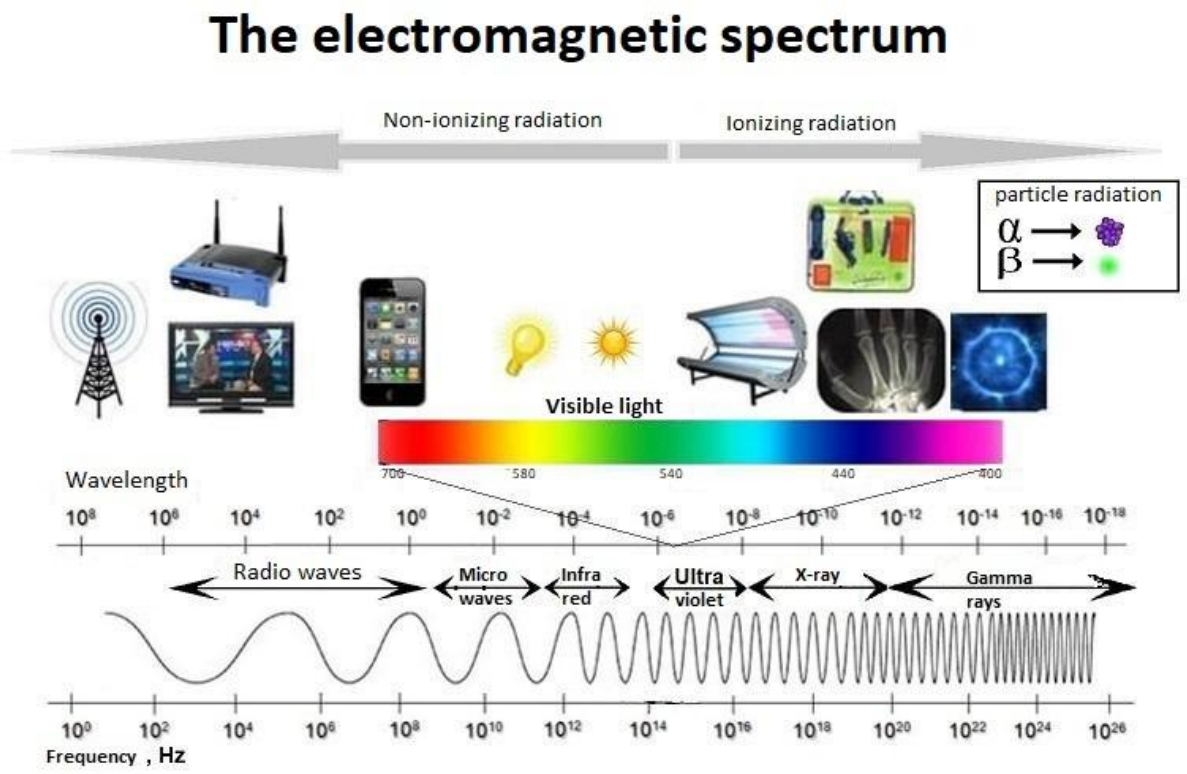

Figure 2.2: Electromagnetic spectrum. Photo: UiB [6].

- Technological use

[5]

The electromagnetic spectrum consist of every conceivable combination of wavelength and frequency of electromagnetic waves. From quite low values for frequencies, where we find radio, TV and microwaves, to visible light and up to high values, where we find ultraviolet light, X-ray and gamma radiation.

The electromagnetic radiation spectrum is divided into categories and structured based on frequency (f or sometimes v [Hz]), and wavelength (λ [m]). Frequency and wavelength are interconnected by

$$f = c_0/\lambda \tag{2.41}$$

where c_0 is the speed of light in a vacuum. The relation between frequency and wavelength is that they are inversely proportional. A high frequency will have a shorter wavelength than a low frequency. This is a result of radiation being linked to the speed of light c, which has a constant value (value is dependant on what medium light is passing through). EM waves with a frequency above visible light on the electromagnetic radiation spectrum carry so much energy that they can ionize atoms. These frequencies are therefore called

ionizing radiation [5]. The higher the frequency of electromagnetic radiation, the more energy the photons carry.

The occurrence of radiation is abundant in the universe we live in. Close to 0.01% of the mass and energy of the universe occur in the form of electromagnetic radiation [5]. Our society and modern technology rely on the phenomena; communication technology and medical services are especially reliant on forms of electromagnetic radiation. In fact, all gas, oil and coal are electromagnetic radiation from the sun that has been stored. The only energy that is not a result of electromagnetic radiation from the sun is nuclear power [5].

Decibel is a logarithmic unit of measurement that is used to measure sound levels, and in common use in electronics, signals and communication. The decibel describes a ratio between two physical quantities e.g. power, sound pressure, voltage, intensity etc. [7]. A single decibel is "10 times the common logarithm of the power ratio" [8]. The decibel is commonly used to express the logarithmic ratio between two magnitudes as in between two electric voltages or currents. 1 dB is equal to 20 times the common logarithm of ratio in cases where the ratio is of a squared quantity [8].

Note on measuring: We will be using dBm to measure the escaping EM radiation from the Faraday cage after quality control. Limits from standards and regulations are detailed in W/m^2. The conversion between these units is detailed in chapter 4.4. The power in the point is converted by equation (2.42a) to convert from decibels (dBm) to watts,

$$P_{dBm} = 10 \log_{10}(\frac{1000 \cdot P_W}{1W}) \tag{2.42a}$$

and by equation (2.42b) to convert from watt to decibel (dBm).

$$P_W = 1W \cdot \frac{10^{\frac{P_{dBm}}{10}}}{1000} \tag{2.42b}$$

2.1.4 EMI & EMP

Electromagnetic interference, abbreviated *EMI*, is the degradation in the performance of a device due to the fields making up the electromagnetic environment. The atmosphere is home to the electromagnetic environment where every electrically powered device present is radiating electromagnetic fields. Devices that radiate these fields are termed *emitter* and can be radio and tv broadcast stations, radar and navigational aids that emit electromagnetic energy when they operate [3, p.644]. Victim devices of EMI (devices that may be influenced by the interference) are termed "susceptors".

Conducted EMI differs from radiated EMI in that the interference is transferred from source to victim device through a physical connection [9].

EMI sources Power supplies, radar transmitters, mobile radio transmitters, fluorescent lights and car ignition systems are all sources and emitters of electromagnetic interference [3, p. 645].

EMP *Electromagnetic pulse*, abbreviated *EMP*, is defined in the Oxford English Dictionary as "n[2]. a pulse of electromagnetic energy, especially a powerful one emitted by a nuclear explosion or nuclear weapon [10]." An electromagnetic pulse can occur naturally in nature, and it can also occur artificially through human actions such as explosions. An electromagnetic pulse is in short a pulse of electromagnetic *energy* that travels outward from its origin in the form of either an electromagnetic field, an electric field, a magnetic field or a conducted electric current pulse.

Sources

Naturally occurring EMPs happen during e.g. lightning, while man-made EMPs can come from e.g. a power line surge, the ignition system on a gasoline-powered internal combustion engine or high-powered explosives. A list of EMP sources can be compiled to, among others; lightning, electrostatic discharge, meteors, plasma in solar winds, electrical switching action, electric motors, gas engine ignition systems, power line surge, nuclear explosion and military non-nuclear EMP weapons.

Many of these sources are phenomena that are natural to protect installations against, but our case is based on protecting the outside world from what takes place inside the laboratory. An assessment has therefore been made; although many possibilities have been mentioned (also more than those mentioned above) where EMI and EMP can occur, I have come to the conclusion that several have no relevance to this thesis. A conscious choice has therefore been made not to go into detail and describe it more precisely in relation to irrelevant sources. Further, the sources described here are direct parallels and analogues to what takes place inside the high-voltage laboratory.

Lightning Lightning is caused by the differential in electrical potential in a cloud or between a cloud and the ground. The clouds, typically of the type *cumulonimbus*, that create lightning exhibit a large amount of vertical movement within the cloud. This vertical movement is causing particles to bounce into and off of each other and become electrically charged particles and separate into a positively charged top portion and a negatively charged bottom portion within the cloud. When this difference in potential

[2]Noun.

becomes large enough, the air forms a plasma that carries a current around 20,000-30,000 ampere, on average dissipating around one to two gigajoule of energy [11].

Of this gigajoule, only 200,000 joules are dissipated in that part of the electromagnetic spectrum as visible light and other radiation. The remaining energy is released to the surrounding air in the form of heat [11].

Electrostatic discharge (ESD) Electrostatic discharge can cause an electromagnetic pulse in the same way that lightning does. The difference between a lightning strike and ESD is the size of the discharge.

2.2 Shielding

There is a particular need to protect sensitive measurements that take place inside the high-voltage laboratory, such as e.g. measurements on partial discharge or corona, against external electromagnetic disturbances (EMI) from outside the HV test room. Furthermore, it is necessary to ensure that electromagnetic activity occurring inside the high-voltage laboratory is not allowed to disturb equipment and installations in the vicinity of the high-voltage laboratory.

Common sources of noise and/or disturbances include:

- Radio stations and radio frequency noise sources
- Welding equipment
- Switching in electrical networks
- Discharges between an object and earth

These disturbances can be transferred to measuring instruments such as capacitive and inductive currents.

To ensure the best possible damping, there are a couple of points that should be striven for:

- Electromagnetic shielding throughout the building
- Pay particular attention to good shielding around doors and gates
- Recommended to have as few openings as possible in the screen structure, if possible: avoid windows
- As few metallic intrusions as possible in the test room as these will act as antennas.

All penetrations must be grounded to the screen structure.

- Permanent structures inside the test room must be connected to the ground.

According to the publication *Electromagnetic environment handbook* (abb.: EMMA) by FMV[3] proper attenuation in the screen system is defined based on different *shell protection classes*, ranging from A to D. Shell protection class SS_A has no specific requirements since equipment included inside the shell already has or does not need protection from HF interference but needs protection from e.g. conducted interference from lightning. Shell protection class SS_B has a requirement of 30 dB in the range of 10kHz to 10MHz. Shell protection class SS_C has a requirement of up to 50 dB in the range of 10kHz to 1GHz. Shell protection class SS_D has a requirement ranging from 30 dB to 70 dB in the range of 10kHz to over 10GHz. These sources have been collected from pages 9 through 11 in part 3 of EMMA [12, pp. 9–11].

Electromagnetic disturbances

Calculations are described by Maxwell's equations with given conditions such as the relationship between the electric and magnetic fields. The ratio between the electric field and the magnetic field of a wave is called the impedance of the wave. The wave impedance varies with the distance between the source of the wave and the point of observation.

1. In the near-field area close to the source, up to a distance equal to $\lambda/2\pi$ where λ = the wavelength of the electromagnetic wave, the wave impedance depends on the source.

2. In the far-field area, when distances are further away than $\lambda/2\pi$, electromagnetic waves will change to become *plane waves*.

The impedance of vacuum is equal to $Z_0 = \sqrt{\frac{\mu_0}{\varepsilon_0}} \simeq 120\pi\Omega$. The speed of light is defined through vacuum to $C_0 = \frac{1}{\sqrt{\mu_0\varepsilon_0}} = 299792458\ m/s$. The wave impedance can thus be rewritten as $Z_0 = \mu_0 C_0$. In other words, the wave impedance only depends on μ_0.

On 20 May 2019, the SI unit system was redefined which changed μ_0 from a defined value to a measured value. Before this happened, μ_0 was defined to the value $4\pi \times 10^{-7}\ H/m$. With the change, the magnetic permeability in a vacuum and the electrical permittivity in vacuum were redefined to experimentally determined values based on the Sommerfeld constant(α):

$$\mu_0 = \frac{4\pi\alpha\hbar}{e^2 c} \tag{2.43a}$$

$$\varepsilon_0 = \frac{1}{\mu_0 c^2} \tag{2.43b}$$

[3]Försvarets materielverk, Sweden.

$$Z_0 = \frac{E}{H} = \sqrt{\frac{\mu_0}{\varepsilon_0}} = 376.730313668(57)\Omega \tag{2.43c}$$

[13], [14].

The power/effect that radiates is connected to the "Poynting vector"($\nabla\mathbf{S}$, shown in equation 2.44) and describes energy flow in a vacuum.

$$\nabla S = -\frac{\partial}{\partial t}(\frac{1}{2}\varepsilon E^2 + \frac{1}{2}\mu H^2) \tag{2.44}$$

Kraus and Carver shows that the Poynting vector is defined to be directly connected to the electric- and magnetic field; $\vec{S} = \vec{E} \times \vec{H}$ [14]. In the far field, $\vec{S}$ is a continuous current moving in the direction away from the source. Metal objects will change the incoming waves as shown in figure 2.3.

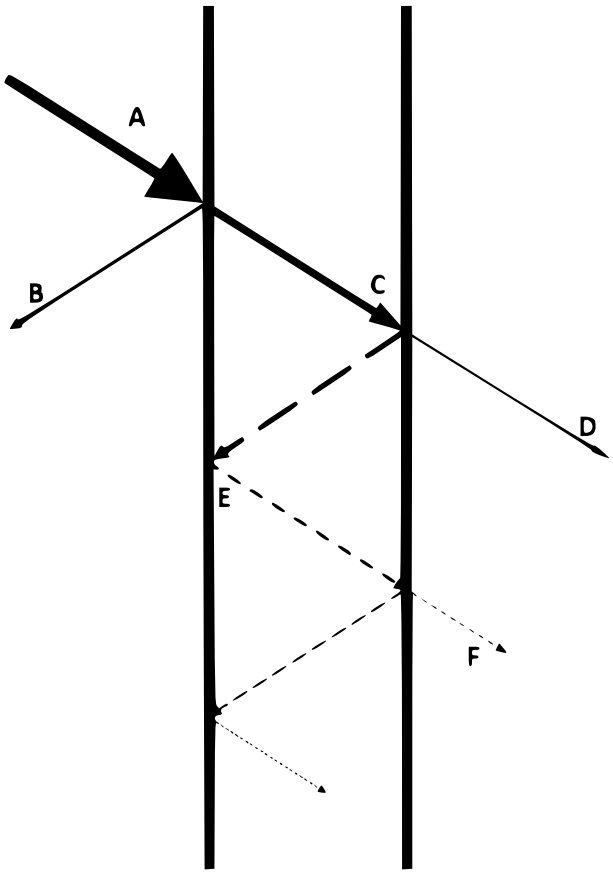

Figure 2.3: Incoming electromagnetic wave being dampened while passing through a metal wall. A: Incident wave, B: Reflected wave, C: Absorbed wave, D: Transferred wave, E: Secondary/tertiary reflected wave, F: Transferred wave.
Photo: Daniel Asle Vingen Endal.

Uniform shielding theory applies to the transmission through the screen material. Generally speaking, the shielding effectiveness (SE) [dB] in a line with free space on both sides will have:

1. Absorption loss inside the barrier
2. Total reflection loss from both surfaces (of the barrier)
3. n-th reflection loss inside the barrier can often look away from n-th reflection as these are absorbed by high absorption figures.

Perfect reflection of a wave will lead to standing waves. The electric field will have a node at the first interface while the magnetic field will have an antinode at the surface of the metal.

The theory mentioned here does not take three-dimensional closed spaces into account and works for plane waves. A few things should be taken into account when designing the shield structure:

1. The screen space is a closed three-dimensional space, not a free-standing wall. Three-dimensional size is important in regards to standing wave due to reflections.
2. The screen space will act as a complicated antenna.
3. Shielding and reflection are produced by currents that arise in the shielding structure and circulate throughout the metal structure.

Screening mechanisms

Shielding mechanisms are often based on the interaction between the magnetic and electric fields. The test room is a large metallic structure exposed to incoming waves. For the sake of simplicity, we can make a couple of simplifications and assumptions to improve understanding.

1. Electric and magnetic fields are considered separately despite being closely connected.
2. The geometry of the room is considered a sphere instead of a rectangular room, but the new spherical shape will have the same volume as the original shape.
    - For the electric field, the sphere will act as a "root antenna" where current is conducted from top to bottom. The current is a displacement current due to capacitive coupling to the electric field.
    - For the magnetic field, the sphere will act as a "loop antenna" where currents are induced by the inductive coupling to the magnetic field and form a closed current loop around the sphere.

The shielded space protects against incoming electromagnetic interference through mag-

netic shielding, electrical shielding and using eddy current shielding.

⇒ Eddy Current-Shielding: Acts against the magnetic field, induced currents are formed in the shield structure and repel magnetic field lines. The metal plates must have a high conductivity (σ) at low frequencies. SE is poor at low frequencies, with no damping at $\omega = 0$, but SE is excellent at high frequencies.

⇒ Electric shielding: Works against the electric field that meets the shielding structure normally. The metal plates must have low conductivity (σ) at low frequencies. SE is excellent at both high and low frequencies.

⇒ Magnetic shielding: Works against the magnetic field in that field lines are absorbed by the shield structure, which makes it important to have high relative permeability ($\mu_r >> 1$). The magnetic field lines that are absorbed by the metal plates in the screen avoid the central volume in the middle of the room. The central volume is thus shielded. SE is good at low frequencies if the walls of the structure are thick enough. Problems arise for SE at higher frequencies as a result of eddy currents gaining a significant size and reducing the relative permeability towards unity ($lim_{\mu_r \to 1}$).

The most important points we can take from the shielding mechanisms mentioned above are to ensure good performance in the presence of eddy currents. The performance under eddy currents is affected by the choices made for screen material, the configuration/performance of the screen and the thickness of the screen structure itself. (Deterioration of performance due to the presence of eddy currents is the reason why calculation methods for SE have a focus on eddy currents.)

Calculation methods

There are several methods for calculating the theoretical shielding efficiency (SE). We present the two methods *electromagnetic field method* and *the circuit method*.

The electromagnetic field method provides an exact solution based on Maxwell's equations with associated boundary conditions. The solution will show the exact behaviour of the screen structure for a large frequency range. **NB!** The electromagnetic field method is only reserved for simple geometric shapes, such as spheres and infinitely long/tall cylinders [1]. Further simplifications can also be implemented if the size of the screen space is much larger than the thickness of the screen structure. This is also the case in our lab, as the smallest dimension for the screen room is the ceiling height of around 3700 mm, which is some magnitudes larger than the screen thickness of $\tau = 2mm$.

2 cases depend on the wavelength of the electromagnetic field:

1. When λ is large compared to the room dimensions, the external field will be dom-

inated by a magnetic field with some presence of an electric field. Rectangular space is replaced by a sphere of equal volume and radius r_{sf}. SE for magnetic field is related to the absolute value of the magnetic field without the shielding (H_e) and the absolute value of the magnetic field with the shielding (H_i) $\rightarrow \frac{H_e}{H_i} \Rightarrow SE_{H//mag} = 20 \log \frac{H_e}{H_i}$.

2. When λ is small compared to the room dimensions, the waves will lead to resonance and standing waves in the screen space.

For inductive currents, the current density along the equator of a sphere of radius r_{sf} and thickness τ is equal to the expression

$$J_{ind} = \frac{3H_e}{2\tau} \tag{2.45}$$

For capacitive currents, the current density along the equator on the same sphere is equal to the expression

$$J_{kap} = \frac{3\omega\varepsilon_0 r_{sf} E_e}{2\tau} \tag{2.46}$$

For plane waves in the far field, the ratio between the current densities will be

$$\frac{J_{kap}}{J_{ind}} = \omega r_{sf}\sqrt{\varepsilon_0\mu_0} = 2\pi\frac{r_{sf}}{\lambda} \tag{2.47}$$

ε_0 is here the electrical permittivity in free space (vacuum) calculated to a value equal to $\varepsilon_0 = 8.8542 \times 10^{-12}\ F/m$ and μ_0 is the magnetic permeability in free space (vacuum) calculated to a value equal to $\mu_0 \simeq 4\pi \times 10^{-7}$. H_e is the magnetic field strength outside the sphere $[A/m]$ and E_e is the electric field strength outside the sphere $[V/m]$. We can see from the expressions 2.46 and 2.45 that the capacitive current is smaller than the inductive current when the wavelength of the frequencies is greater than the dimensions of the screen space.

The circuit method gives a good and simple picture of the parameters involved in the screen mechanism. The results we get from the circuit method are close to the results from the field method up to/up to the frequency range where the skin depth becomes significant.
For high-frequency waves, the value of the calculated attenuation will be lower than the actual attenuation of the screen structure (as a result of the skin effect). The screen space behaves like a short-circuited coil shaped like a cylinder with radius r_c and thickness τ [2]:

$$\frac{H_e}{H_i} = \frac{R + j\omega L}{R} \quad , \quad R = 2\rho\pi\frac{r_c}{\tau} \quad , \quad L = \mu_0\pi(r_c)^2 \tag{2.48}$$

The values R and L are the equivalent resistance $[\Omega m]$ and equivalent inductance $[Hm]$ of the screen structure, and ρ is the specific resistance of the screen material.

SE for a cylinder is given by the expression

$$SE_{mag(cyl)} = 10\log(1 + (\frac{\mu_0\omega r_c\tau}{2\rho})^2) \tag{2.49}$$

If we replace the radius of the cylinder in equation 2.49 with $r_c = 2r_{sf}/3$, we can use the same formula for SE shielding to a sphere expressed by [2]

$$SE_{mag(sf)} = 10\log(1 + (\frac{\mu_0\omega r_{sf}\tau}{3\rho})^2) \tag{2.50}$$

Electromagnetic shielding of laboratory

It is natural that (SE) the shielding of the screen structure varies depending on which frequency [Hz] is to be attenuated. If you plot the relationship between damping and frequency, we will get a figure that shows us a majority of regions as outlined in figure 2.4 [1].

R_1: $(0 < f < f_1)$ Covers the area of the graph where the attenuation is below 3 dB (SE $<$ 3 dB). The reason for the poor damping is the presence of eddy currents in the screen structure. Both the field method and the circuit method give approximately the same results in this area. SE is often low up to frequencies below 10 Hz.

R_2: $(f_1 < f < f_2)$ In this range, large rooms will have good damping even with thin screen plates on the surfaces. This is because the magnetic SE depends on the product of the room dimensions and the thickness of the screen (SE depends on $r_{sf} \cdot \tau$). At f_2, the skin depth will be equal to the thickness of the material.

$$f_2 = \frac{\rho}{\pi(\mu_r \cdot \mu_0)\tau^2} \tag{2.51}$$

For steel, this region will be relatively narrow as steel has a high relative magnetic permeability. Likewise, this region will be relatively wide for copper and aluminium due to their respective low values of relative magnetic permeability. The ratio between f_2 and f_1 is equal

$$\frac{f_2}{f_1} = \frac{2r_{sf}}{3\mu_r\tau}$$

R_3: $(f_2 < f < f_3)$ The real value of the shielding in this region will be higher than the one plotted in this graph. This is due to the skin effect. The field method will here provide a correct solution. The current flowing in the screen will flow on the outside of the screen structure, which disconnects the fields inside the screen structure from the fields on the outside.

R_4: $(f_3 < f < f_4)$ Imperfections and unevenness in the surface of the screen structure will lead to limitations in the total attenuation of the screen structure above the frequency f_3. The effect of these irregularities in the screen structure is difficult to predict based on calculations, nor is it adjusted for based on previously measured experiments. A fictitious assumed maximum attenuation of 120 dB is set, reflected in figure 2.4 by the shaded area.

R_5: $(f_4 < f)$ High frequencies cause plane waves and can lead to standing waves and cavity resonance in the screen space. The resonance frequency is dependent on the screen space's dimensions in addition to the presence of large objects in the screen space. Large metallic objects can lead to concentrations of electric fields and create unwanted capacitances (stray capacitances) in addition to the concentration of magnetic fields around conductors.

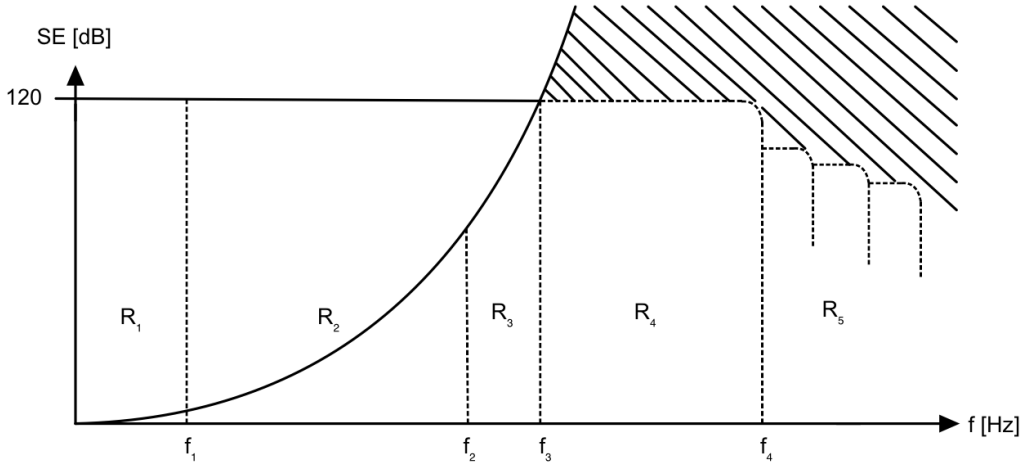

Figure 2.4: Sketched graph showing theoretical damping calculated using the circuit method. Photo: Agathe Bjelland Eriksen [15].

In order to shield the high-voltage test room, there are usually two methods that are considered based on current construction methods for the structure [1].

1. For concrete structures under construction, it can be recommended to include wire mesh that is immersed in the concrete. Joints and knots on the netting are welded together before immersion.

2. For other buildings under construction as well as buildings already built, it is recommended to use overlapping metal sheets. To achieve satisfactory damping, it is important to ensure good electrical contact between the plates. This can be done by e.g.:

   (a) Screen panel is screwed or clamped together. If corrosion occurs in the joints, this can cause an increase in contact resistance and lower the performance of the screen structure.

   (b) Cover joints between screen panels with conductive tape. Tape with low enough resistance to carry this out is hard to come by.

   (c) Joints can be covered or filled with conductive gaskets or conductive glue. This will be an expensive solution.

   (d) The panels can be welded together.

The ceiling in the test room can be shielded in the same way as the walls are shielded. In the floor, metal sheets or a mesh can be used which is submerged during the construction of the building. If desired, screen plates in the test room can be perforated. This will provide sound attenuation in the room but will come at the expense of SE and give a somewhat poorer performance for higher frequencies.

Power cables act as sources of noise and it is recommended to have as few conductive cables as possible exposed inside the screen structure by instead laying cables in the wall on the outside of the screen structure.

The window should be shielded all around with netting or with vertical wires embedded in the glass. Vertical wires are less disturbing to human vision than horizontal wires are. The netting/wires in the window must be electrically connected to the screen structure. Material options for the screen structure are copper, aluminium and steel. The price for these can be decisive for the choice of material, and after a quick uncritical google search we can estimate that the raw materials will have respective prices per metric ton of 7937 USD for copper; 2,225 USD for aluminium; 700 USD for steel. We prefer to use steel in the shield structure as steel has a higher relative magnetic permeability which will provide better magnetic shielding.

Chapter 3

Methodology

3.1 Design

3.1.1 Requirements

Standardisation and mandatory requirements

The construction of the Faraday cage is subject to various regulations and laws that must be maintained, in addition to the descriptive section produced by COWI in [16]. The various regulations and laws that I will be referring to during this thesis consist of the following:

FEF-2006 - Even though the high-voltage laboratory is defined as a test facility [16, p. 43], it is chosen to still regulate it by FEF-2006 because the facility does not fall under any of the points mentioned in the list of § 1-2 of FEF-2006. Further, it is its own supply facility with a 10kVA transformer connected to 230 volts.

NEK400:2018 - The low-voltage part of the installation is subject to NEK400:2018 as it can be considered part of point c) "*properties for public use*" (by being part of a government-owned institution) as well as point o) "*low voltage supply facilities*" in the list of section 11.1 [17, p. 9]. NEK is an acronym for "Norsk Elektrotekniske Komite", which translates to the "Norwegian Electrotechnical Committee".

NEK440-2015 - According to a note included in [16], the high-voltage laboratory is not directly regulated by NEK440, but it has been concluded that the safety distances presented in NEK440-2015 are adequate for the facility, and the regulation has therefore been used to determine the high-voltage safety distances [16, p. 43]. The note on page 43 of document [16] further informs that the regulation refers to the norm "NEK EN 60071-2 Tillegg A", developed and change into "NEK EN 60071-1 Tillegg A. The norm

in question informs that it is permitted to use equipment when a facility is tested and there are no problems with flashover present with the distances used during the testing.

Strålevernforskriften - This Norwegian regulation informs that if no national guidelines and/or limit values exist for optical radiation or electromagnetic fields, then the latest update of the "Guideline on limited exposure to non-ionizing radiation" from ICNIRP is applicable and the norm for what is considered "good practice". As of November 2022, the previous update to these guidelines were done in May of 2020 [18] The guideline can be summarized in a broad stroke by the following table 3.1. The table refers to "table 5" from [18, p. 495] which contains reference levels for averaged exposure across a timespan of 30 minutes over the whole body, both for the general public and occupational scenarios. [19]

Table 3.1: Reference levels for exposure the general public [18].

Frequency range:	Action value for: [W/m^2]	
	Occupational	General public
10 - 400MHz	10	2
400 - 2000MHz	10 - 50	2 - 10
2 - 300GHz	50	10

DSA - DSA is the acronym of the Norwegian "Direktorat for Strålevern og Atomsikkerhet"[1]. It is "*the authority and competence body for nuclear safety, all uses of radiation, for natural radiation and for radioactive contamination in the environment*" [20]. DSA has conducted a study published in the report *Radiofrekvente felt i våre omgivelser - målinger i frekvensområdet 80MHz - 3GHz* which has a focus on the exposure from e.g. base stations, as well as other common sources of electromagnetic radiation in our surroundings. The report reflects the general worldwide consensus and limits values put forth by ICNIRP and utilises the limit values for the general public to scrutinize the measured values of the report [21, p. 12].

HVL imposed necessities

Minimum attenuation The Faraday cage/shielded room needs to have a minimum attenuation of at least 25 dB across all frequencies from 10kHz to 3GHz [22].

EMC A device is electromagnetic compatible when it is working satisfactorily and as intended without exposing other nearby devices, or the surrounding electromagnetic environment, to intolerable disturbances [3, p. 644].

[1]Directorate for Radiation Protection and Nuclear Safety

According to Norwegian regulations,

> The facility must be planned and executed and must be maintained so that it does not produce electrical and electromagnetic interference that exceeds a level where radio and telecommunications devices and other devices or facilities cannot function as intended.
>
> The plant and the equipment included in it must have sufficient internal immunity to external electromagnetic influence so that the plant can function safely and as intended [23].

Educational priority HVL had to choose how students would get a good return from using the high-voltage laboratory. This means that they had to choose how the students should observe trials, experiments and lab tasks. The two most relevant options turned out to be the installation of a window, an analogue solution, and the installation of a camera with video transmission to the outside of the test room. Discussion about what the two alternatives had as advantages and disadvantages became relevant. Windows would involve a weakening of the Faraday cage and are thought to make the protection against electromagnetic radiation less effective at lower frequencies. The camera would need to transfer data to the outside of the display room, in addition to the camera having to withstand the radiation it would be exposed to inside the display room. The cameras would need shielded boxes mounted to the inside of the test room with an optical converter for data transmission to the outside so that the information stream would not be degraded by EMI. Power supply to the cameras would also be a necessity, requiring a separate power supply with a filter to supplement safe power for the equipment. In the end, HVL went with the choice of windows.

Minimum distance from testing volume to surface of Faraday cage Requirements from HVL that there must be a minimum 1100mm air gap from the test area to conductive surfaces in the screen room [16, p. 43]. This is based on testing carried out in the high-voltage laboratory. Since the system has been tested with a safety distance of 1100 mm without problems with flashover, it is therefore approved for use with a safety distance of 1100 mm per norm NEK EN 60071-1 Appendix A and NEK440:2015 [24].

3.1.2 Grounding

Earthing is a defined reference point that is further considered zero point for an electrical system. The term grounding includes earth conductors in the plant, the connected earth electrode, and the soil that encloses the electrode.

Features expected by grounding systems for use in high voltage involve, among other things:

1. The grounding system should act as a return road for current floating on the earth side when tests are performed for surge and preventing measurement errors from the presence of parasitic streams.

2. The grounding system should act as protection for the electrical equipment by quickly spreading over electrical surges through a conductive low impedance orbit. This will ensure effective discharge for large currents to soil and safeguard that electrical potential is limited to values within given design guidelines.

3. The grounding system should be a safety for personnel working in the laboratory by reducing the electrical potential of values that are tolerable to humans.

[1, p. 69][25, p. 41][24, p. 22].

Security requirements impose restrictions on step voltage and touch voltage [25, p. 18].
Step voltage is the difference in electric potential between two points on the Earth's surface with a distance 1 meter apart that is imposed on a person walking on the surface [24, p. 14].
Touch voltage is the voltage between leading parts when touched at the same time as a person [24, p. 13].

It is the grounding system in collaboration with the steel screen plates that constitute the construction of the Faraday cage. In other words, the test room is regarded as a completely sheltered structure. Grounding electrodes are a necessity because:

1. The building can be hit by lightning (though this can happen for K1 at HVL Campus Kronstad, there are separate earth electrodes installed in the building for this purpose).

2. Short circuit to soil inside the test room near a source, such as a transformer, can cause the electrical potential of the entire building to increase without a proper connection to the soil. An increase in voltage in this way can leak into low-voltage systems or telecommunications networks if no proper filter is installed and the systems are not properly insulated.

The choice of an earthing electrode is made based on criteria dictated by NEK440:2015 [24] and the design/dimensioning of the earthing system must take into account: *The value of the fault current*, *the duration of the fault*, and *the characteristics of the soil*. Factors that have an impact on these parameters:

- For the value of fault current
  - Magnitude - Waveform - Frequency
- For the duration of failure
  - Method for earthing the neutral point - Design of the earthing system - Selection of protective relays
- For the properties of the soil
  - Composition - Temperature - Moisture content

It may seem that all the criteria mentioned above can be solved by making sure that a single factor is as low as possible; make the grounding resistance as low as possible. Tests with overvoltage in the high-voltage laboratory mean that the presence of rapidly changing transient currents $[i_T(t)]$ from the discharge of the overvoltage generator may occur. This can produce significant transient inductive voltage losses, given by $[v_L(t)]$

$$v_L(t) = L_{gr}\frac{di_T(t)}{dt} \tag{3.1}$$

The resistance to ground is the resistance between the ground electrode and an imaginary reference electrode located at ∞. As the current spreads outwards, the cross-section will increase and the resistance will decrease; 90% of the earth resistance is present within 3 meters of the earth electrode. Resistance in a homogeneous material is proportional to the product of the resistivity of the material and the length of the material, and inversely proportional to the cross section of the material [4, p. 823].

The implemented earthing system is subject to Norwegian norms and regulations, i.a. FEF 2006 and NEK440:2015. This is because there are no separate regulations for high-voltage laboratories. The facility is from an official perspective not to be considered a supply facility but it is decided by HVL that it should be subject to the current regulations for this. The grounding system inside the test room/screen room consists of a $95mm^2$ ground rail in solid copper mounted on insulators around the entire room and has a distance of 150mm from the floor surface in the test room up to the bottom edge of the ground rail. The ground rail is connected to both single entry (SE) frames SE1 and SE2. The metal surfaces that make up the walls in the test room are grounded via single entry frame 1. The path to earth leaves the test room through SE-frame 1.

Inside the test room, there is permanent equipment which must also be earthed. Of the permanent installation, the following equipment is covered by grids to protect against overvoltages; and the grids that cover the *extinguishing gas pipe, ozone sensor & microphone, fire alarm, socket* are therefore connected to the earth.

Of other permanent equipment that is not covered by high-voltage grids, we have *LED*

lighting fixture, SE-frame 2, metal plate for test area (floor), metal plate (suspended, ceiling). The metal plate on the floor and the metal plate on the ceiling are both connected to the ground rail with a separate $95mm^2$ copper connector. The remaining equipment belonging to the test room is *high-voltage test equipment* and *220V/100kV AC transformer.*

The high-voltage grounding system continues outside the test room and is connected to the grounding system on the inside via single entry frame 1 under the windows. Equipment in the high-voltage laboratory is *ozone central*, *control desk for old system*, *control desk for new system*, *combinator*, *connection box (relay and PLC, lighting fixtures)* and *the cable shielding* on the *power supply to the light fixture in the test room*, *the connection to the isolation transformer*, *the cable from the junction box to the light fixture* connected to the high-voltage grounding system. As previously mentioned above, the high-voltage ground is connected to the ground bolt on SE-frame 1 and runs from the ground bolt through the floor to the floor below. On the floor below, high-voltage earth is led through a cable shaft down to the basement. In the basement, the earth conductor is connected to a crow's feet earth electrodes in the ground beneath the building. In the basement switchboard room, high-voltage earth is connected to the main earth busbar in the main distribution cabinet via an equalization cable [26].

Floating ground is used to separate and electrically isolate circuits and equipment from a common ground. This can cause danger due to the possible build-up of potential.

Conductivity in soils

An ideal ground plane is basically presented as a zero-potential, zero-impedance body, and is used as a reference for all signals in associated circuits and to receive unwanted currents to eliminate the effect [3, p. 647].

For low frequencies, the earth resistance will be a purely resistive load. At higher frequencies, the impedance term will have an increasing effect on the earth resistance. The skin effect may be partly to blame for this, as less of the cross-section of the electrode is used in the transmission to the soil. Soil resistivity can vary down to a depth of a few meters as a result of changes in humidity. It is also important to take into account that soil resistivity can vary greatly with depth, as soil usually appears in clearly divided different layers [24, p.56, part 2].

Earth electrodes must be separated by a distance at least equal to the length of the earth spear [24, p.60, part 2], to prevent overlap of interfaces to earth.

Preventing overlap is important as ensuring good electrical contact with the earth involves a connection between a conductor and a semiconductor and thus not a point-to-point connection, but a conductor-to-surface connection. This type of connection requires the ground electrode to be surrounded by a significant volume of soil to complete the connection [27, pp. 4–5]. A detailed overview of resistance for various soil types is given in table 3.2 of NEK440:2015.

Table 3.2: Earth resistances for alternating current. Source: NEK440:2015.

Soil type	**Soil resistivity** ρ_E [Ωm]
Marshy soil	5 to 40
Sand-mixed clay soil, clay, topsoil	20 to 200
Sand	200 to 2500
Gravel	2000 to 3000
Soft rock	usually under 1000
Sandstone	2000 to 3000
Granite	up to 50000
Moraine	up to 30000

The composition of the soil can provide an indicator of what values can be expected for the earthing resistance. Furthermore, ground electrodes should be laid at a frost-free depth to ensure that low temperatures and cold degrees do not reduce the functionality of the ground [24, p.34, part 2]. Given that moisture remains constant, increasing soil temperature will ensure a lower soil resistance. Furthermore, increasing humidity will also lead to a lower resistance in the soil [27, p. 3].

It is beneficial to know the specific resistance ρ_E (in Ωm) to earth when designing an earthing system. The value for specific resistance to soil can be obtained from tables, for example table 3.2, but ideally the value should be acquired using on-site tests, for example using the Wenner method. Due to the existing grounding system for building K1, this is not necessary.

Four point method - *Wenner-method* four temporary electrodes are driven into the soil along a straight line, separated by a distance a and to a depth b. A device, a so-called *megger*, reads the value of the earth resistance R_m in ohms which is used in the equation 3.2. The value ρ gives the average specific resistance of a layer of soil at depth b.

$$\rho = \frac{4\pi a R_m}{1 + \frac{2a}{\sqrt{a^2+4b^2}} - \frac{2a}{\sqrt{4a^2+4b^2}}} \tag{3.2}$$

Materials and corrosion in grounding electrodes

Current materials to fabricate grounding electrodes from should have desired properties such as:

- Mechanical strength
- Long duration/durability
- High conductivity
- High ability to resist corrosion

Steel, iron, copper and aluminium are all possible candidates for making earth electrodes from, but steel and aluminium have a low potential compared to copper, and will therefore corrode more easily. Steel and aluminium in contact with moisture and/or oxygen form "rust". Steel rust expands and falls off, which exposes new steel material and allows the process to start over again and again. Rust on aluminium is called aluminium oxide, and forms a hard layer around the aluminium and acts as protection. When a layer of aluminium oxide has formed on the entire surface of the aluminium, the process will stop[28]. Aluminium, on the other hand, is not as mechanically strong as copper or steel and is therefore not as relevant a choice. Copper, on the other hand, is resistant to corrosion, has high conductivity, and high durability and is stronger than aluminium. The choice is therefore copper as a material for the grounding electrodes.

Table 3.3: Conductivities of different metals @ 20°C

Material	σ [S/m]
Iron	10^7
Lead	4.55×10^6
Tin	9.17×10^6
Brass	1.1×10^7
Aluminium	3.5×10^7
Copper	5.88×10^7

Corrosion is the result of an electrochemical reaction that takes place between metals and their surroundings [29]. From Bardal it is informed that the corrosion process for wet corrosion (electrochemical corrosion) consists of an anodic and a cathodic reaction. During the anode reaction, the metal is dissolved and transferred to the corrosion

medium/electrolyte. In the case of a cathode reaction, a reduction of oxygen can be made, for example, that hydrogen formed by means of electrolysis [29, p. 7]. One metal in contact with two different electrolytes can also lead to corrosion. Two metals surrounded by electrolytes will create a potential that sets up a current from cathode to anode. The current causes corrosion of the anode and forces ions away from the anode and into the electrolyte. The potential difference between cathode and anode is a contributing factor to the rate of corrosion. A large difference in potential between the metals accelerates the corrosion rate, while a lower difference in potential between the metals will lower the corrosion rate. The difference in potential is a function of the metals' relative position in relation to each other's electrode potential.

Table 3.4: Standard electrode potential @ 25°C [29, p. 24]

Material:	Potential [V_{ep}]
Magnesium	-2.37
Aluminium	-1.66
Zinc	-0.76
Iron	-0.44
Lead	-0.13
Copper(divalent, Cu^{2+})	+0.34
Copper(monovalent, Cu^{+})	+0.52

(Note for table 3.4 [2])

Metals (e.g. Iron and aluminium) with negative electrode potential are chemically active metals and react with conductive surroundings by corroding. Metals with positive electrode potential (e.g. copper) are considered noble metals and are inert. If noble metals are combined with metal that is chemically active, it will create a significant difference in potential and turn the chemically active metal into an anode that will undergo frequent corrosion. A copper earthing system will expose iron pipes, in addition to other metallic structures, to corrosion.

The rate of corrosion depends on the type of soil and the type of underground structure present.

Corroding soils are generally acidic and contain a significant amount of moisture, clay and organic matter.

Soils with high resistivity reduce corrosion current and corrosion rate, but also increase the grounding resistance of the entire system. We can see this in table 3.5 from [30].

One possibility is to isolate each of the different metallic structures. This will provide

[2] monovalent copper lacks reliable source, figures found in the master thesis "Design of high-voltage lab in Ohio, 1987".

Table 3.5: The soil's degree of corrosive nature by soil resistivity [30, p. 2].

Soil resistivity [Ωm]	Classification
0 - 10	Extremely corrosive
10 - 30	Very corrosive
30 - 50	Corrosive
50 - 100	Moderately corrosive
100 - 200	Mildly corrosive
Over 200	Non-corrosive

better protection against corrosion, but it will also lead to an increased risk of static shock as a result of the build-up of static charge. One possible way to do this is to treat the metallic structures with a protective layer, for example, varnish.

Ground measurement report

Measurement of the transition resistance to high-voltage earth has been carried out by LOS Elektro AS using the "3-point method" on the instrument Fluke 1623 / ground tester geo. The result for the transition resistance is measured to be 0.12Ω [31].

3.1.3 Calculated shielding effectiveness

To make calculations on Shielding Effectiveness, we need to know the volume of the screen space.

Based on measurements from floor plans and measurements taken with a laser meter in the room, we know the dimensions for the floor and calculate that the floor surface has a total area of ≈ 33 m^2.

$$\begin{aligned}
\text{Floor area } &= 5.75m \times 6.25m - A_{nor} - A_{sou} \\
A_{nor} &= 3.4m \times (5.75m - 5.22m) \\
&= 3.4m \times 0.53m = 1.802\text{m}^2 \\
A_{sou} &= 1.685m \times 0.725m - diagonal \\
diagonal &= \frac{393^2}{10^3} \cdot \frac{1}{2} = 0.0772245\text{m}^2 \\
A_{sou} &= 1.685m \times 0.725m - 0.0772245\text{m}^2 \\
A_{sou} &= 1.1444005\text{m}^2 \\
\text{Floor area } &= 35.9375\text{m}^2 - 1.802\text{m}^2 - 1.1444005\text{m}^2 \\
&= 32.9910995\text{m}^2
\end{aligned}$$

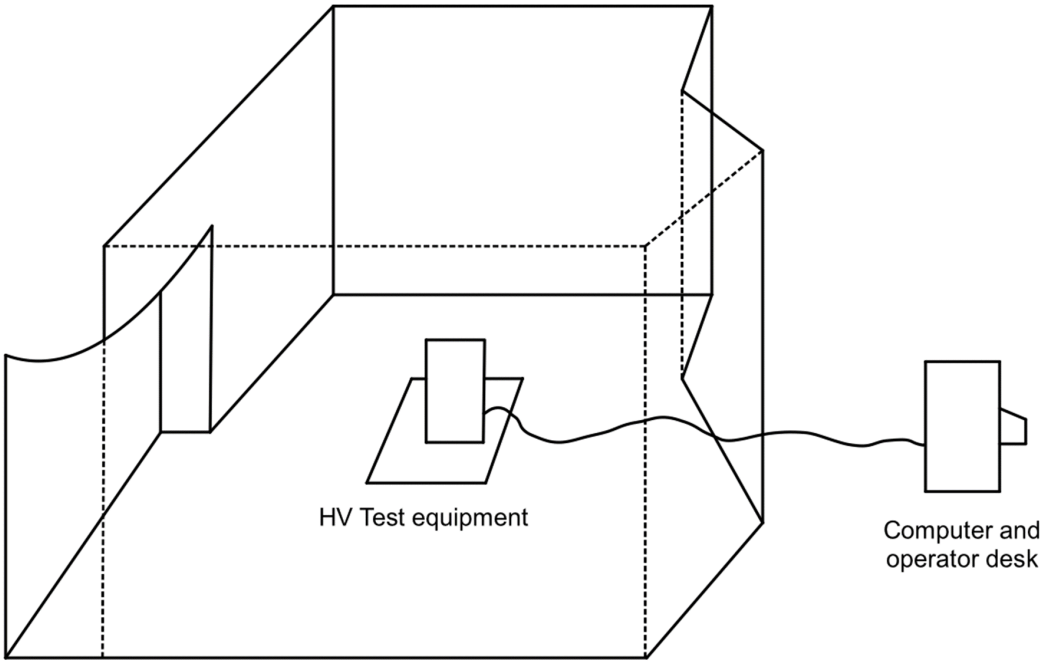

Figure 3.1: Sketch showing the general shape and layout of the high-voltage test laboratory and connection between control desk and HV test equipment. Photo: Agathe Bjelland Eriksen [32].

The area consists of a niche that narrows the area in the horizontal plane at a height of 310cm, above this height, the area is [3] given by

$$\begin{aligned} \text{Floor area}_{ON} &= 32.9910995\text{m}^2 - A_{niche} \\ A_{niche} &= 2.85\text{m} \times 0.53\text{m} = 1.5105\text{m}^2 \\ \implies \text{Floor area}_{ON} &= 32.9910995\text{m}^2 - 1.5105\text{m}^2 \\ \text{Floor area}_{ON} &= 31.4805995\text{m}^2 \end{aligned}$$

The height of the niche is measured to be 310.660377cm. The volume of the entire test room is given by the volume with the niche (V_{fa}) and the volume above the niche (V_{niche}), where the height from the niche up to the ceiling in the screen room is equal to 59.3396226cm:

[3] Floor area$_{ON}$ is the area of the horizontal plane above the height at which the niche terminates.

$$
\begin{aligned}
V_{fa} &= 32.99...\text{m}^2 \times 3.106...\text{m} \\
&= 102.4902741\text{m}^3 \\
V_{niche} &= 31.4805995\text{m}^2 \times 0.593396226\text{m} \\
&= 18.6804689\text{m}^3 \\
V_{tot} &= V_{fa} + V_{niche} \\
V_{tot} &= 102.4902741\text{m}^3 + 18.6804689\text{m}^3 \\
&= 121.170743\text{m}^3
\end{aligned}
$$

Converts the volume from a complex rectangular volume to a smooth sphere.

$$
\begin{aligned}
V_{sphere} = \frac{4}{3}\pi r^3 \rightarrow r_{sphere} &= \sqrt[3]{V_{tot} \cdot \frac{3}{4\pi}} \\
r_{sphere} &= \sqrt[3]{121.170743\text{m}^3 \cdot \frac{3}{4\pi}} \\
r_{sphere} &= 3.069750324\text{m}
\end{aligned}
$$

We use the established theory from 2.2 with the associated equations.

$$
\text{Equation (2.50) gives } SE_{sf} = 10\log\left(1 + \left(\frac{\mu_0 \omega r_{sphere} \tau}{3\rho}\right)^2\right) \tag{3.5}
$$

We have calculated that the radius of a volume-equivalent sphere is equal to $r_{sphere} = 3.069750324\text{m}$. Furthermore, we exemplify with the same frequencies on which the measurements have been made in table 5.2.

The value for magnetic permeability in free space/vacuum is approximate $\mu_0 = 4\pi \times 10^{-7}$ [13]. We can allow ourselves to use the old definition since the resulting uncertainty is of an acceptable level. $\omega = 2\pi f$, f = frequency, $\tau = 2\text{mm}$ = the thickness of the screen, $\rho =$ the specific resistance of the screen material. We take the steel "ASTM A525 Galvanized Steel" as our starting point with a specific resistance equal to $\rho = 0.000000170\Omega m = 1.7 \times 10^{-7}\Omega m$. The reason why we start with this steel is that it is a commercially available galvanized steel imported from Sweden and satisfies the European standard *NS-EN 10346:2015* for *"continuously hot-dip coated steel flat products for cold forming - technical delivery conditions"*. It is therefore considered acceptable to use data from [33] for commercial quality zinc-coated (galvanized) steel (ASTM A525 Galvanized Steel).

NB! *This candidate has not succeeded in acquiring the specific or relative magnetic permeability of the galvanized steel used in the screen solution, nor data for the electrical permittivity. Measuring these values for the material has also not been an option (due to*

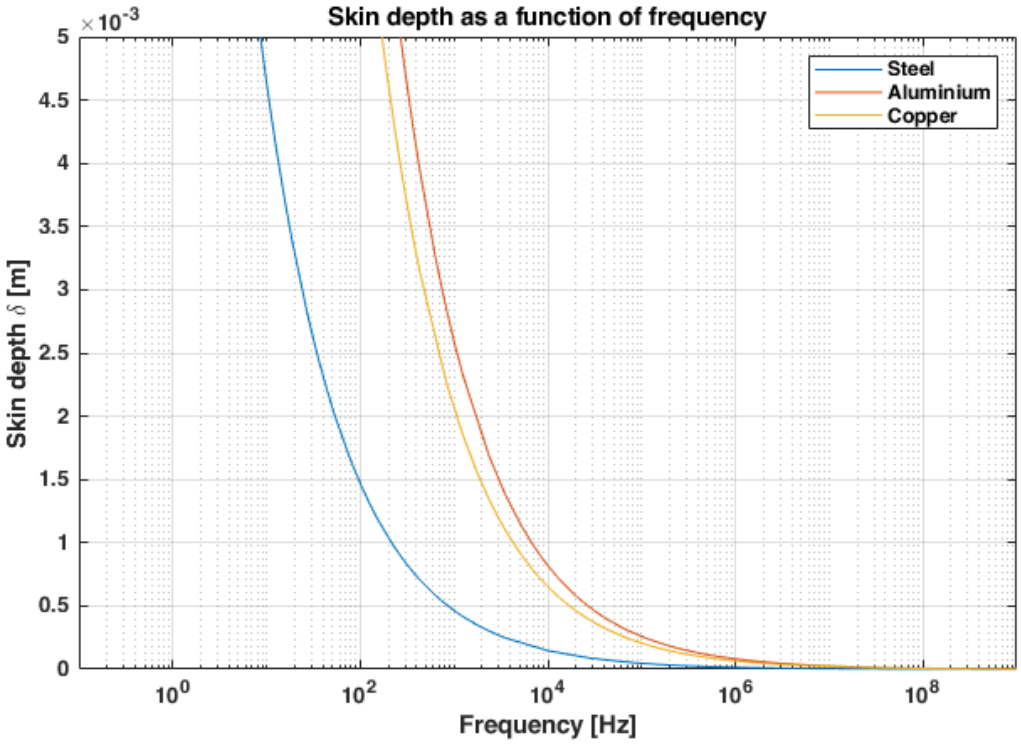

Figure 3.2: Shows the skin depth of the materials *steel*, *aluminium* and *copper* as a function of frequency. Photo: Daniel Asle Vingen Endal.

time). It has therefore been chosen to use the respective values for general steel; $\mu_r = 200$ *[1], where this is applicable.*

"The **skin depth** is a measure of the depth to which an **EM** wave can penetrate the medium [3, p. 426]." The skin depth is given by equation 3.6.

$$\begin{aligned} \delta &= \sqrt{\frac{\rho}{\pi f \mu_0 \mu_r}} \\ &= \sqrt{\frac{1.7e(-7)}{\pi \cdot f \cdot \pi 4e(-7) \cdot 200}} \\ &= \sqrt{\frac{\rho}{\pi \mu_0 \mu_r}} \cdot \frac{1}{\sqrt{f}} \\ \delta &= \frac{0.01467336073}{\sqrt{f}} [\text{m}] \end{aligned} \tag{3.6}$$

f_1 is given by where the attenuation is 3 dB; find frequency by solving equation (2.50) for SE = 3 dB

$$\begin{aligned} 3dB =& 10 \log(1 + (\frac{\pi 4e(-7) \cdot 2\pi \cdot f \cdot 3.069... \cdot 2e(-3)}{3 \cdot 1.7e(-7)})^2) \\ \implies & f \simeq 10.5Hz \end{aligned} \tag{3.7}$$

The frequency f_2 is given where the skin depth is equal to the thickness of the screen panels and is calculated using (2.51).

$$f_2 = \frac{\rho}{\pi \cdot \mu_0 \cdot \mu_r \tau^2}, \quad \rho = 1.7e(-7), \mu_0 = 4\pi e(-7), \mu_r = 200, \tau = 2e(-3) \tag{3.8}$$

$$f_2 = 53.8268788Hz \tag{3.9}$$

f_3 is given by where $SE = 120dB$; equation (2.50) gives $f_3 = 1.06e7Hz$, that is 10.6MHz.

f_4 depends on the design of the room and arises as a result of resonant frequencies and standing waves. It is therefore difficult to predict which frequency this will have.

3.2 Student safety

This safety part of the thesis consists of sections 3.2 through 3.2.5. I utilize and build upon the work of Askvik, Svensson, Hantveit, *et al.*(2016 [34]) and present it to the reader since this is the basis that future iterations of safety procedures will evolve from when necessary.
Previous versions of the high-voltage laboratory at HVL developed such a high potential that sustained electric arcs with a length of 5 mm were generated from the window frame to a measuring probe during the mapping and evaluation of electrical fields for the laboratory [34, fig.7]. This was remedied by giving each of the window frames a separate connection to the earth to equalize the electrical potential.
The bachelor group of Askvik, Svensson, Hantveit, *et al.* was tasked with mapping the functionality of the then-present high voltage laboratory in 2016. During work on their bachelor thesis, they designed a safety procedure to be used in the high-voltage laboratory, and the procedure will continue to be used further in future iterations of the high-voltage laboratory.

3.2.1 Definitions

Since the high voltage laboratory is to be considered a station facility when tests are being performed, the definitions here are collected from standards and norms of "NEK" - Norwegian Electrotechnical Committee, such as NEK400:2014, NEK440:2015 and/or NEK445:2009.

High voltage Electrical facility for nominal voltage higher than 1000 V AC, or higher than 1500 V DC [17, p.27].

Low voltage Electrical installation for nominal voltage up to and including 1000 V AC or up to and including 1500 V DC [17, p.32].

Dangerous area The area around live parts is delimited by the minimum distance (DL) and which is not fully protected against direct contact [24, p. 17].

Reference earth Part of the Earth that is considered conductive, whose electrical potential per definition is considered equal to zero, and which is outside the influence area of all grounding systems [17, p.28].

Earth electrode Conductive part in electrical contact with the Earth, and which may be buried in soil or enclosed by a specific conductive medium, for example, concrete or coke [17, p.28].

Grounding conductor A conductor that forms a conductive current path, or part of a conductive current path, between a given point in a system, installation or equipment and an earth electrode or an earth electrode system. [17, p.29]

Equipotential bonding Arrangement of electrical connections between conductive parts to achieve an equipotential [17, p.44].

Potential The voltage between a given point and reference earth [24, p. 20].

Exposed conducting part Conductive part of electrical equipment that can be touched, and which is not normally live, but which can become live when the basic insulation fails [17, p.44].

Other conducting part A conductive part which forms no part of the electrical installation and which can attain a potential, usually the electrical potential of a local earth [17, p.17].

Corona The ionization of air caused by a high enough potential V_m such that the air becomes a conductor, resulting in a current visible in a dark room is called *corona discharge*. Corona discharge is characterized by its blue glow. The maximum potential V_m is dependent on the dielectric strength of air (E_m) and the radius of curvature for a conducting object exposed to an electric field. The larger the curvature radius of the object is, the higher potential it can withstand before causing the surrounding air to ionize and become conducting.[4, p. 766]

Emergency shutdown Switching off a switch to remove an electrical supply to an electrical installation in order to prevent or reduce the consequences of a dangerous situation [17, p.35].

Emergency stop Function intended to stop a movement that has become dangerous as soon as possible [17, p.34].

Operations manager The person tasked with coordinating all planned operations of the high-voltage laboratory, including checking that all decisions regarding training and testing of the high-voltage laboratory are carried out in accordance with current safety routines and requirements in regulations and standards [34, p. 13].

Lab engineer Person responsible for all work that takes place in the laboratory [34, p. 13].

Safety manager Leads the experiment and is responsible for the current HSE regulations for the high-voltage laboratory being followed. The safety manager is responsible for the key to the door to the high-voltage laboratory [34, p. 13].

Lab operator Controls either the operator desk or the computer and is responsible for the operator key [34, p. 13].

Connection manager The first to enter the laboratory when the voltage is switched off. The connection manager must check that all exposed conductive parts are equalized with earth [34, p. 13].

High-voltage laboratory The *high-voltage laboratory* refers to the entire electric power laboratory, D418. This includes the test room, both control desks, cables, the isolation transformer and the area around the test room. The high-voltage laboratory is to be considered a station facility when tests are in progress and is therefore subject to NEK440 – Stasjonsanlegg over 1 kV (Station facilities above 1kV) [34, p. 13].

Test room The test room, D416, is the actual room where the high-voltage equipment is located and the experiments are carried out. The entire test room is to be considered a "dangerous area" [34, p. 14].

Ozone gas Ozon is a toxic gas formed by spilt oxygen atoms attaching to oxygen molecules in the air. The Norwegian Labor Inspection Authority has dictated a maximum value of 0.1 ppm, or 0.2 mg/m^3 [35].

Permissible touch voltage The permissible touch voltage is given by the graph in figure 4-2 of FEF 2006 [25, p. 43]. Touch voltage is regulated in order to limit the current passing through the body.

3.2.2 Safety routines

The lab engineer must always be present during the use of the high-voltage laboratory. If the lab engineer leaves the lab, all work must stop immediately. Work in the laboratory must take place in groups with a minimum of 3 people in each group, with the possibility of more participants. Each individual is assigned a unique role. Each group must have one security officer, one connection officer and one lab operator. It is the lab engineer who decides and assigns the roles. If the lab engineer wishes, the roles can be changed during the experiment, otherwise each person retains their role for the entire duration of the experiment. Each of the participants in a group must familiarize themselves with the safety measures of the laboratory. Responsibilities are then determined, assigned and fixed before the start of an experiment.

Safety manager Leads the experiment and is responsible for ensuring that the HSE regulations are followed by everyone involved in the experiment. Must be wearing a reflective vest. Responsible for the key to the doors to the test room in the high-voltage laboratory. Responsible for ensuring that protective masks with activated charcoal filters are used if the concentration of ozone gas in the air inside the test room is above the limit value set by the Norwegian Labor Inspectorate.

Lab operator Controls either the digital operator console or the analogue operator console. Responsible for the operator key that turns on the operator's desk.

Connection manager Must be the first person to enter the test room after the lab operator has switched off the voltage and handed over the operator key to the connection manager. The switch operator cannot enter the test room without the operator key.

3.2.3 Procedure: Securing a de-energized test room

The test room must be considered energized until it is confirmed de-energized. Before the group is allowed to start an experiment, the group, together with the lab engineer, must confirm that the ground rod is connected to the earth.

- The lab operator must ensure that the voltage supply to the test room is disconnected.

- The lab operator must lock the operator's desk and hand over the operator key to the connection manager.

- The safety manager must unlock the doors to the test room and open both doors in the security lock.

If the concentration of ozone gas inside the test room is above the limit value, the protective mask must be sufficiently fixed over the face and must be tight. When the safety manager has confirmed that protective masks are sufficiently attached, the safety manager can open the doors to the test room.

- The connection manager lifts the grounding rod out of the position where it is connected to the grounding sensor and checks that the grounding attachment at the end of the grounding rod is sufficiently secured.

- The connection manager uses the grounding rod to equalize all conductive parts in the system and ensures that the system is 100% voltage-free. The connection manager then connects the grounding rod to the output terminal of the transformer as visible grounding.

All exposed and conductive parts in the room must be equalised. It is particularly important that all capacitors are discharged. Equalization must first take place through the resistor mounted at the end of the grounding rod, then directly to earth at the innermost part of the grounding rod.

- The safety manager checks that the connection manager follows the procedure.

When the earth is visibly connected to the output terminal of the transformer, the test room is considered de-energized. The safety manager must stand by the door to the test room as long as the door to the test room is unlocked and/or a person is inside the test room. The lab operator must be at the operator's desk when people are inside the test room and the door is unlocked.

- The safety manager confirms that the test room has been de-energized.

With the exception of the connection manager, no one has access to the test room without the permission of the safety manager.

- When work has been carried out and the test room has been evacuated, the connection manager disconnects the earthing rod from visible earth and onto the earthing sensor.

- The safety manager confirms that the test room is evacuated and empty.

- The safety manager locks the test room.
- The connection manager shall be the last to leave the test room. The connection manager hands over the operator key to the lab operator. The safety manager can now initiate an experiment.

3.2.4 Procedure: Shutting the laboratory at the end of an experiment

When the experiment is over, the test room is to be secured and the facility is to be confirmed de-energized. Students must follow "Procedure: Securing a de-energized test room".

The grounding rod must be connected to the output terminal of the transformer. When the transformer is earthed, the connection manager can, after receiving approval from the safety manager, switch off the supply transformer.

- The safety manager confirms that the transformer has been switched off.
- The test room is locked and left with the earth rod on the output terminal of the high-voltage transformer.
- The lab engineer confirms that the procedure has been followed. The shutdown is approved by the lab engineer.

(NB!) Students cannot leave the premises of the high-voltage laboratory until the lab engineer has approved the shutdown.

3.2.5 Closing

In the event of observation or suspicion that routines for the use of the high-voltage laboratory are not being followed, the lab engineer and/or operations manager have the mandate to close the laboratory.

In the occurrence of a shutdown, all work must stop immediately. The test room is secured under the direction of the lab engineer or operations manager.

3.3 Description of HVL Faraday cage

The high voltage laboratory is located in the D-block on the 4th floor of the main building, K1, of Western Norway University of Applied Sciences (abb.: HVL). The laboratory consists of a room with the dimensions 6.25 meters in width, 5.75 meters in depth and

3.7 meters in height where every surface of the room is covered by 2-millimeter thick steel plates.

Surfaces All the steel plates in the enclosure are joined together by either soldering or spot welding.

Steel plates on the walls and the ceiling are mounted flush against each other and fastened to their respective surfaces with steel screws. With external steel profiles clamping down on the joints between each plate in order to increase the dampening and reinforce the seams, good mechanical- and electrical connection is ensured in a redundant manner. These steel profiles are commonly referred to as lasks[4]. A structural steel girder in the ceiling is protruding closer to the Faraday cage, necessitating extra measures in order to lead any arcing from the testing volume to the ceiling. A corrugated steel plate weighing several hundred kilos is therefore mounted to the ceiling above the test area as a backup to air-gap dampening. This corrugated steel plate is suspended from the building structure, yet electrically isolated from the concrete structure that is the building. An equivalent plate is placed on the floor of the shielded enclosure, which the testing equipment is placed on top of. Both of these plates are connected to the high-voltage ground. Further, the bolts are electrically and mechanically connected to the surrounding Faraday cage. The surfaces can be viewed in fig. 3.3, while more detailed representations of the pictures are found in the appendix under C.1 and C.2.

(a) (b)

Figure 3.3: A view of the different surfaces of the shielded room taken along the diagonal NE/SW-axis running through the room. From left to right in each picture, fig.3.3a shows the west wall and north wall, and fig. 3.3b shows the east wall and the south wall (with windows). Photos: Daniel Asle Vingen Endal.

[4]Lask: Traditionally a flat wood or metal piece that connects two adjoining boards, beams or rail ends in the longitudinal direction. Metal is used in our case.

Cage openings

Wave traps All channel openings for ventilation are covered by shielded ventilation panels, termed "wave traps"[5], with a honeycomb-shaped pattern. Wave traps are manufactured by *Holland Shielding Systems BV, Netherlands*. The wave traps ensure that ozone created by electric arcs during high-voltage experiments can be ventilated out while the electromagnetic fields are kept inside the room. The optimal dampening based on measurements performed under laboratory conditions portrays a minimum dampening of 40 dB across all frequencies, with a peak dampening of 110 dB between 10MHz and 100MHz [36].

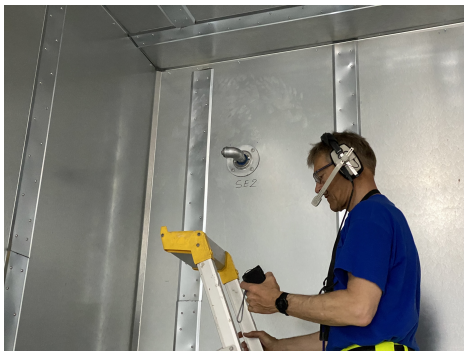

(a) SE for NOVEC fire suppression system.

(b) SE for cable pass-through. Viewed from inside Faraday cage.

(c) Access hatch. North-west corner.

(d) Example of wave trap.

Figure 3.4: Images of cage openings. Photos: Daniel Asle Vingen Endal.

Single Entry frame All cables and tubes enter the screened room through the two single entry frames (SE-frame). The Single entry frames and accompanying modules are manufactured by *Roxtec INT., Sweden*. The main single entry frame is located under window No.3 (see measuring results for window #3 in table A.2), furthest into the laboratory in relation to the screened door. It has the capacity for 102 cables and tubes of varying dimensions to pass through the wall.

[5]Directly translated from the Norwegian word "bølgefelle".

Figure 3.5:
Shielded door.
Photo: Daniel Asle Vingen Endal.

The door is custom designed by Holland Shielding Systems BV for good dampening of frequencies in the EMI wave band with a compression seal on the door and a copper finger seal on the frame.

The windows are made by Holland Shielding Systems BV. Since the first provided solution for the windows did not meet expectations, a second solution was implemented in place of the first. The build-up of the window panes for both solutions was the same; the three windows each consist of two layers of glass with a finely woven mesh (130 OPI) laminated between the windowpanes. The three original windows were to be mounted in a cradle-like fashion, where the mesh was laminated between the steel frame holding the glass unit and the steel wall of the Faraday cage, as shown in figure 3.7a. This way of mounting showed itself to provide insufficient shielding in comparison to the quality assurance specification sheet provided by the manufacturer in the magnetic spectrum of the waveband.

For the improved mounting solution, the windows were returned to the manufacturer, who then fabricated integrated mounting hardware for each window. A key requirement from HVL of these windows is the ability to dismount them, in order to clean the surfaces of the windows in the fire cell that the shielded structure is built within. The laminated mesh connects electrically and magnetically to the window frame now through a conductive gasket that seals along the perimeter of each laminated pane unit, which is bolted to individual steel frames also fabricated by Holland Shielding Systems. Holland Shielding

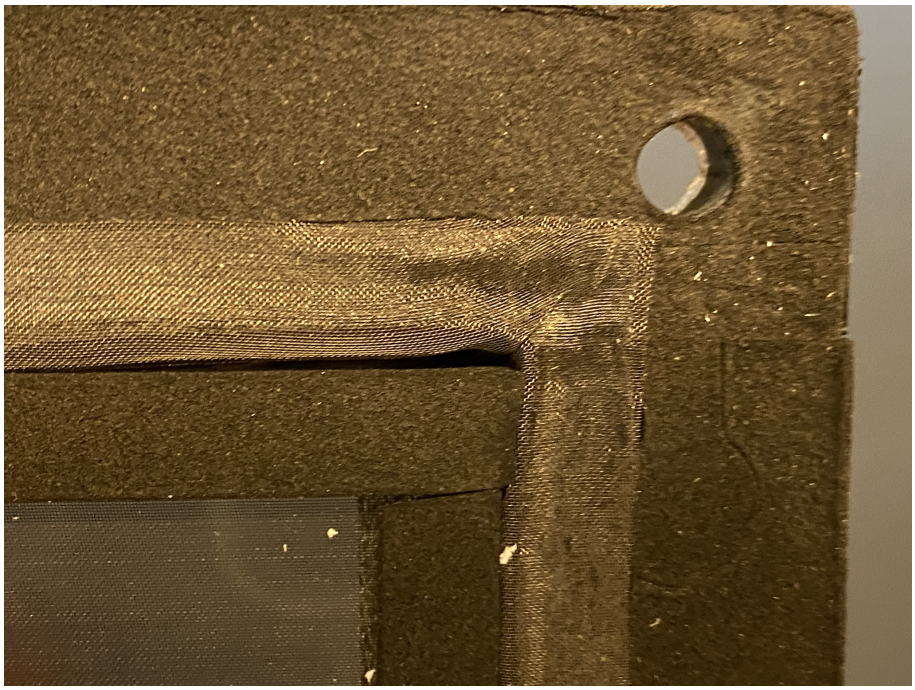

Figure 3.6: Shown is the connection form of the wire mesh for when it is mounted to the window frame. Photo: Daniel Asle Vingen Endal.

Systems have provided best-case specifications obtained by conducting laboratory tests for the new windows. The best-case dampening characteristics can be viewed in figure D.4. A detailed view of the rubber gasket can be seen in appendix C.4. The steel window frames are mounted with an additional nickel-coated copper mesh gasket between the window frame and the Faraday cage. A steel plate lask is then bolted over the joints between each window.

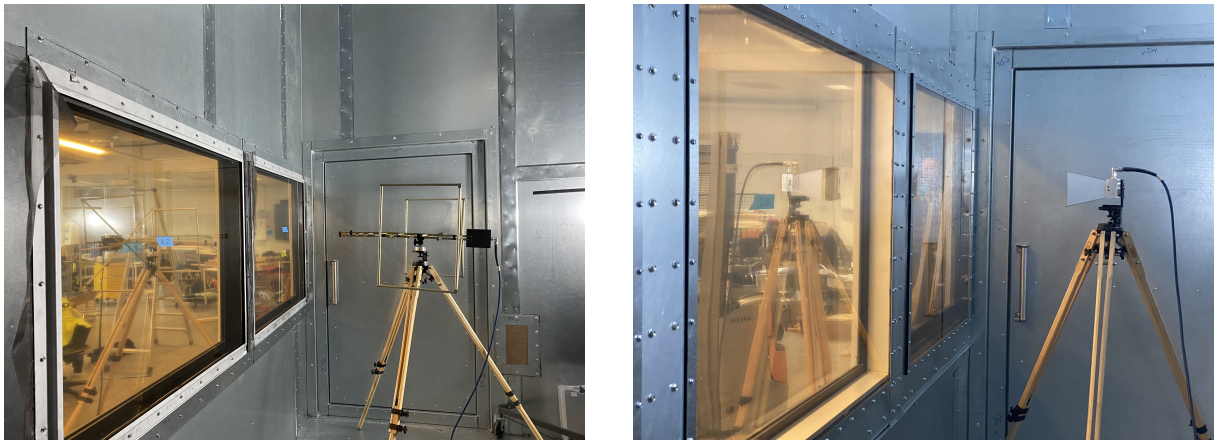

(a) (b)

Figure 3.7: 3.7a shows the original cradle-sandwich-like mounting solution for the windows, while 3.7b shows the currently implemented and improved mounting solution for the windows. Photos: Daniel Asle Vingen Endal.

Chapter 4

Methods

This chapter is based on information and excerpts taken from test reports received [37] for the screened high voltage laboratory produced by EB Consulting AS, as well as thoughts and reflections from the candidate about the content of the report and the days of measurements at HVL.

The tests were conducted by the company EB Consulting AS with assistance from Daniel Asle Vingen Endal. EB Consulting AS is based in Kristiansand, Norway and delivers services for testing and control measurements of screened structures. The tests were performed in compliance with the de facto adopted standard for testing civilian installations; IEEE standard 299 [38]. The terms dampening and attenuation will be used interchangeably.

4.1 IEEE standard 299

The standard describes and includes:

- Description of the tested facility
- Execution and method
- Test setup and instruments
- Test frequencies and levels
- Test results
- Structure and content of the test report

The test standard is strictly limited to the points mentioned above. It does not require the mention of any errors, a problem description, or possible solutions if unacceptable results are measured and the attenuation requirements should not prove to be met [37].

4.2 Calibration and preparation for testing

The IEEE standard 299-2006 is used for measuring the shielded room. The test period takes place over the course of a week, with preparations followed by measurements throughout large parts of the day. Test points are marked on walls, floors and ceilings, and positions for receiver antennas are calculated for surfaces on adjacent floors and in adjacent rooms. The measuring antennas must be at least 40 cm away from the nearest conductive material. This is so that the impedance of the measuring equipment is not affected by conductive material in the vicinity.

The equipment must be calibrated for the measurements to be made based on the minimum distance to the nearest conductive surface and the thickness the signal has to pass through. The calibration is done by lining up the antennas with (in this case) 1 meter of distance between the tips of each antenna. It is important that the antennas are lined up as accurately as possible in such a way that they point at each other along the same axis. The signal generator is set with a gain level so that the receiving equipment achieves a 0-level, to the extent that this is possible. 0-level gain for each test frequency is noted in order to reproduce the reference transmission when the dampening of the screen structure is to be measured. If the gain is maxed out on the signal generator and the 0-level is not achieved on the spectrum analyzer, the measured attenuation will be boosted by the remaining gain value required to reach the 0-level. This value is written down to later adjust the recorded measurements. Deviations from the notation or the calibration setup here will give higher attenuation values due to an incorrect distance through which the signals pass, the impedance of the antenna being affected because it is too close to conducting materials, or because there will be an incorrect adjustment for the gain of a frequency when measuring results are to be recorded. The tests carried out with the equipment in question require a person inside the room to operate the receiving equipment, and a person outside the room to operate the transmitting equipment. Once the equipment has been calibrated, it can be positioned using known points in the structure of the building which can be found on the floor plans for the building. Accurate measurements are carried out to ensure that the antennas are positioned correctly and pointing at each other to avoid uncertainty in measurement data. Adjustment for floor height and varying wall thickness is taken into account.

During dampening tests, according to the IEEE 299-2006 standard, the room was empty with the exception of the required testing equipment. The SE-frames were completely set up with all cables and tubes routed through. The cables were all shorted and connected to the ground in order to avoid so-called ”antenna leaks” during testing. Novec fire suppression system and Honeywell fire detection system were not fitted during dampening tests.

4.3 Test methods

4.3.1 Test method according to IEEE standard 299-2006

The measurements were carried out as CW tests in accordance with IEEE std. 299 with some adjustments. Transmitter and receiver instrument levels; respectively signal generator and spectrum analyzer; were calibrated for floor, wall and ceiling thicknesses before the measurements started. See table 4.1 below [37].

Measuring location with a spectrum analyzer and receiver antenna is established inside the Faraday cage with a corresponding signal generator and antennas are placed outside. Measurements were done at points chosen based on contractor experience for what has to be tested in order to verify the attenuation properties of the screened structure.

The chosen measurement points were applied signals in three frequency bands in accordance with the standard. The measured dampening between the transmitter and receiver was corrected according to calibration values and gives the actual dampening property in the defined test points.

The measurement equipment inside the screened structure was supplied from an external fuse course via a power filter mounted to the Single Entry frame 1. Communication was done via a temporary connection cable connected via a "telefilter" in the Single Entry frame 1.

Table 4.1: Calibration specifications for test method according to IEEE 299 [37, p. 9].

Calibration	Between antennas	Notes
Loop (LF/magnetic fields, 156kHz-10MHZ)	100 cm	30 cm to screen + wall/roof thickness (25-40 cm) + 30 cm to wall or roof.
Bilogical (RR/ electric fields, 52MHz-1GHz)	100 cm	
Horn (HF/ electric fields, 1GHz-18GHz)	100 cm	
Test	Between antennas	Notes
Loop (LF/mag. field)	30 cm to inside of screen and 30-40 cm to building body. Total of 100 cm including wall/roof.	Minimum 45 cm distance to other conductive (metal) components in and outside the screen space to avoid antenna impedance mismatch.
Bilogical (RR/el. field)		
Horn (HF/el. field)		
Note: The tests were conducted with horizontal or vertical antenna polarization depending on what was practically possible.		

The locations of the test points can be seen in figures 4.1, 4.2 and 4.3. A principle sketch showing the procedure of conducting measurements can be seen in figure 4.4.

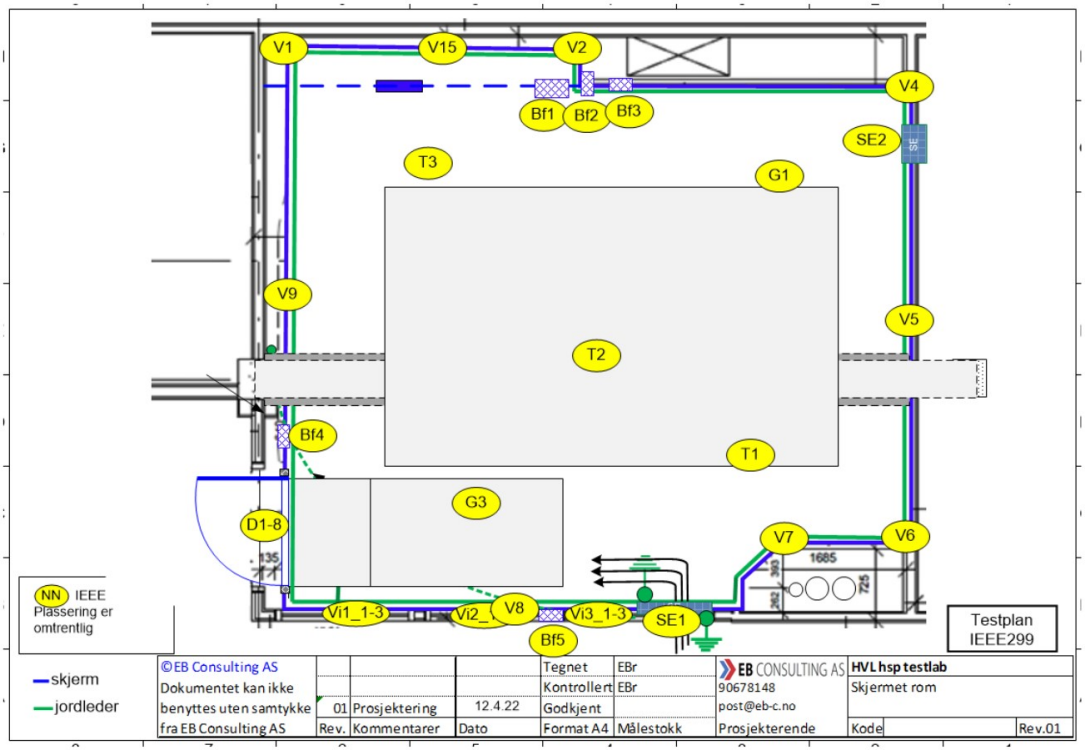

Figure 4.1: Location of measuring points within the shielded enclosure. Courtesy of EB Consulting AS [37].

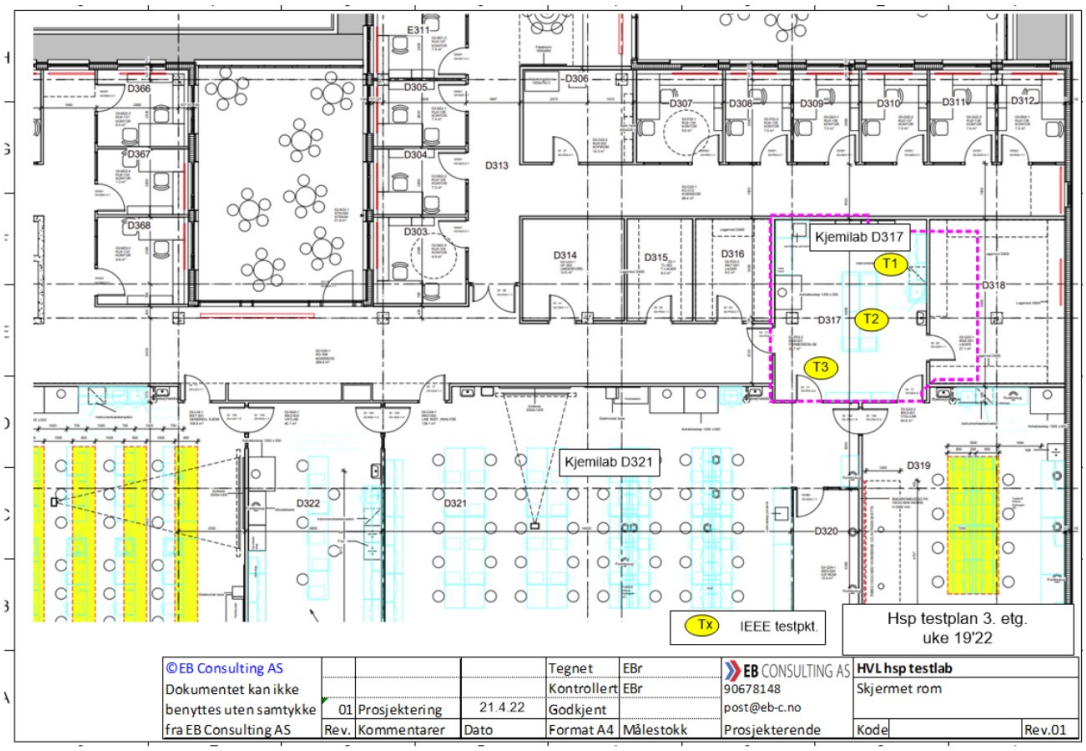

Figure 4.2: Location of measuring points on the 3rd floor, below the shielded enclosure. In order to measure the dampening of the floor in the Faraday cage. Courtesy of EB Consulting AS [37]

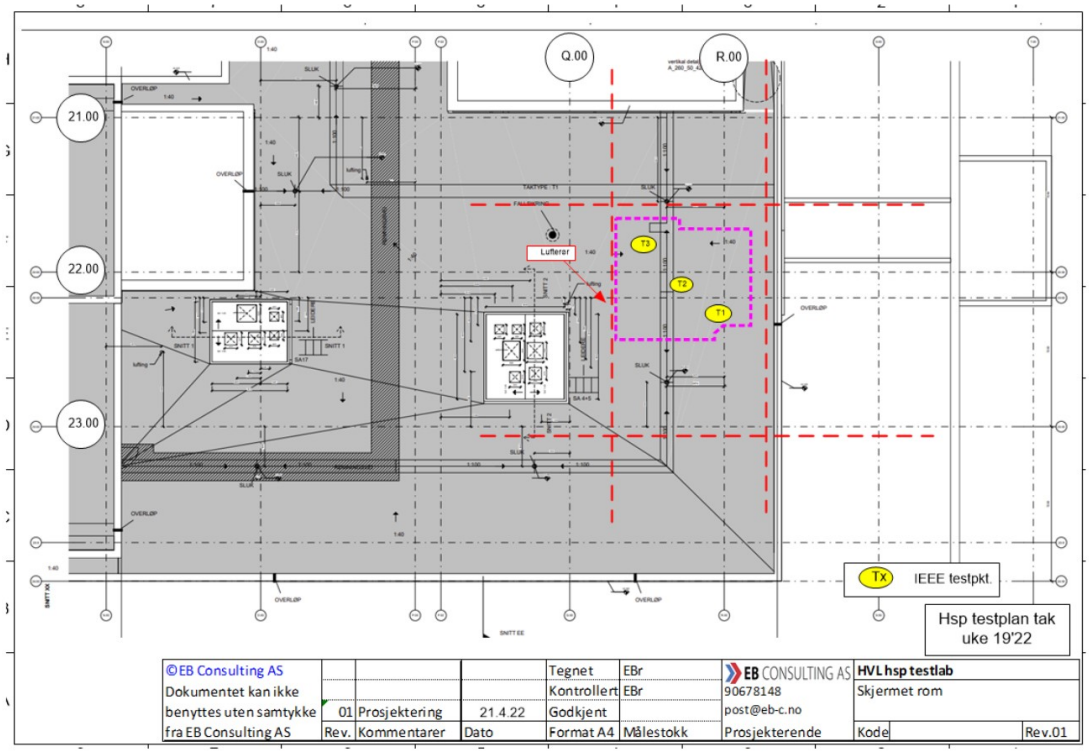

Figure 4.3: Location of measuring points on the roof above the shielded enclosure. In order to measure the dampening of the roof in the Faraday cage. Courtesy of EB Consulting AS [37]

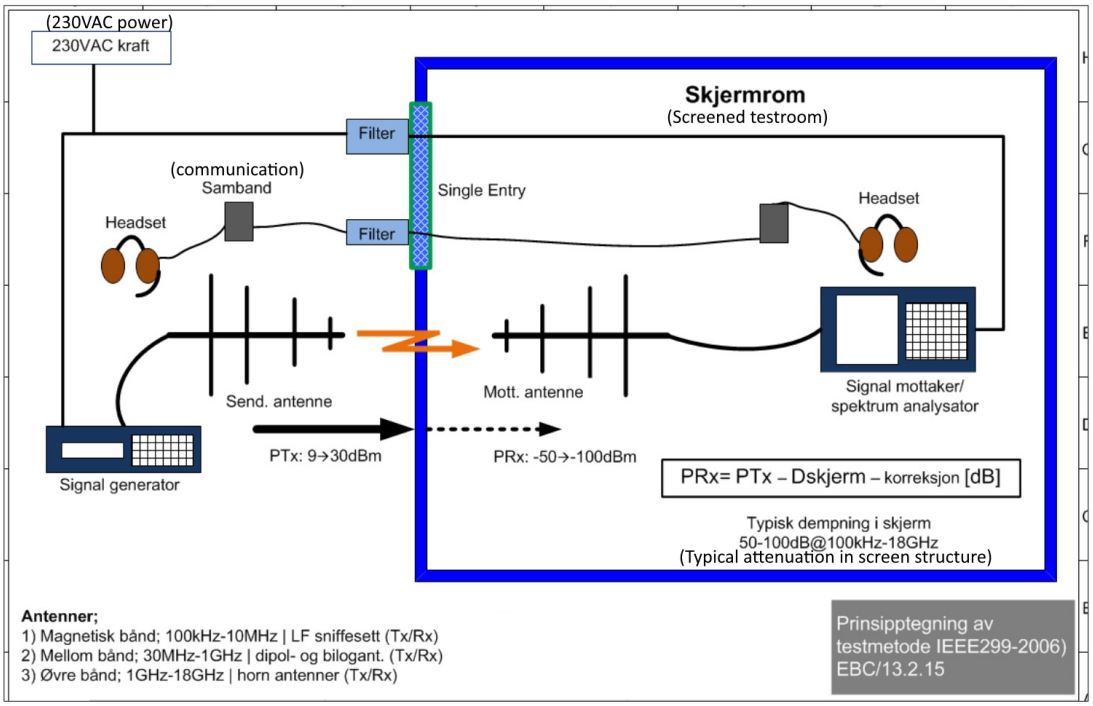

Figure 4.4: Principle sketch for test method IEEE std. 299. Photo: EB Consulting AS [37, p. 9].

4.3.2 Test method for high-voltage tests

As measurements were wrapping up, there were also performed measurements of electromagnetic fields outside the screened room while HVL were performing real high-voltage tests in the high-voltage laboratory. High-voltage testing equipment was rigged for up to 75kV RMS (100kV peak) test voltage. It was not possible to conduct tests with higher test voltages since the equipment was not installed and prepared for it at the time of testing. During the tests, the applied voltage was increased gradually in order to achieve corona and subsequent flashover on a high-voltage insulator as the test object. Any leakage of electromagnetic field on the outside of the screen room was measured at two points with a spectrum analyzer and associated antenna, see figure 4.5 and table 4.1 for details. Measurements were made with the screen structure closed and with the screened door opened in order to compare results (with measurements from 2021) and verify the attenuation properties of the Faraday cage.

Measured values were recorded and saved on the spectrum analyzer, as well as videotaped with a digital camera. The measuring equipment used is detailed below.

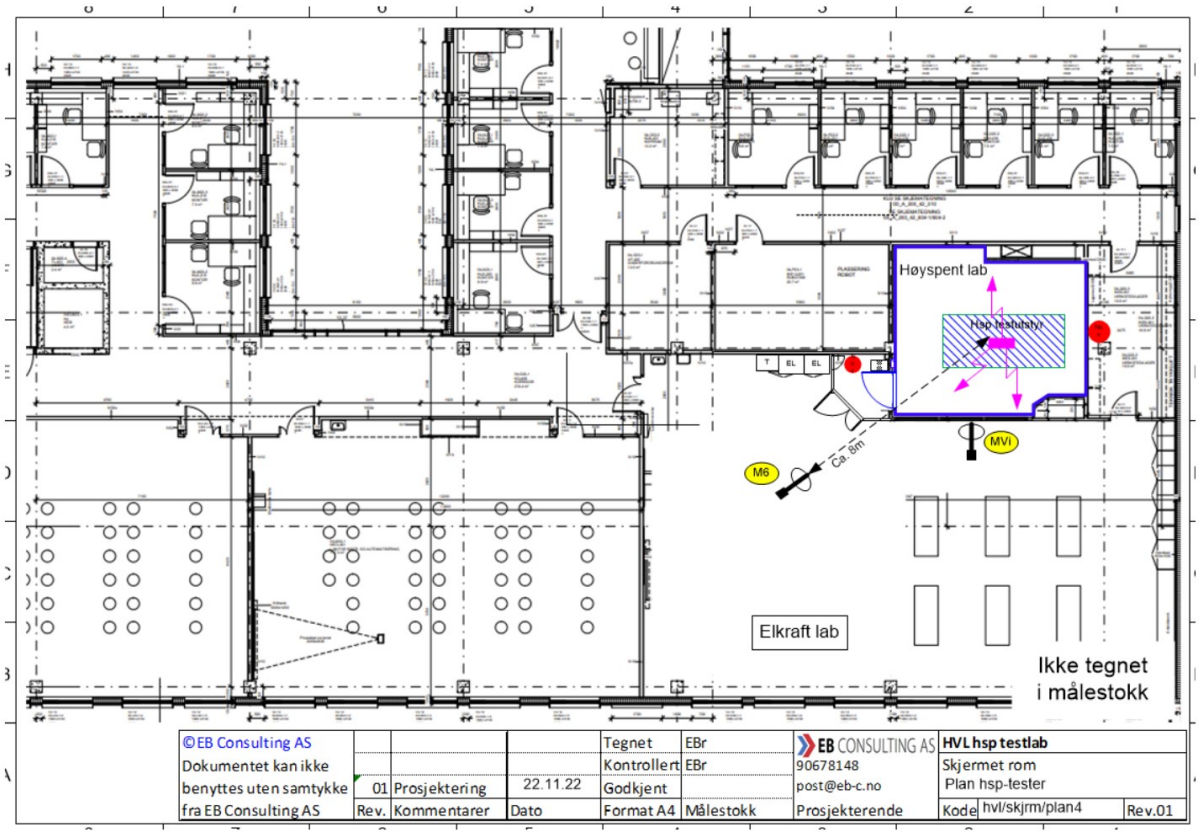

Figure 4.5: Floor plans showing the location of measuring points in connection with real high-voltage tests. Photo from EB Consulting AS [39, p. 8].

4.3.3 Test equipment

Equipment list IEEE standard 299 tests

1. Signal generator; 0.1Hz-20GHz; type Anritsu Signal Generator; mod. MG3692C. Calibrated 2018.
2. Spectrum analyzer; 9kHz-20GHz; type Anritsu Spectrum Analyzer; mod. MS2720T. Calibrated 2015.
3. 1 set bilogical antennas type AH Systems; mod. SAS 521F-2 (25MHz-2GHz). Calibrated 2016.
4. 1 set horn antennas type Poam Electronics ab; mod. RTF-118A (1GHz-18GHz). Calibrated 2015
5. 1 set of LF/HF loop antennas "sniffers"; 10kHz-10MHz; signal generator and accompanying receiver; type Euroshield RF-Leak detector/att. Meter; mod. MF 9F. Calibrated 2017.
6. Tripods type AH Systems; mod. ATU 510 and antenna "lift" Dovre.
7. Various antenna cables, connectors, dampening links and cable filters.

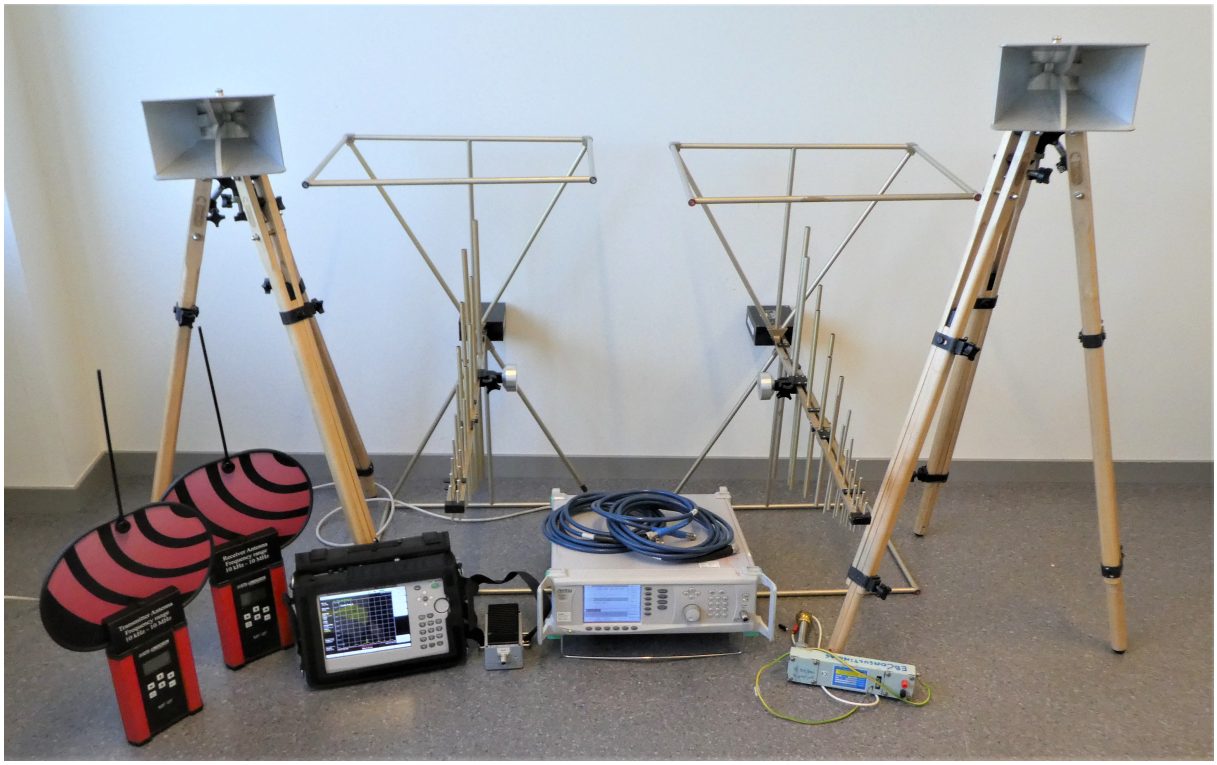

Figure 4.6: Photo: EB Consulting AS.

Equipment list High-Voltage tests

1. Directive loop antenna;
    - 9kHz-20MHz; type Rohde&Schwarz R&S HE200HF.
    - 20MHz-200MHz; type Rohde&Schwarz R&S HE200RF_mod. 1.
    - 500MHz-3000MHz; type Rohde&Schwarz R&S HE200RF_mod. 3.
2. Isotropic "room" antenna; Anritsu 2000-1791-R Isotropic antenna, E-field, 0.7GHz - 6GHz.
3. Spectrum analyzer; 9kHz-20GHz; type Anritsu Spectrum Analyzer; mod. MS2720T. Calibrated 2015.
4. Tripods type AH Systems; mod. ATU 510.
5. Various antenna cables, connectors, dampening links and cable filters.
6. Videocamera

Manual containing antenna factor for R&S HE300 antenna can be found in [40]. We expect that since antenna modules are compatible between the 200 version and the 300 version, information in the manual is compatible too.

(a) (b) (c) (d)

Figure 4.7:
4.7a: Measuring instrument for high-voltage testing. Photo: Rohde & Schwarz [41].
4.7b: Isotropic antenna, manufacturer: Rohde & Schwarz. The photo was taken from EB Consulting AS test report [39].
4.7c: Spectrum analyzer to visualize incoming electromagnetic radiation. Photo: Anritsu [42].
4.7d: Isotropic antenna, manufacturer: Anritsu. The photo was taken from EB Consulting AS test report [39].

4.4 Converting received measured values

In order to compare the measured results from the spectrum analyzer to the values in ICNIRP guidelines [18], we need to establish and present some equations and formulas published by various antenna manufacturers and others.

Our sources for these equations are Rohde & Schwarz [43], Everything RF [44], and antenna characteristics and properties [40], Aaronia AG [45] and A. H. Systems [46]. Including some calculations to be used in the discussion in order to compare results presented in the table 5.3 to ICNIRP guidelines [18]. The amount of energy that passes through the shielded enclosure can be converted from dBm to W/m^2 in several manners. The peak recorded value during flashover with a RMS voltage of 75kV is -120 dBm.

I will here attempt to derive two ways to estimate the energy density at the point based on our measurement value for the field intensity **E**. One method is logarithmic and one method is numeric linear. With logarithmic recorded values one can use a method from the webpage "Everything RF" [44], while for SI-unit values a method is described by StackExchange forum user "neonzeon" [47] which is better described in a document published by R&S [43]. Both methods yield somewhat similar results. Further, we get the antenna factor (AF) of the R&S HE200HF antenna in the frequency range of 10-20MHz from the antenna manual. The antenna used for the measurements was an R&S HE200HF antenna, but the antenna modules are interchangeable between the 300-version and the 200-version, so we suspect that the antenna characteristics for the 300-version are applicable to the 200-version. The antenna factor (during passive mode) is approximately between 42dB/m (@10MHz) and 40 dB/m (@20MHz) depending on frequency [40, p. 42].

Firstly, the gain and antenna factor is read from figures 5-13 and 5-14 in the antenna manual [40]:

Table 4.2: Gain and Antenna factor visually read from graphs in antenna manual. Source [40, pp. 41–42].

Frequency: [MHz]	Gain: (G_{dBi})[dBi]	Antenna Factor: ($K_{a(dB)}$)[dB/m]
10	-52	42
20	-45	40
75	-16,5	24
125	-10	22

For the logarithmic method, our peak value is first converted from dBm to dBμV, then adjusted with AF [44]. The result is then converted from decibel-micro-Volts-per-meter [dBμV/m] to decibel-Volts-per-meter to electric field intensity **E** [V/m] and then finally

we get the measured power flux density[W/m^2]. These operations are based on formulas from a compendium sheet published by Aaronia AG [45] and a similar document from A. H. Systems [46], as well as the website "Everything RF" [44].

$$V_{[dB\mu V]} = P_{dBm} + 107dB \tag{4.1a}$$

$$E_{[dB\mu V/m]} = V_{[dB\mu V]} + AF_{[dB/m]} \tag{4.1b}$$

$$E_{[V/m]} = 10^{((E_{[dB\mu V/m]} - 120)/20)} \tag{4.1c}$$

$$S_{[W/m^2]} = \frac{E^2[V/m]}{Z_0[\Omega]} \tag{4.1d}$$

These equations can be found in [46] and [44]. Equation (4.1a) converts the received power that the spectrum analyzer from dBm (P_{dBm}) to decibel-micro-Volts, [46]. Equation (4.1b) adds the antenna factor, giving the electric field strength in decibel-micro-Volts-per-meter, [44]. Equation (4.1c) converts the electric field strength from decibel-micro-Volts-per-meter to electric field strength E in V/m, [46]. Equation (4.1d) calculates the measured power flux density S from the electric field strength E and the impedance of free space, [46].

For the numeric linear method, we first need to express AF in volts instead of decibels using the formula provided by Rohde&Schwarz [43, p. 6], then we can use the method presented by neonzeon and antenna manufacturer Rohde & Schwarz together with formulas provided by Aaronia AG [45] and A.H. Systems [46] to convert dBm to power [W], then calculate field intensity **E** by using a formula from [43] and then convert to energy density.

Gain is converted to numeric value G_n [48]:

$$G_n = 10^{G_{(dBi)}/10} \tag{4.2}$$

The numeric gain is then used to calculate the numeric antenna factor [43, p. 6]:

$$K_a = \sqrt{\frac{4 \cdot \pi}{G_n \cdot \lambda^2} \cdot \frac{Z_0}{Z_i}} \tag{4.3}$$

The wavelength is based on the relation between frequency and the speed of light in a vacuum, as shown in equation (2.41).

We use equation (4.3) and wavelength from 4.3 to get the numeric value for the antenna factor, then check it using equation (4.4) to see if it correlates to the value from graph

Table 4.3: Wavelength of test frequency.

Frequency	Wavelength
10MHz	30m
20MHz	15m

5-13 from the manual mentioned above.

$$K_{a(dB)} = 20 \cdot log_{10}(K_a) \tag{4.4}$$

Table 4.4: Calculated numeric antenna factor.

f [MHz]	λ [m]	$G_{(dBi)}$	G_n	K_a $[m^-1]$	$K_{a(dB)}$ $[m^-1]$
10	30	-52	6.309...e-06	129.172...	42.223...
20	15	-45	3.162...e-05	115.398...	41.244...

As we can see from table 4.4, the calculated numeric antenna factor K_a is quite close to the value we read from the graph in the manual. We can therefore proceed. I will now present the remaining equations to perform the conversion:

$$P_W = 10^{((P_{dBm}-30)/10)}\ [W] \tag{4.5a}$$

$$U_r\text{: } P_W = \frac{U_r^2}{Z_i} \implies U_r = \sqrt{P_W * Z_i}\ [V] \tag{4.5b}$$

$$E = U_r \cdot K_a\ [V/m] \tag{4.5c}$$

$$S = \frac{E^2[V/m]}{Z_0[\Omega]}\ [W/m^2] \tag{4.5d}$$

These equations can be found in [43]. Equation (4.5a) converts the received power that the spectrum analyzer reads from dBm (P_{dBm}) to Watts (P_W) [46], equation (4.5b) extracts U_r which is the voltage that the spectrum analyzer receives [43], equation (4.5c) turns the received voltage U_r into the electric field strength **E** [43], and equation (4.5d) calculates the measured power flux density **S** from the electric field strength **E** and the impedance of free space [46].

Chapter 5

Results and Discussion

This chapter presents the measured dampening response from the site-built Faraday cage through the respective surfaces and necessary installations in the construction during quality control, as well as during actual use.

Initially, EB Consulting AS carried out mapping measurements during live high-voltage tests in week 24, 2021 to establish the conditions in the high-voltage laboratory.

The screen room has been designed by EB Consulting AS to meet the requirements from HVL, with a minimum requirement of 25 dB attenuation over all frequencies.

First, two rounds of damping measurements have been carried out in week 19 and week 33 of 2022 as described in chapter 4.3.1 to check the real damping of the construction against design and theoretical analysis. The first week of measurements went mostly as expected, with the exception being measured values for the shielded windows and the shielded door. During this week, measurements were made for all the wall points, the door, windows, wave traps, roof and floor. The recorded values from the windows and the door were rejected. This was due to poorer-than-expected shielding effectiveness resulting from complications or deficiencies in parts delivered from subcontractors. Measurements could not be completed during the first week because of this.

The second round of measurements occurred after new windows and the missing mounting gasket had been delivered from Holland shielding systems. The lack of this gasket affected the measurements for both the door and the windows, in addition to wave trap No.4 located right next to the door. Following the installation of the missing gasket and mounting of improved shielded windows, new measurements were carried out and replaced previous values in the new test report.

Furthermore, calculations have been made based on the theory of what could be expected values of shielding effectiveness for the construction based on the material and design choices that have been made.

Finally, real attenuation measurements have been carried out by measuring for leakage of EM waves during "live" HV tests, described in chapter 4.3.2, with the door to the screen room in the fully open position, and with the screen room completely closed.

Due to the reproduction of figures from test reports produced by analysis tools, the candidate has not had the opportunity to change the assigned labels, figure texts and abbreviations presented in this chapter.

5.1 Results

The results obtained during this thesis will be presented in this chapter, and then discussed later in chapter 5.2.

The goal of figure 5.1 is not to show all the measured values in an organized way, it is to show where most of the measured dampening results are concentrated.

Figure 5.1 shows all 1200+ measurements that were carried out during the two weeks of measurements. Each series has an 80% transparency. The intention of this graph is to highlight the trend for damping in the shielded construction. This is demonstrated by how dark the graph is on the y-axis.

Note for the frequency segment from 100MHZ to 170MHZ for figure 5.1: due to the impact on the measured values, probably from resonance in the screen room, the applied frequencies were varied to achieve more accurate values. The values in the graph have been collected to the nearest common frequency, but exact frequencies for each value can be viewed in appendix A.

5.1.1 Measurement results of the shielded enclosure from IEEE 299 standardised procedure

A summary of the measurement results from the standard is presented in table 5.1. Table 5.1 compiles all the data from appendix A.

Table 5.1: Summary of IEEE299 test results compiled from tables in appendix A. Source: [37, p. 16].

Object	Dampening result [dB] Min. - max.
Walls	31 - 111
Roof	32 - 117
Floor	43 - 112
Shielded door	30 - 93
Access hatch	52 - 98
SE-frame	32 - 98
Wave traps for air	31 - 104
Windows, 10kHz-1MHz	5 - 32
Windows, 10MHz-18GHz	26 - 83
Assumed measurement accuracy; ± 3 dB	

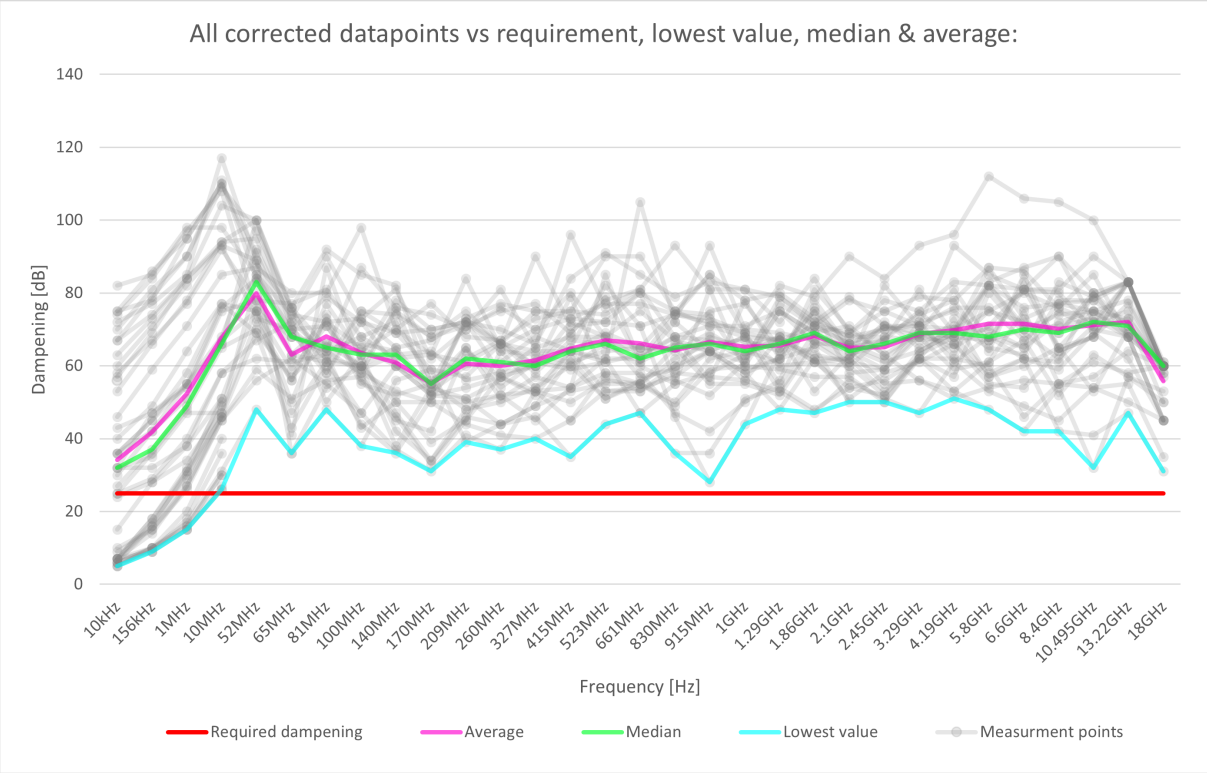

Figure 5.1: Line diagram showing the measurements as well as the trend of the shielded enclosure. Photo: Daniel Asle Vingen Endal.

Steel surfaces and access hatch

Figure 5.2 shows the measured dampening response of all the steel surfaces and the access hatch located above the niche on the north-facing wall. The data in figure 5.2 is discussed in chapter 5.2.1 under "surfaces" and chapter 5.2.1 under "access hatch". The figure compiles data from table A.3 and table A.7.

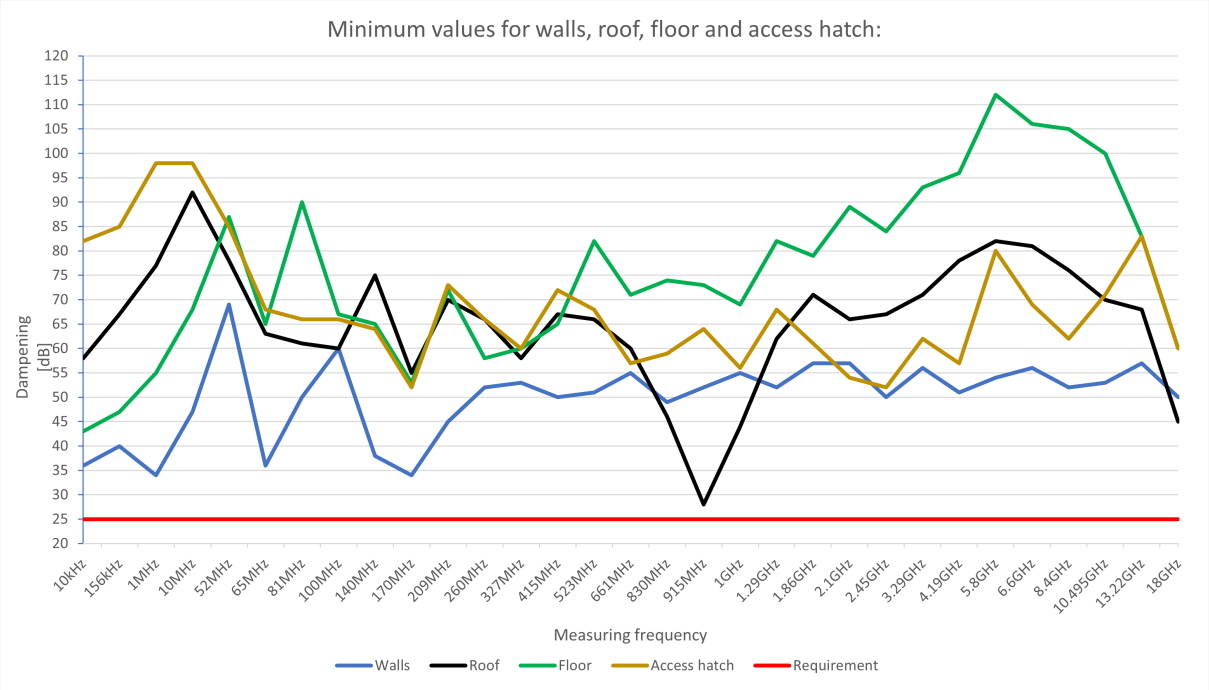

Figure 5.2: Lowest dampening values for steel surfaces and access hatch. Photo: Daniel Asle Vingen Endal, inspired by [37].

Windows

Figure 5.3 presents the overall lowest measured dampening across all three windows. The lowest measured dampening value for each individual window is presented in figure 5.4. Figure 5.5 presents the dampening of the window frame in the transition from the window to the Faraday cage.

Figure 5.3, figure 5.4 and figure 5.5 all utilize data from table A.2 but have different focus areas. Figure 5.3 gives a quick overview, figure 5.4 shows the individual response of each window, while figure 5.5 shows the dampening of the window frames. The data presented in the figures of this section are discussed in 5.2.1.

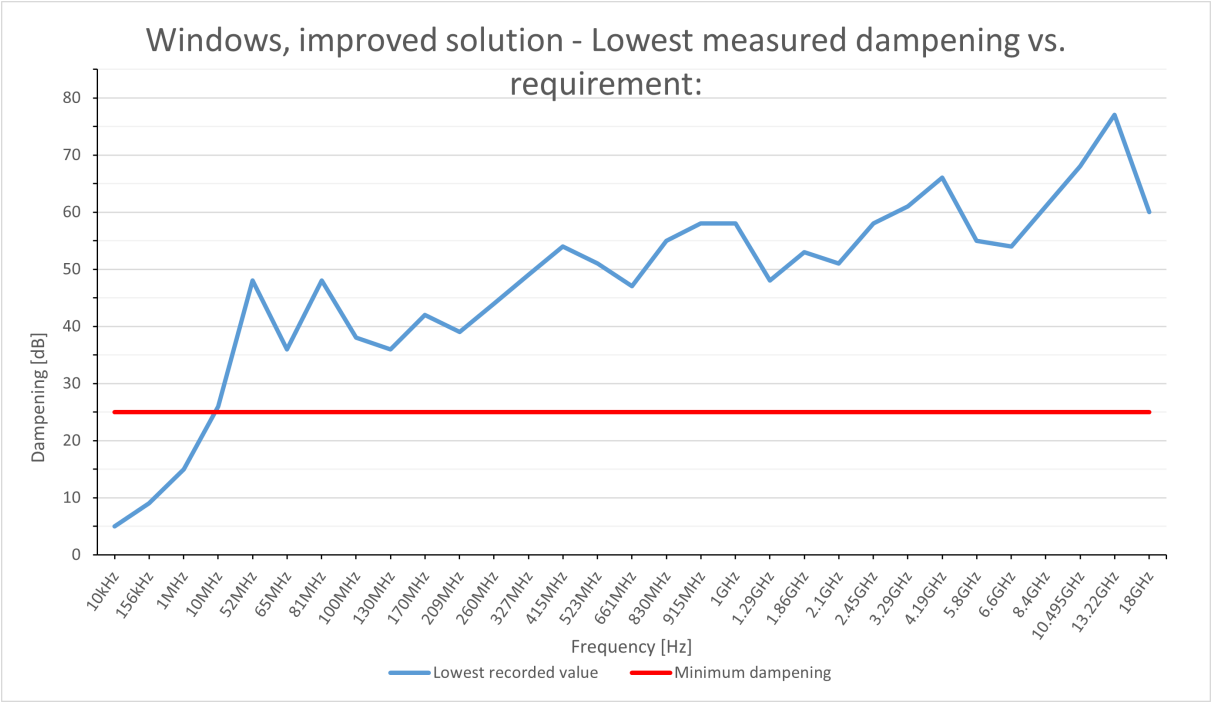

Figure 5.3: Lowest dampening value in each measured frequency across all surfaces of the Faraday cage. Photo: Daniel Asle Vingen Endal.

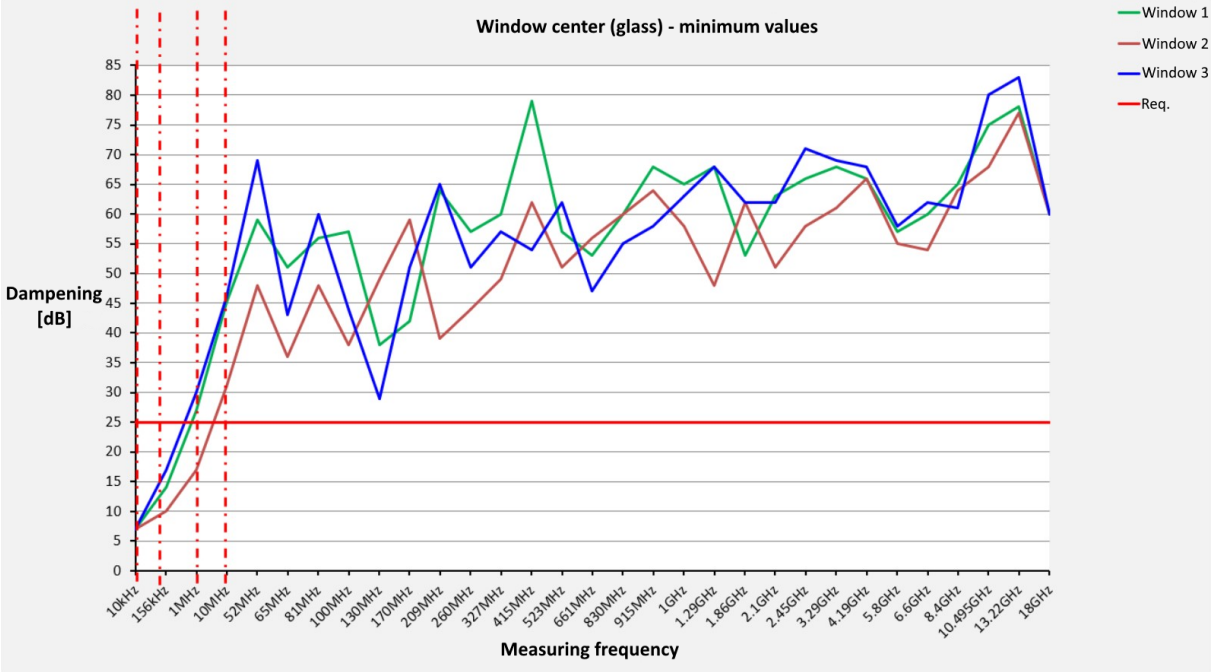

Figure 5.4: Minimum value measured in the centre of each improved window. Photo: EB Consulting AS [37].

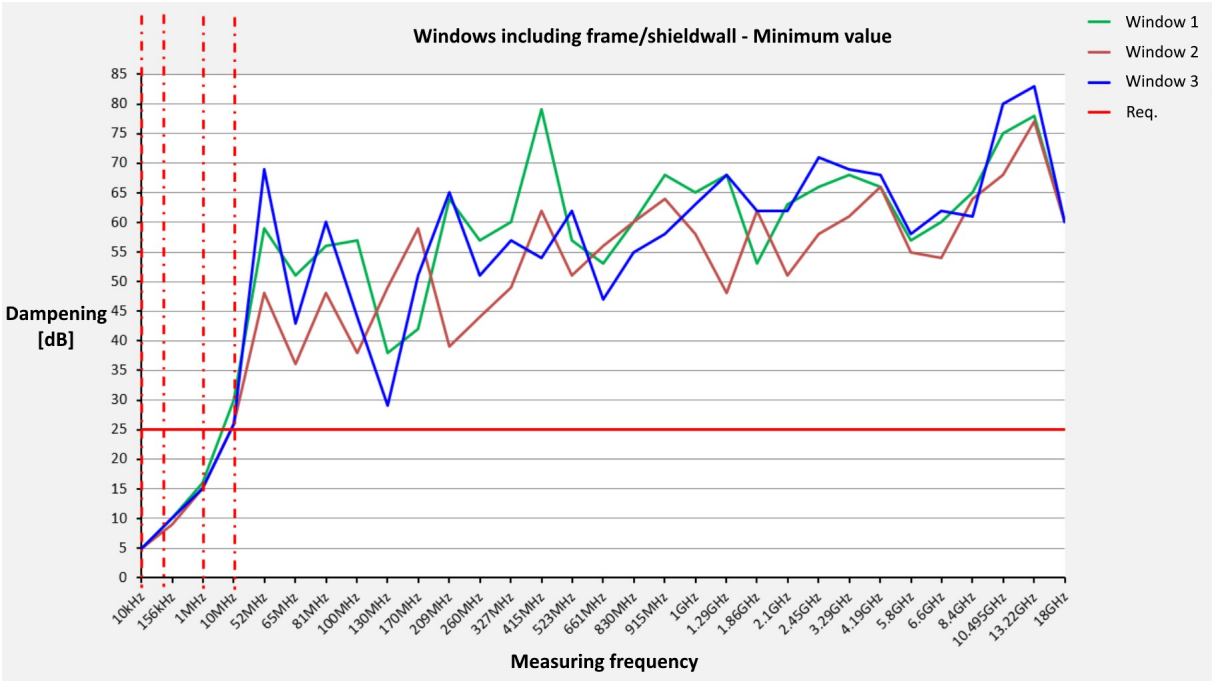

Figure 5.5: Lowest value of measurement from window frame on each window. Photo: EB Consulting AS [37].

Initial results, windows from week 19 2022 Because of small changes done to the windows between measuring sets, the inclusion of old obsolete measurements is deemed necessary to compare results from before and after these changes. The graphs in figure 5.6 use the measurements results from week 19 2022, which can be seen in table A.1.

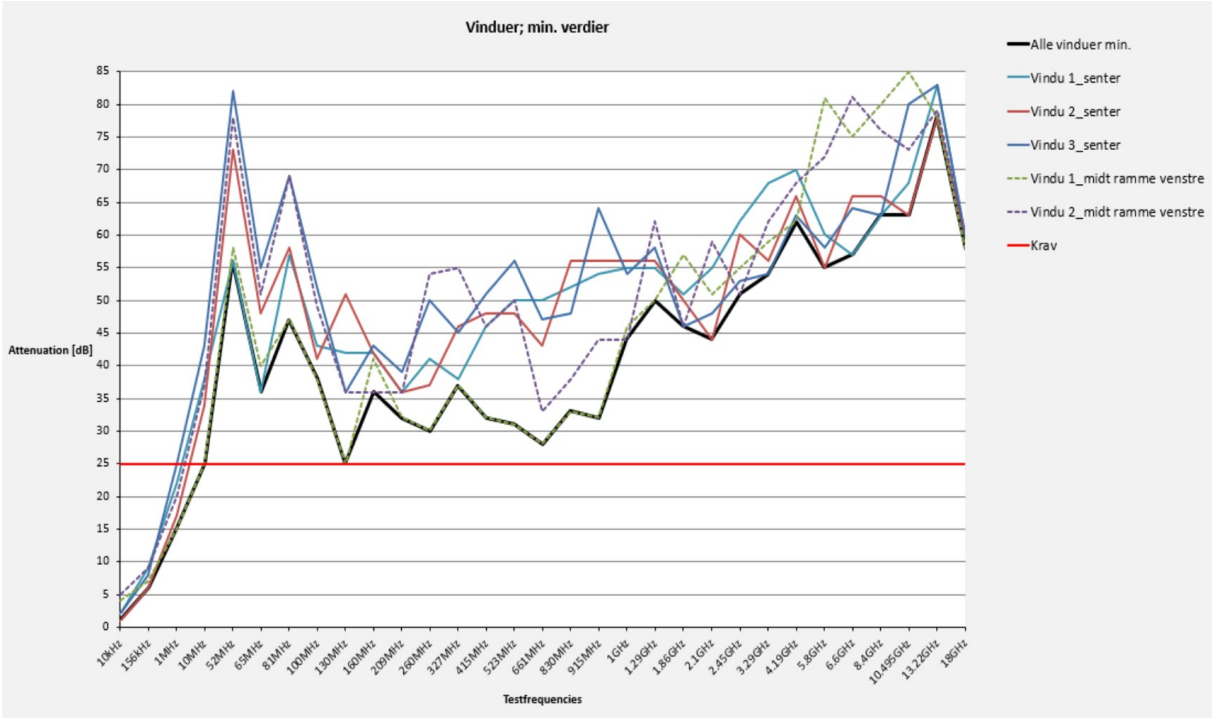

Figure 5.6: Measurements of windows with the original mounting solution. Photo: EB Consulting AS [49].

Door, Wave traps and Single entry openings

Figure 5.7 shows the measured dampening of the shielded door, the single entry frames and the wave traps for air mounted in front of ventilation openings in the shielded room. The figure compiles the data from tables A.4 and A.7.The data presented in this section are discussed in 5.2.1 (Wave traps), 5.2.1 (Single entry frames) and 5.2.1 (shielded door).

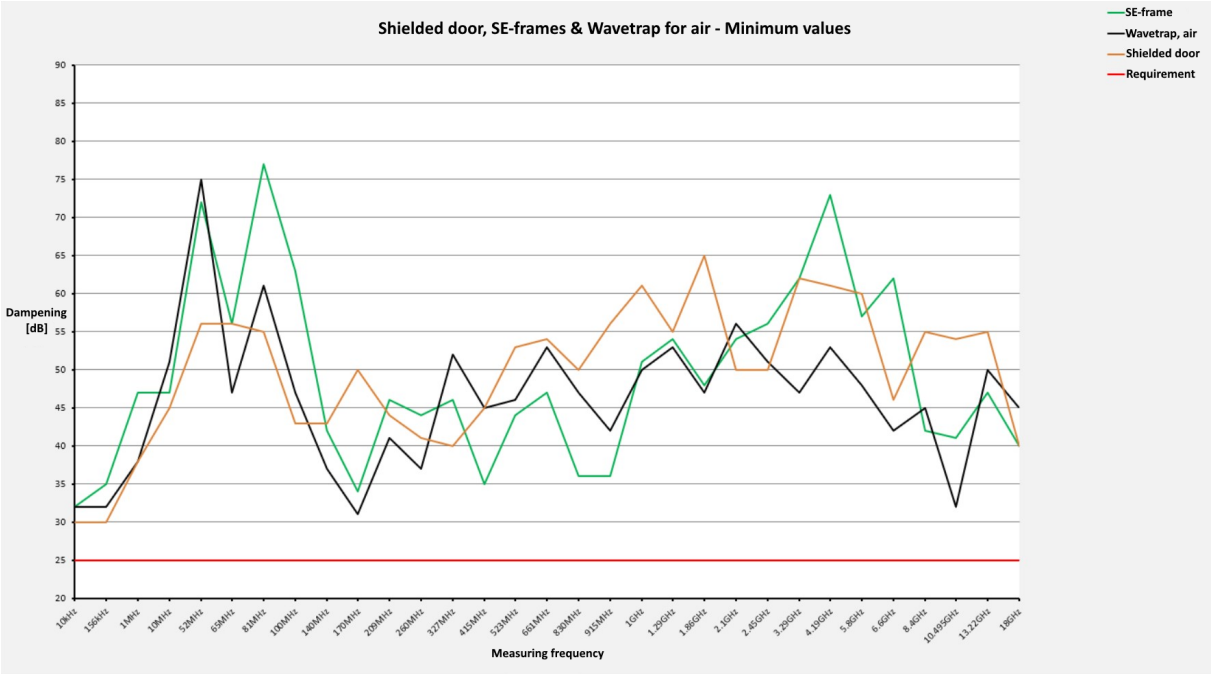

Figure 5.7: Lowest measured dampening value for Shielded door, Wave traps and Single entry openings. Photo: EB Consulting AS [37].

Initial results, door/SE-frame/WT/AH from week 19 2022 Since the installment of the missing gasket in the door can affect the performance of the windows, and vice-versa, the inclusion of old obsolete measurements is deemed appropriate to compare results from before and after the changes. Both figure 5.8 and 5.9 are retrieved from [49] (with permission). The measuring series for figure 5.9 was started at measuring point D7 with the intent to measure the remaining points D1 through D8 but concluded after measurements for point D7 were finished. The measurements were cut short due to the discovery that the secondary gasket was missing. Figure 5.9 utilizes this series of measurements, which can be found in appendix A in table A.5. Figure 5.8 utilizes measurements found in table A.6.

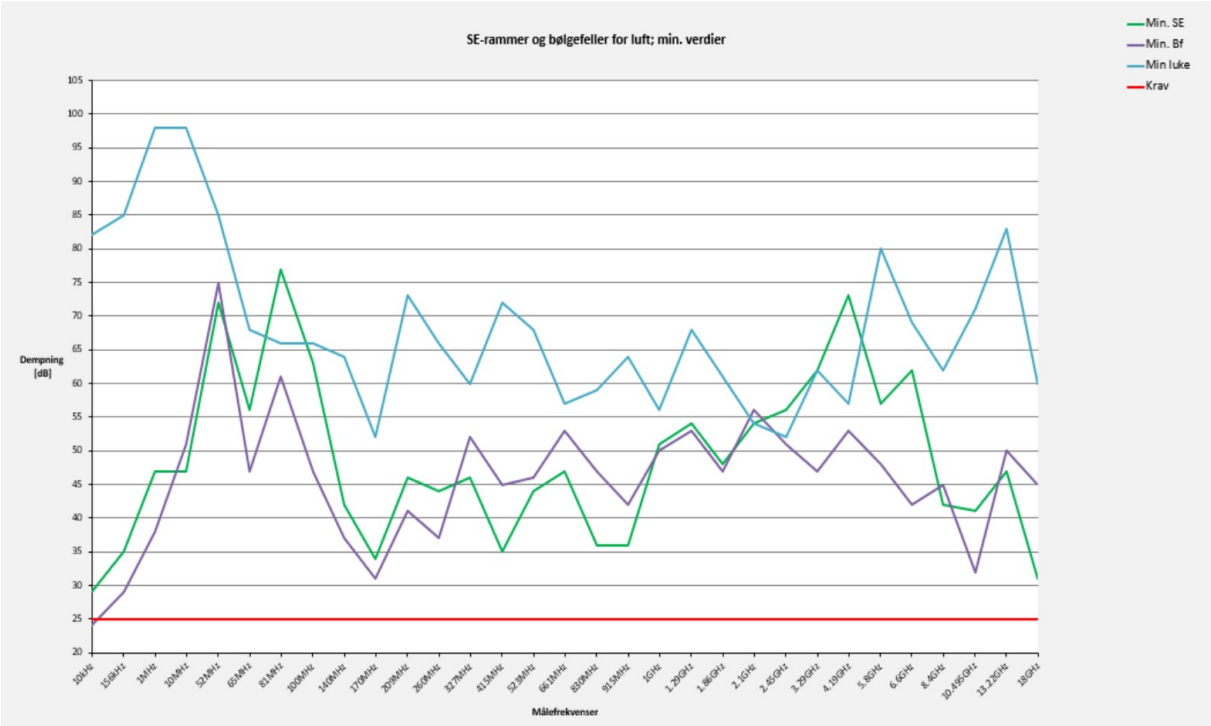

Figure 5.8: Old measurements of the SE-frames, Wave traps and Access hatch from May 2022. Photo: EB Consulting AS [49].

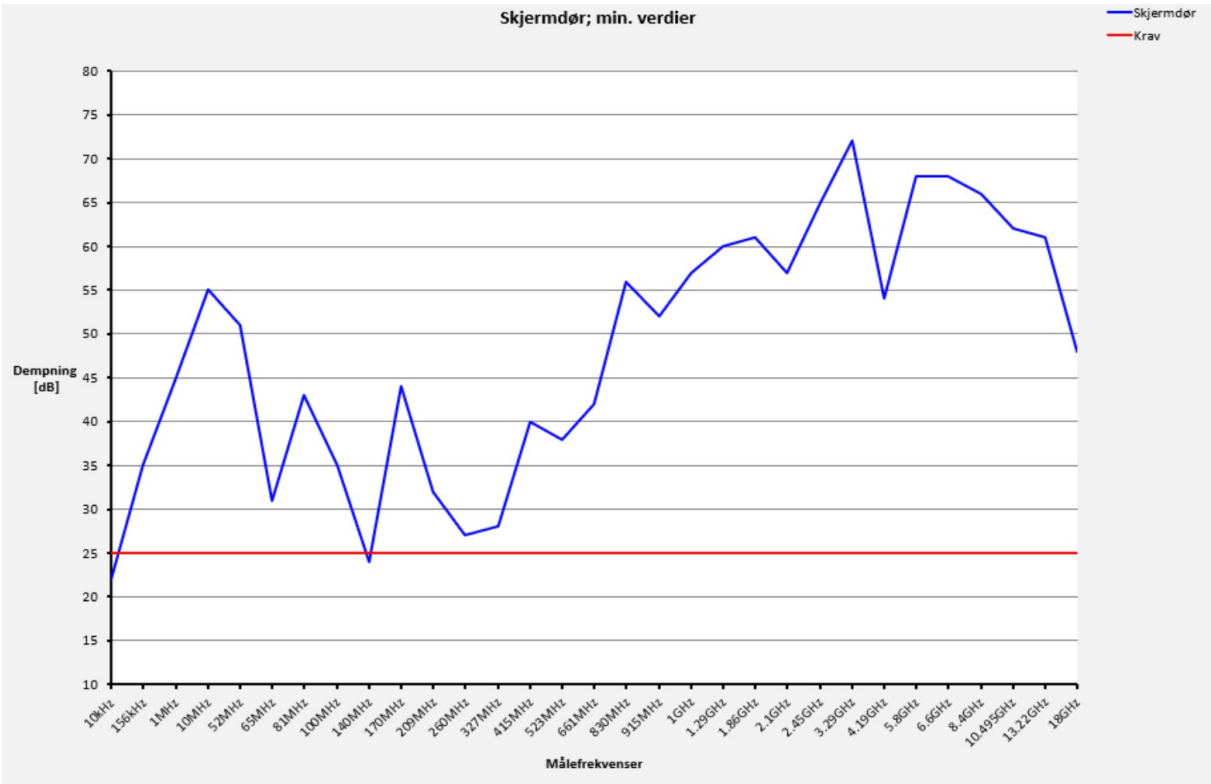

Figure 5.9: Obsolete measurements of the shielded door. The secondary gasket was missing when the shielded door was delivered and this did not perform 100% according to technical specifications. Photo: EB Consulting AS [49].

5.1.2 Calculated dampening

Theoretical dampening is estimated with the method presented in chapter 3.1.3 with the established values for the different factors mentioned. The resulting values are presented in table 5.2 for the frequencies used to measure the shielding effectiveness according to IEEE standard 299.

Table 5.2: Theoretical dampening of a shielded uniform sphere with a radius of approximately 3.069 m and a wall thickness of 2 mm. Values estimated with equation (2.50) according to the method in chapter 3.1.3.

Magnetic fields:															
Frequency:	10kHz	156kHz	1MHz	10MHz											
SE [dB]:	60	83	100	120											
Electric fields and plane waves:															
Frequency:	52MHz	65MHz	81MHz	100MHz	130MHz	170MHz	209MHz	260MHz	327MHz	415MHz	523MHz	661MHz	830MHz	915MHz	1GHz
SE [dB]:	134	136	138	140	142	144	146	148	150	152	154	156	158	159	160
Plane waves:															
Frequency:	1.29GHz	1.86GHz	2.1GHz	2.45GHz	3.29GHz	4.19GHz	5.8GHz	6.6GHz	8.4GHz	10.495GHz	13.22GHz	18GHz			
SE [dB]:	162	165	166	167	170	172	175	176	178	180	182	185			

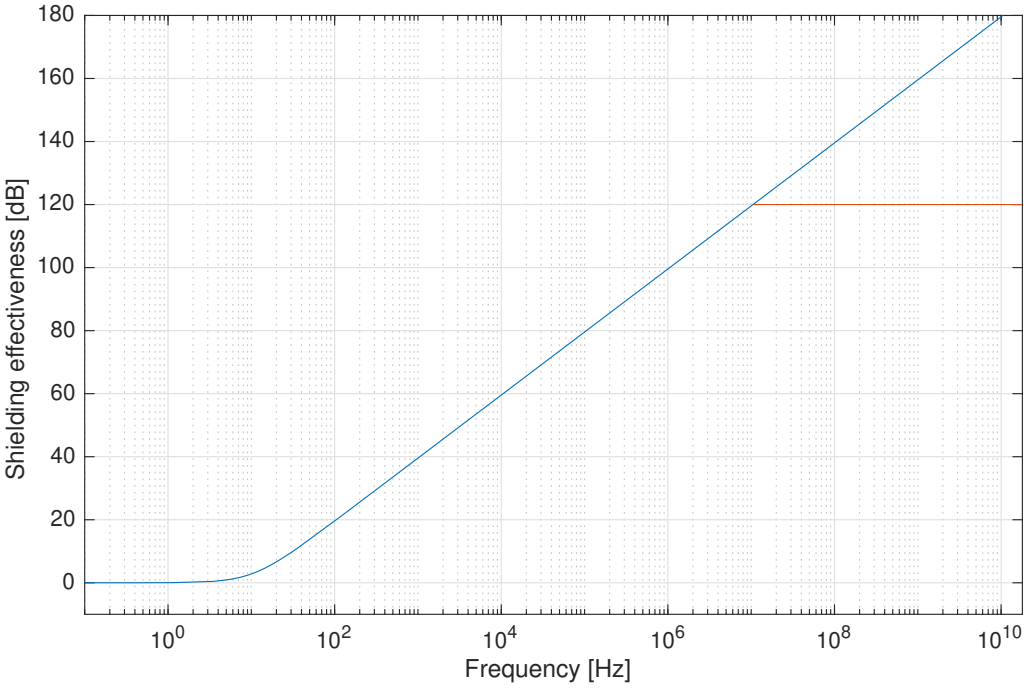

Figure 5.10: Calculated dampening based on the material choices made and the volume of the room represented as a perfect sphere. Logarithmic x-axis and linear y-axis. Orange line shows theoretical maximum dampening. Photo: Daniel Asle Vingen Endal.

5.1.3 Live high-voltage tests

Table 5.3: Containing measurement results from the high voltage experiment tests. From EB Consulting AS test report [39].

EB Consulting AS

HVL Screened room - High voltage tests						Date: week 47'2022, week 33'2022 and week 24'2021			
Source; high voltage insulator during test						**Measuring values**			
Source; high voltage insulator during test	**Floor**	**Meas. Point**	**Distance to high voltage source [m]**	**Test antenna (1)**	**Freq. [MHz]**	**Field strength/level [dBm] Comparing before and after shielding of high voltage laboratory**			
						Corona		**Flashover**	
Test location						Open door	Closed room	Open door	Closed room
Week 47, 2022 - Completed screened structure. HV test max: 380kVAC rms									
Elektrolab	4	M6	8	1	10 - 20	approx. -115 to -120	approx. -120 to -125	approx. -110 to -115	approx. -120
Elektrolab	4	MVin	2	2	75 - 125	N/A	approx. -85	N/A	approx. -80
Week 33, 2022 Completed screened structure. HV test max: 75kVAC rms									
Elektrolab	4	M6	8	1	10 - 20	approx. -115 to -120	approx. -125	approx. -110 to -115	approx. -120 to -125
Elektrolab	4	M7	6	1	10 - 20	approx. -115 to -120	approx. -125	approx. -110 to -115	approx. -120 to -125
Week 24, 2021 - before constructed screened structure. HV test max: 75kVAC rms									
Elektrolab	4	M6	8	1	10 - 20	approx. -100 to -110	N/A	approx. -80 to -90	N/A
Elektrolab	4	M7	6	1	10 - 20	approx. -100 to -110	N/A	approx. -80 to -90	N/A

Noise floor approx. -125dBm

After constructed screened structure room — approx. 30dB improvement of test results; (approximately 1000 times)

Test antennas (1) Rx					
Nr.	Type	Freq. Range:	Nr.	Type	Freq. Range:
1	R&S HE300HF	9kHz-20MHz	5	Anritsu isotrop	700MHz-6GHz
2	R&S Loop 1	20MHz-200MHz	6	Bilog	25MHz-2GHz
3	R&S Loop 2	200MHz-500MHz	7	Horn	1GHz-18GHz
4	R&S Loop 3	500MHz-7,5GHz			

Week 24 2021 & Week 33 2022

Table 5.3 shows the measured electromagnetic radiation leakage from the shielded structure in point M6 and point M8[1] (see figure 4.5 for relation to source) expressed in dBm at 6 and 8 meters from the source. Measurements were done with the screened door open and with a fully closed shielded room.

Following are pictures of the spectrum analyzer showing the registered values during our testing.

Images containing spectrum analyzer measurement results from week 24 of 2021 can be viewed in figure 5.11a and 5.11b for point M6.

Images containing spectrum analyzer measurement results from week 33 of 2022 can be viewed in figure 5.12a and 5.12b for point M6.

[1]Point M8 is in line with the dotted line from M6, but approximately 2 meters closer to the source.

Bilde 4 | eksempel korona og høyspent overslag i **uskjermet hsp-lab**

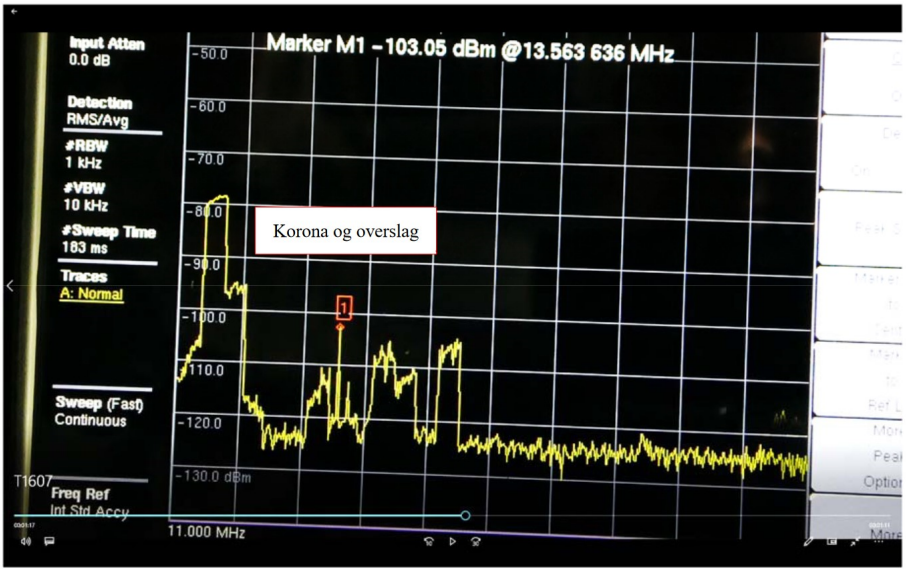

(a)

Bilde 5 | eksempel korona og høyspent overslag i **uskjermet hsp-lab**

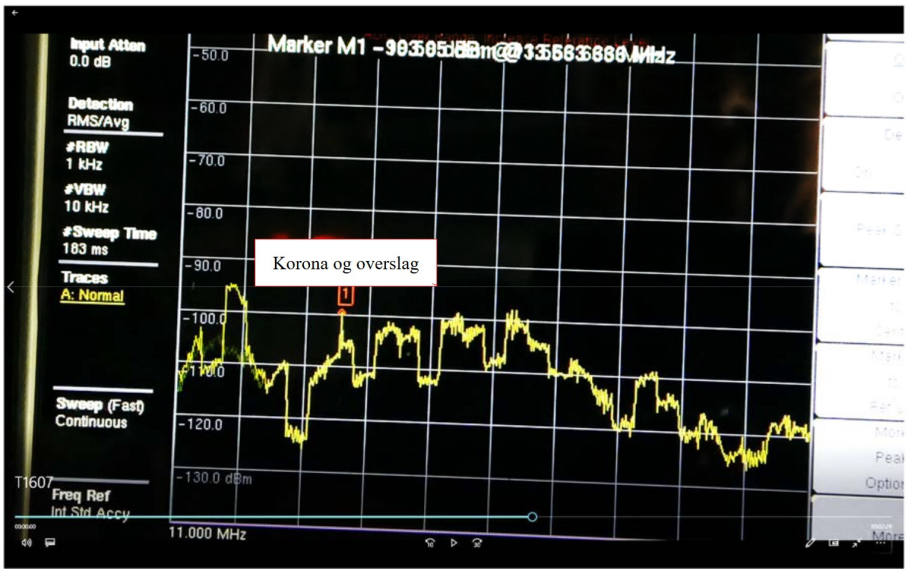

(b)

Figure 5.11: Pictures of spectrum analyzer during testing of week 24, 2021. Figures 5.11a and 5.11b show the measured electromagnetic field 6 meters away from the source. Large amounts of electromagnetic radiation that interfere with e.g. spike @ ca. 13MHz (shown in fig. 5.12a and 5.12b) for RFID door access card reader-system. The images are taken from the 3rd test report by EB Consulting AS [37].

Bilde 1 | eksempel måleresultat lukket dør

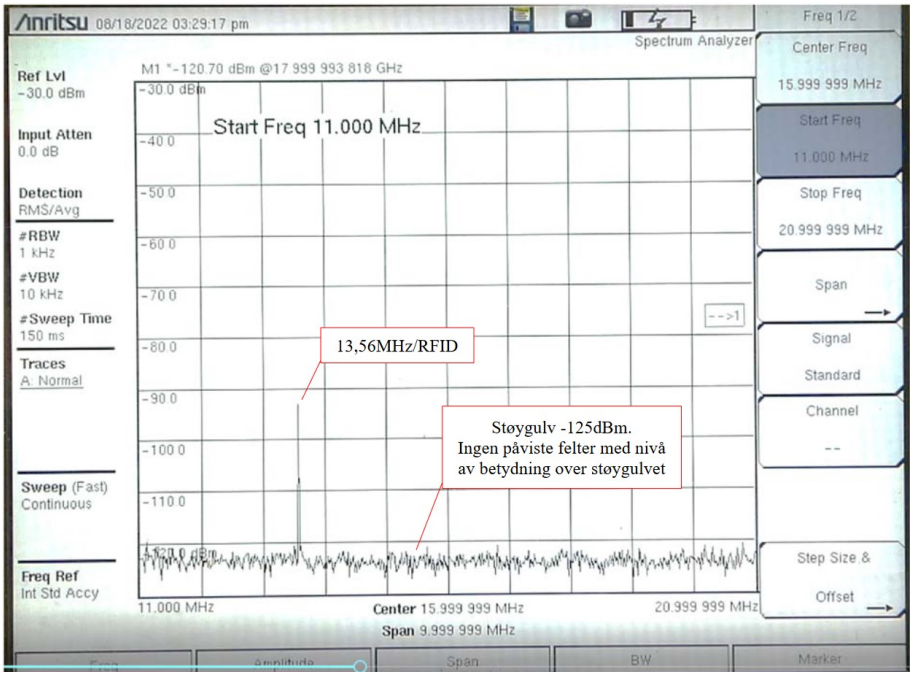

(a)

Bilde 3 | eksempel korona og hsp overslag **åpen dør**

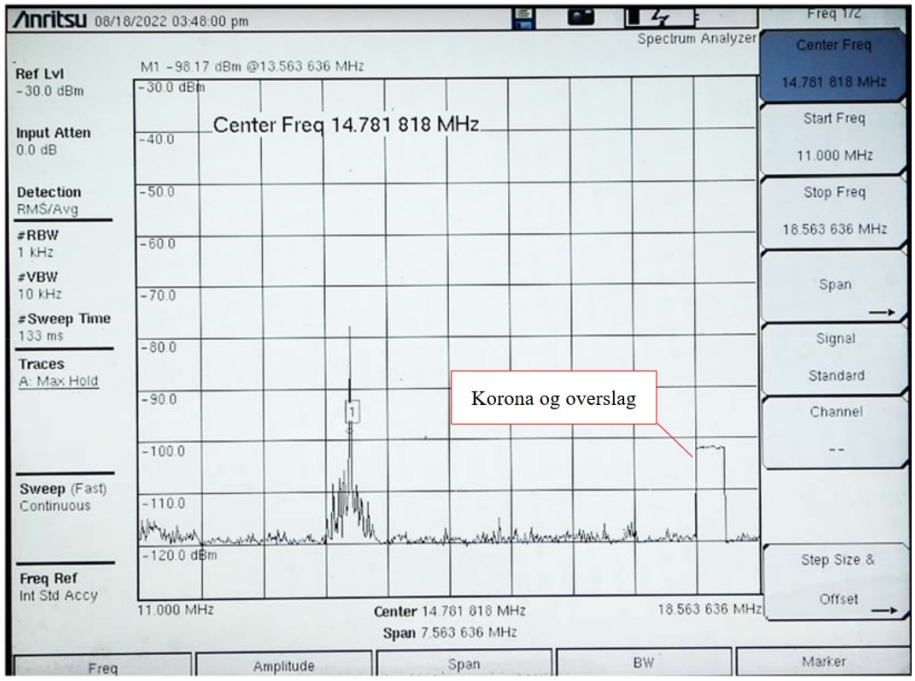

(b)

Figure 5.12: Pictures of spectrum analyzer during testing of week 33, 2022: The pictures show the measured electromagnetic field passing through the shielded enclosure. Spike @ ca. 13MHz is from the RFID access card reader for entering the "Elkraft lab" mounted on the wall outside the "Elkraft lab"-entrance. The images are taken from the 3rd test report, EB Consulting AS [37]. 5.12a: Sealed enclosure, no electromagnetic fields were measured. 5.12b: The door to access the inside of the Faraday cage was fully open. Some electromagnetic fields were measured.

Week 47 2022

Electromagnetic leakage from the shielded structure was measured in point M6 and point MVin (see figure 4.5 for relation to source). Images containing spectrum analyzer measurement results can be viewed in figure 5.13 a and b for point M6, and in figure 5.14 for point MVin.

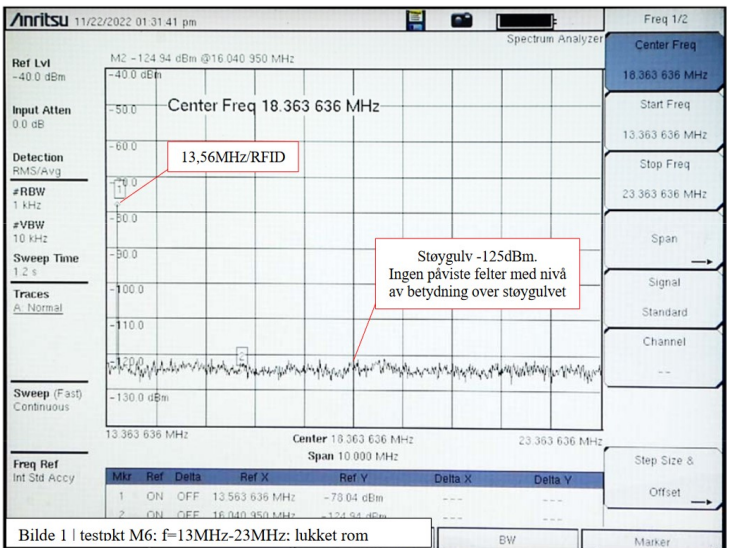

(a)

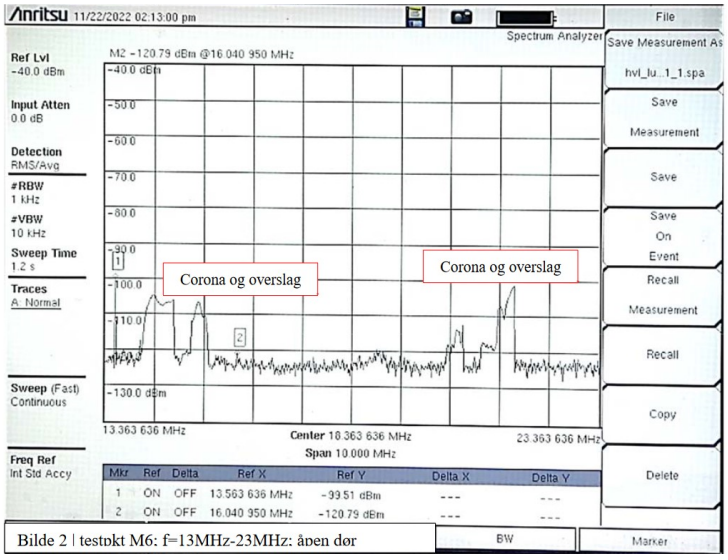

(b)

Figure 5.13: Pictures of spectrum analyzer during testing of week 47, 2022: The pictures show the measured electromagnetic field passing through the shielded enclosure. Spike @ ca. 13MHz is from the RFID access card reader for entering the "Elkraft lab" mounted on the wall outside the "Elkraft lab"-entrance. The images are taken from the 3rd test report, EB Consulting AS [39].
5.13a: Sealed enclosure, no electromagnetic fields were measured.
5.13b: The door to access the inside of the Faraday cage was fully open. Some electromagnetic fields were measured.

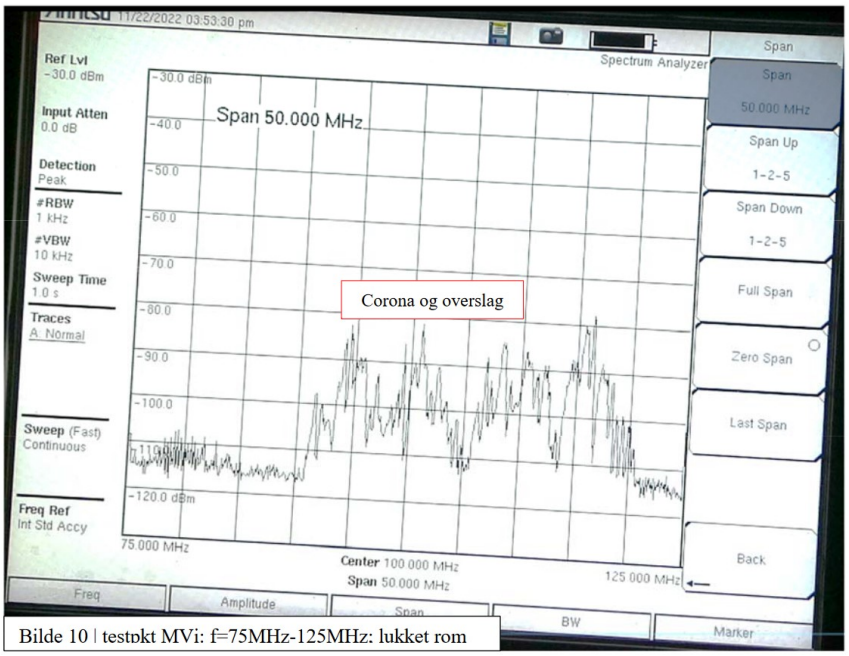

Figure 5.14: Picture of spectrum analyzer shows the EM field strength during corona and flashover measured through the shielded window with a frequency range of 75MHz to 125MHz. The images are taken from the 3rd test report, EB Consulting AS [39].

Comparing measured values from HV tests to ICNIRP guideline values

The power flux density in the measurement point can be estimated based on our recorded measurements with the calculation methods presented in chapter 4.4. Following is a presentation of tables containing the input data from specific points and the output data based on the two described methods.

For the logarithmic method, the measured power flux density in the point is estimated based on equations presented in chapter 4.4, being equations (4.1a) through (4.1d). Converted values for corona are shown in table 5.4. Converted values for flashover are shown in table 5.5.

For the numeric method, the measured power flux density in the point is estimated based on equations presented in chapter 4.4, being equations (4.2) through (4.5d). Converted values for corona are shown in table 5.6. Converted values for flashover are shown in table 5.7.

Table 5.4: Measured field strength during Corona passing through the shielded Faraday cage while the door was open and closed. Converted using the logarithmic method. Derivation with intermediate values can be found in table B.1.

Shielded Door	Freq. f [MHz]	Received power [dBm]	S - Eq. (4.1d) $[pW/m^2]$ (10^{-12})
Week 47, 2022:			
(M6)Closed	10 - 20	-125	0,4203 - 0,6662
(M6)Closed	10 - 20	-120	1,3294 - 2,1069
(M6)Open	10 - 20	-120	1,3294 - 2,1069
(M6)Open	10 - 20	-115	4,2039 - 6,6628
(MVin)Closed	75 - 125	-85	66,6283 - 105,599
Week 33, 2022:			
(M6)Closed	10 - 20	-125	0,4203 - 0,6662
(M6)Open	10 - 20	-120	1,3294 - 2,1069
(M6)Open	10 - 20	-115	4,2039 - 6,6628
Week 24, 2021:			
(M6)Open	10 - 20	-110	13,2941 - 21,0697
(M6)Open	10 - 20	-100	132,941 - 210,697

Table 5.5: Measured field strength during Flashover passing through the shielded Faraday cage while the door was open and closed. Converted using the logarithmic method. Derivation with intermediate values can be found in table B.2.

Shielded Door	Freq. f [MHz]	Received power [dBm]	S - Eq. (4.1d) $[pW/m^2]$ (10^{-12})
Week 47, 2022:			
(M6)Closed	10 - 20	-120	1,3294 - 2,1069
(M6)Open	10 - 20	-115	4,2039 - 6,6628
(M6)Open	10 - 20	-110	13,2941 - 21,0697
(MVin)Closed	75 - 125	-80	210,697 - 333,932
Week 33, 2022:			
(M6)Closed	10 - 20	-125	0,4203 - 0,6662
(M6)Closed	10 - 20	-120	1,3294 - 2,1069
(M6)Open	10 - 20	-115	4,2039 - 6,6628
(M6)Open	10 - 20	-110	13,2941 - 21,0697
Week 24, 2021:			
(M6)Open	10 - 20	-90	1329,41 - 2106,97
(M6)Open	10 - 20	-80	13294,1 - 21069,7

Table 5.6: Measured field strength during Corona passing through the shielded Faraday cage while the door was open and closed. Converted using the numeric method. Derivation with intermediate values can be found in table B.3.

Shielded Door	Freq. f [MHz]	Received power [dBm]	[W] (4.5a)	S - Eq. (4.5d) $[pW/m^2]$ (10^{-12})
Week 47, 2022:				
(M6)Closed	10 - 20	-125	3,162E-16	0,5585 - 0,6997
(M6)Open	10 - 20	-120	1E-15	1,7661 - 2,2129
(M6)Open	10 - 20	-115	3,162E-15	5,5850 - 6,9978
(MVin)Closed	75 - 125	-85	3,162E-12	68,9902 - 110,94
Week 33, 2022:				
(M6)Closed	10 - 20	-125	3,16228E-16	0,5585 - 0,6997
(M6)Open	10 - 20	-120	1E-15	1,7661 - 2,2129
(M6)Open	10 - 20	-115	3,16228E-15	5,5850 - 6,9978
Week 24, 2021:				
(M6)Open	10 - 20	-110	1E-14	17,6615 - 22,1293
(M6)Open	10 - 20	-100	1E-13	176,615 - 221,293

Table 5.7: Measured field strength during Flashover passing through the shielded Faraday cage while the door was open and closed. Converted using the numeric method. Derivation with intermediate values can be found in table B.4.

Shielded Door	Freq. f [MHz]	Received power [dBm]	[W] (4.5a)	S - Eq. (4.5d) $[pW/m^2]$ (10^{-12})
Week 47, 2022:				
(M6)Closed	10 - 20	-120	1E-15	1,76615 - 2,21293
(M6)Open	10 - 20	-115	3,162E-15	5,58505 - 6,99789
(M6)Open	10 - 20	-110	1E-14	17,6615 - 22,1293
(MVin)Closed	75 - 125	-80	1E-11	218,166 - 350,824
Week 33, 2022:				
(M6)Closed	10 - 20	-125	3,162E-16	0,558505 - 0,699789
(M6)Closed	10 - 20	-120	1E-15	1,76615 - 2,21293
(M6)Open	10 - 20	-115	3,162E-15	5,58505 - 6,99789
(M6)Open	10 - 20	-110	1E-14	17,6615 - 221,293
Week 24, 2021:				
(M6)Open	10 - 20	-90	1E-12	1766,15 - 2212,93
(M6)Open	10 - 20	-80	1E-11	17661,5 - 22129,3

5.2 Discussion

A brief introduction to the discussion The requirement from HVL of a minimum 25 dB dampening across all frequencies was not met regarding the original windows that were meant to be used. As previously detailed in chapter 3.1.1, some exceptions had to be made here due to special wishes from HVL of an analogue viewing experience. This demanded the use of actual windows with shielding capabilities in place of for example cameras streaming live video feeds to monitors mounted outside of the shielding enclosure. It was expected that the dampening values for the windows would be lower when compared to the dampening values of the wall since there would be a conductive mesh in place of the 2 mm thick steel plates used elsewhere in the room. It was also expected that choices for the mesh, such as the number of openings in the mesh per inch (OPI) and the thickness of the mesh, would affect the obtained dampening values for the windows. What was not anticipated was the difficulty of getting a good mechanical connection between the window mesh and the rest of the screened room. This resulted in lower dampening values in the LF magnetic range than anticipated based on information from the fabricator, as is shown in the initial results presented in figure 5.6 (for $f < 10\text{MHz}$).

As a note previously mentioned in the introduction, one of the triggering factors instigating the need for a Faraday cage in the high-voltage laboratory was that the nearby card readers stopped functioning correctly during high-voltage tests, preventing employees and students from getting in or out of offices and premises.

A less expensive version of the constructed solution would likely still fulfil the requirements and wishes put forward by the owner and at the same time provide sufficiently good shielding effectiveness. Choices that could lower the material costs include utilizing a metal fire door (in place of shielded door), thinner metal plates on surfaces, and windows that cannot be dismounted from the wall. Thinner metal plates would mean lower shielding effectiveness for magnetic fields, as it is the thickness of the shield that provides the attenuation for these frequencies. Another option for windows is to use vertical wires in front of glass windows, but this would likely yield poor SE values for both lower frequencies, as well as for higher frequencies. The cheapest option for windows would be to not include them, but this was unacceptable due to the impact it would have on the learning outcome for attending students. While such a solution would likely provide sufficient SE and dampen the EM radiation enough to be within the ICNIRP guidelines, this could possibly become a limitation for future iterations of the laboratory.

The candidate finds it important to note that the majority of costs connected with a contractor designing and building a Faraday cage is for the time used, while the costs associated with the components and materials for the Faraday cage are a fraction of

the cost compared to the hours and expertise spent designing a solution. In the case of implemented solutions with lower costs, it is conceivable that new and more expensive rounds of engineering would then be necessary when the need for upgrades arises, and a greater amount of funds in total would be used to get a final solution.

Surrounding the safety question in the introduction, a case is made that no shortcuts should be used when it comes to the aspect of safety. The regulations should be imposed on the Faraday cage/HV laboratory in order to ensure that no fatal currents are allowed to conduct through nearby humans. The discovery made by Askvik, Svensson, Hantveit, *et al.* mentioned in the introduction of chapter 3.2 regarding the buildup of electric potential in the window frames further justifies this. It is common knowledge for engineers working with electricity that currents as low as 30 mA are fatal when passing through the body. This can be achieved by following graphs published in regulations mentioned in chapter 3.2.1.

5.2.1 Discussion of IEEE 299 measurements

Steel surfaces The measuring results of the dampening across the steel surfaces that make up the Faraday cage are mostly as we expected.

As shown in figure 5.2, the lowest measured dampening values of each frequency is generally between 35 dB and 90 dB. The poorest performing surface seems to be the walls of the enclosure when looking at the minimum dampening value. The line representing the wall measurements should be seen in context with the recorded measurement results of table A.3, and the location of each relevant test point as presented in figure 4.1. It is then possible to make an educated deduction that most of the low values presented in figure 5.2 are from the test points V8 and V7.

With the test point V8 being the nearest neighbour to the screened windows, it should be considered that there is a high probability that the poor values for the measured performance are due to leakage through the shielded windows. This is further backed up by the apparent correlation of the outlier frequencies of the steel surfaces (1MHz, 65MHz, 140MHz, 170MHz) when comparing to the performance of the windows in figure 5.3. While the steel surface of point V8 show improvement upon the dampening of the windows for $f = 1MHz$, the performance for the rest of the previously mentioned frequencies is tangent to the attenuation for the respective frequencies in the windows. It is therefore probable that the cause for the poor performance of the steel surfaces is in reality leakage from the windows.

Based on measurement results presented in table A.3, the performance of the steel surfaces when ignoring test point V8 is generally between 60 dB and 80 dB, and up towards 90-100

dB in many cases. This is well above the required 25 dB dampening from HVL.

This is further reflected in the shielding performance of both the floor and the roof, with the exception of the single entry of 28 dB dampening @ 915MHz in test point T1 (point in the roof). The reason for this low measured value is somewhat unknown, and it is taken note of this sudden drop in dampening compared to the 80+ dB dampening measured for T2 and T3 for the same frequency. Still, the measured value is above (or at) the required 25 dB (even if adjusted for measurement accuracy), and thus not necessarily a problem.

For the measurement results of the floor, It should be noted that there is an extra metal plate of corrugated steel sheet suspended from the roof above the test volume and that an equivalent plate is present on the floor that the testing equipment is placed on top of. Both of these plates are connected to the ground as described in section 3.3. It should be noted that we were having difficulties acquiring measurements when using the bilogical antenna because of the false roof and permanently mounted plumbing and various structures present in the false roof on the third floor. As a result, the distance between the antennas exceeded the intended measurement distance of 1 meter that they were calibrated with, resulting in a most likely higher measured dampening value. The immediate vicinity of the suspended profiles supporting the false roof may have affected the antenna impedance as well. However, since there were no such problems with the measurements for the roof, it is likely not an alarming amount of possible sources of error that this will amount to, since it is the same dimensions for the steel plates used for both roof and floor, and the only difference between the roof and the floor is the construction method; the construction method in the floor should be providing better shielding than the construction method in the roof (welded plates for the floor versus lask connections for the roof).

Windows As described in chapter 3.3, the original windows were mounted in a cradle-like steel profile fabricated in-house that held the windows in place while sandwiching the laminated mesh in the windows to the Faraday cage. This resulted in lower dampening values than expected in the magnetic waveband, as seen in frequencies 10kHz - 1MHz in table A.1 and in figure 5.1.1. The mounting solution for the windows had to be adjusted. Before finalizing tests in August 2022, the screened windows were changed to windows using a more serviceable fastening solution constructed by the manufacturer. The new solution uses threaded steel rods welded around the perimeter of a steel window frame, steel nuts then tighten down on a steel border which holds the gasket that ensures a satisfactory connection/seal around the laminated window panes to the main structure of the Faraday cage [37].

Figure 5.5 presents the quality of the connection that each of the window frames provides

for the individual window by the lowest measured dampening value of each window frame. What is interesting here is that the common denominator for these windows is a poor shielding performance in the LF band, which is also reflected in figure 5.4, but not to the same extent as for the frames.

When comparing the measured dampening values in figure 5.6 and 5.3 by examining the problematic frequency range of 10kHz-1MHz, some improvements can be observed for all of the frequencies, ranging from a couple of dB for 10kHz and 156kHz, and up to a 10 dB improvement for 1MHz in window centres. One explanation for poor values for shielding effectiveness could be the thickness of the mesh in the windows. In order to maintain visibility, the mesh cannot be of great thickness. This can be a preventative factor for the attenuation of magnetic fields in frequencies of 10MHz and below.

Because the SE characteristic of the window centre increases at greater increments than the SE of the frame, one can speculate if the poor dampening in the transition is due to a variety of factors such as; mounting pressure, frame surface area, gasket surface area, etc.

One possibility is that the thickness of the mesh has less impact on the connection quality, while the size or number of openings in the mesh might be a factor, albeit small. This is a possibility because these factors can directly affect the surface area impressed on the shielded structure by the gasket (while the mesh thickness does not).

In figure 5.6, observe the old original windows which seem to have quite good dampening properties in the LF-end of the electric field portion of the spectrum we have analysed when compared to the results of the new solution shown in figure 5.4. This may be because of the potentially larger surface area of the conductive mesh that was clamped between the cradle-like mounting mechanism and the Faraday cage for the original windows, but as we can also see, the attenuation is still not good enough in the magnetic field portion of our spectrum (below 10MHz). This was, however, expected based on the laboratory test results shown in figure D.4 from the manufacturer and accepted as a compromise prior to the installation of the windows.

In hindsight, it could be speculated whether or not changing out the windows was the best choice; if sacrificing up to 13 dB dampening (when comparing centre values of window 3 @ 52MHz) is worth the improvement of 2-6 dB better dampening for 10kHz (when comparing lowest overall measured centre values). In reality, it is known that the lowest frequencies for the windows are the weakest points for the Faraday cage. It is therefore likely a better solution to improve these weaknesses when the overall dampening characteristics of the enclosure, in spite of the impacts, are still maintained.

Access hatch (AH) The graph for the dampening response of the steel access hatch is depicted in figure 5.2. Both from this figure and from table 5.1, we can see that the access hatch has the best low-frequency dampening response of all the test points, with the lowest dampening value across all frequencies in the series being 52 dB. It is reasonable to question what gives this response. Possible explanations may include the thickness of the material being different or the antenna impedance being influenced by nearby conducting metals. We can see in figure 3.4c that the access hatch is bolted securely to the Faraday cage. With the correct gasket and correct mounting pressure, attenuation properties like the one seen in the above-mentioned graph can be obtained. But if this is a result of the antenna impedance being influenced or an increase in the distance between the antennas, we should have seen an increase in the dampening response across the whole spectrum. With the assumption that the above statement is true, we can state that the high measured value for dampening is because of the proper mechanical- and electrical connection between the AH panel and the Faraday cage.

Shielded door While the dampening performance shown in 5.9 of the shielded door without the secondary gasket was for the most part adequate, there were some deviations from the required 25 decibels. The first measurements were conducted on a single test point on the side of the door adjacent to the windows. The performance could have been affected by the poor dampening of the windows for the lower deviation, but when looking at figure 5.6, the window dampening may not explain the deviation from the requirement at 140MHz.

If we look for an explanation by examining the dampening of wave trap No.4 adjacent to the door, figure 5.8 shows that the minimum dampening of all the wave traps at the frequency in question was well above the requirement. However, we see that the wave traps also have a deviation; this will be discussed later in the appropriate section. Thus, the wave trap cannot be blamed for this deviation either and the deviation is most likely caused by the missing secondary gasket.

When looking at figure 5.7 which depicts the minimum dampening of the shielded door after the secondary gasket has been fitted, we can see that both deviations have been remedied and that the door has dampening characteristics above the requirement across all frequencies.

The candidate would like to mention that in table A.4, the values from measuring points D6 and D7 are not included as the lowest measured dampening response in figure 5.7 because these values are directly next to the shielded windows, as shown in figure C.5. When looking at the measured dampening response of the frame for window 1 (the window

adjacent to the shielded door) for these frequencies[2], it becomes clear that the values recorded in points D6 and D7 are not representative of the dampening response of the door in these points.

It would be misleading to use the values for these frequencies in these door test points, and they have therefore been overridden by values from the half of the door furthest away from the shielded windows. It is however interesting how the dampening value for the door along the edge of the window is lowest in the middle of the door/bottom of the window frame (9 dB), followed by the bottom of the door (15 dB), and then the top of the door/top of the window frame (25 dB).

The candidate expected that the top of the door would have a lower value for shielding effectiveness compared to the bottom of the door because of the proximity to the top portion of the window, in contrast to the over 50 cm distance between the bottom of the door and the bottom of the window. Overall, when comparing the shielding effectiveness in point D7 with the secondary gasket (tab: A.4) and without the secondary gasket (tab: A.5), we do see an overall general improvement across most frequencies.

Considering the impact that the window has on the SE values of the door, we find that the shielding performance of the door lives up to the requirement made by HVL.

Single Entry frames Measurement results of the single entry frames can be viewed in figure 5.7, which presents the lowest measured attenuation value of each frequency.

In this high-voltage test laboratory, there are 2 single entry frames; the one for cables is termed "SE1" and is located below the shielded window number 3, and the second one is termed "SE2" and is located near the ceiling towards what would be the north-west corner of the room. It lets the tubes for the Novec fire suppression system pass through the shielded wall.

While all the recorded dampening values for the single entry frames are above the required 25 dB, we do see some values being a bit lower than what we would expect from the SE-frames. It is specifically the values for SE1 that are a bit lower when compared to SE2, with SE1 often providing around 50% of the dampening that SE2 provides, and sometimes less than 50% too. In fact, over 30% of the measured values for SE1 are performing below 60% of the performance in their corresponding frequency provided by SE2. SE1 actually provides all of the minimum values for the single-entry frames. If we see the values for SE1 in relation to the values for Window 3, it can be observed from the measured values that there may be some leakage through the window frame. This could also be a result of either all the cables that are passing through the SE-frame forming loops and acting as antennas

[2]Window 1, "Rig.": 5 dB @ 10kHz and 10 dB @ 156kHz. Rig. = short for right.

for some of the frequencies, even though they were grounded during the measurements, or that it is not the best connection between the SE-frame and the structure of the cage. The location of SE1 is also rather unfortunate. Not only is it located near the weakest portion of the shielded enclosure, but it is also located near two corners, which further impacts the shielding performance of the single entry frame.

Typical shielding effectiveness values should be around 40-80 dB.

The SE-frames are provided by manufacturer Roxtec INT. Sweden and need to meet certain requirements from the factory to pass QC, so this is most likely not the fault factor. It should however be noted by the reader that there were only conducted measurements for the window frames for the lowest frequencies, in the magnetic portion of the frequency band, and that we could be more certain and have a more thorough discussion if dampening values around all of the frames were recorded as well, but that would mean the need to conduct at least an additional 270 measurements, as is indicated by the white spaces from 52MHz to 18GHz in table A.2.

Since we recorded dampening values above the required 25 dB for both all of the windows and SE-frame 1, this was deemed unnecessary in the work of performing QC on the Faraday cage. However, it would provide greater insight and a possible explanation as to why the recorded attenuation values for SE1 are so much lower than the values for SE2.

It will be noted as a possible addition for future work since it would be interesting to know if the sub-optimal performance is due to the windows/transition from the windows to the Faraday cage, or if there is a different reason than the ones mentioned above, or possibly an entirely different reason we are not yet aware of.

Additionally, the location of SE1 being located so close to several angles/corners could have a negative impact on the shielding effectiveness.

I would like to end the discussion of the single-entry frames by stating that the measured performance is, in spite of being termed "sub-optimal" by the candidate, still above the required dampening and will perform adequately.

Wave traps for air Measurement results of the wave traps for air can be viewed in figure 5.7, which presents the lowest measured attenuation value of each frequency. The location of each wave trap can be seen in images C.1, C.2 and C.5 in appendix C.

We can see the initially measured dampening response recorded in table A.6 portrayed figure 5.8 and as mentioned previously in the discussion for the shielded door, we can see at first glance that there is only one deviation in the measurements taken in May for the wave traps; but this is fixed by the time we acquire new measurements in August after

adding the secondary gasket as indicated by figure 5.7.

The shielding performance of all the wave traps is above the required dampening after the new windows are mounted and the secondary gasket is installed on the door. Still, we should examine our recorded measurement results and see if there is anything we can learn from them. All the measured values are however above the requirement, except for the 10kHz frequency for wave trap 5 located above the shielded windows.

This measurement is probably below the requirement due to all the penetrations and holes on this side of the room. Wave trap 5 being located close to both the windows and to the edge of the Faraday cage where the wall meets the roof may also be a factor that impacts the dampening at this point.

The measurement results for wave traps 1 through 5 can be observed in table A.7 by the entries of BF1-BF5 that the general values of these measurements are quite good, with almost 85% of the values above a dampening value of 45 dB and usually ranging all the way up to around 70 dB dampening. The remaining 15% of the values are between 30 dB and 45 dB, with the exception of dampening values at 10kHz and 156kHz for wave trap No.5.

As shown in appendix D.2, the dampening response is greatest around 40-50MHz, which can be seen some tendencies for in some of our measurements (see values for BF1-BF3, A.7). The likely reason that the wave traps do not follow the dampening response to a point is because of the generally sub-optimal placements of the wave traps; by that, I am meaning they are all located near an edge in the Faraday cage shielding structure and not directly in the middle of a surface as it should preferably be.

5.2.2 Discussion of theoretical calculations

The theoretical calculations presented in chapter 5.1.2 with the method presented in chapter 3.1.3 are based on the assumption that the volume of the test room is a uniform sphere, and with assumed values for the properties permeability and permittivity of the materials used. The manufacturer of the steel plate did supply a value for electric resistivity ρ. This means that, while the calculations are supposed to give an indication of what dampening values we can expect, they cannot be compared directly. We can see in figure 5.10 that the theoretical dampening has an exponential growth[3] as the frequency increases. A theoretical maximum dampening of 120 dB is then enforced when calculations go above this level of dampening.

Further, we know that for the higher frequencies, standing wave patterns can emerge in

[3]Due to the logarithmic x-axis, the growth appears as linear.

the shielding enclosure based on the dimensions of the room. The presence of large pieces of test equipment and other large objects that have been placed in the test room can affect what frequencies the standing wave patterns appear at.

The standing waves can lead to a diminished dampening in the shield structure than what is indicated by the theoretical calculations.

It is difficult to determine which frequencies will provide standing waves for any shielded enclosure as this is based on previously mentioned factors. The equipment can also easily be moved around and/or be replaced with other equipment, which means that the frequencies where standing waves will occur easily and often change.

There will therefore be a drop-off in shielding performance at higher frequencies, but it is difficult to determine these through theoretical calculations because of the many changing variables.

5.2.3 Discussion of live high-voltage measurements

A discussion around the actual performance of the shielded structure is due after conducting several high-voltage tests.

Week 24, 2021 EB Consulting AS conducted leakage measurements in 2021 during HV tests with a test voltage of 75kV RMS in order to establish a baseline of the existing conditions before the shielded structure was built. In table 5.3, we can see that the measured electromagnetic radiation during corona and flashover had an amplitude around 15-25 dBm and 35-45 dBm (above the -125 dBm noise floor) respectively at both measuring points. NB. Registered values of maximum -80 dBm. The values mentioned above are relative. Where -80 dBm is equal to $1 \cdot 10^{-11}$ W, while 45 dBm is equal to approximately 31 W. With no shielding present, no measurements with a closed shielded room were conducted. This establishes the baseline that the performance of the constructed shielded enclosure is compared to.

The estimated power flux density is presented in tables 5.4 - 5.7 show that the recorded values are within the 2 W/m^2 of the ICNIRP guidelines for 30 minutes of exposure during both corona and flashover.

Please see the note about measurement uncertainty at the end of the discussion for "Week 47, 2022" (5.2.3) surrounding estimated values based on measurements from HV tests.

Week 33, 2022 Replication of the experiments done in 2021 was conducted at the end of week 33, 2022. Two additional values were recorded this time, being values for corona and flashover with a closed Faraday cage. Table 5.3 shows that the amplitude of

the measuring results was reduced from an amplitude of 15-25 dBm to an amplitude of 5-10 dBm for corona phenomena with the door of the Faraday cage in the open position. Furthermore, we can see that for the closed room, the measured response is the same as that of the noise floor; -125 dBm. This indicates that no electromagnetic radiation escapes from the shielded Faraday cage in the measured frequency band of 10-20MHz while corona is occurring inside the Faraday cage.

During flashover, we can see in table 5.3 an improvement from the previously mentioned amplitude of 35-45 dBm baseline to a measured amplitude of the electromagnetic radiation of 10-15 dBm. This is an improvement of at least a 20 dBm decrease (in amplitude) in a worst-case scenario, and up to a decrease of 35 dBm (in amplitude). All the while the door of the shielded enclosure was open during these measurements.

With a closed shielded enclosure, a response was measured during flashover with peaks of electromagnetic radiation with a peak amplitude of 5 dBm being measured above the noise floor for the frequency band 10-20MHz.

The amount of energy that passes through the shielded enclosure can be converted from dBm to W/m^2 as shown in tables 5.4, 5.5, 5.6 and 5.7. As we can see in the tables, we have done measurements with both a "compromised" shielding solution where the door was open and with a fully enclosed Faraday cage shielding structure. The test room shall only be used while the test room is fully closed and constitutes a completely shielded structure. It is therefore quite interesting to see that the highest values recorded for estimated flux density are in the tables for flashover (tables 5.5 and 5.7) with the shielded door open, and the measured values are in the range of 20-23 pW/m^2. Based on the guidelines on consumer electronics presented in [21, p. 12] and the ICNIRP guidelines, this is well within the 2 W/m^2 power density limit for frequencies up to 200MHz. Something very interesting is when we take a look at figure 5.12a, we can see that there is a radiation peak with an amplitude of -93 dBm which has been identified as the RFID card reader system for the doors at Western Norway University of Applied Sciences. This measurement is larger than any of the measurements that we recorded when testing the Faraday cage with an RMS voltage of 75kV. This means that the card readers are emitting more energy into the air than the high-voltage laboratory is doing during experiments.

Please see the note about measurement uncertainty at the end of the discussion for "Week 47, 2022" (5.2.3) surrounding estimated values based on measurements from HV tests.

Week 47, 2022 A new round of experiments was done in week 47, 2022. This time, original test point M6 and new test point MVin located approximately 2 meters away from the source were utilized. The voltage utilized during these tests was increased from 75kVAC RMS to 380kVAC RMS.

Table 5.3 shows the amplitude of the measured values in point M6 had the same values as during testing with a voltage of 75kVAC RMS for corona with open and closed structure, as well as during flashover with a closed room.

The recorded values indicate that little electromagnetic radiation escaped from the Faraday cage during testing in the frequency range of 10-20MHz while the corona is occurring inside the Faraday cage.

During flashover, we can see in table 5.3 that a small increase for values measured in M6 (10-20MHz) during flashover to approximately -120 dBm instead of ranging between -125 to -120 dBm. This is likely because of the large increase in voltage used.

For the new test point situated 2 meters from the source outside the window, new values were recorded during corona and flashover while the door to the Faraday cage was closed. The recorded values lack data to compare with previous tests, but one is still able to extrapolate information from these data values.

A value of approximately -85 dBm was recorded for leaked electromagnetic radiation through the shielded window during the corona. A new value of -80 dBm was recorded at the time of the flashover. These measurements were conducted in the frequency range of 75-125MHz.

The amount of energy that passes through the shielded enclosure can be converted from dBm to W/m^2 as shown in tables 5.4, 5.5, 5.6 and 5.7. Since the recorded values from point M6 are the same during tests with an HV voltage of 380kVAC and an HV voltage of 75kVAC, I refer to the discussion for week 33 for these values.

The point MVin sports the highest recorded measurement values obtained during testing. The leaked electromagnetic radiation during corona reaches values ranging between 60 and 120 pW/m^2. Further, the same measurements during flashover reach values ranging from 210 to 350 pW/m^2, depending on what frequency the radiation leaks through the Faraday cage.

Looking at and comparing the images in figures 5.14 and 5.13, the amplitude of flashover in point MVin approaches the recorded value of the RFID signal from the card reader. However, this is likely nothing to worry about, as the frequencies have a separation between them and no problems entering or exiting the high-voltage laboratory/"Elkraft labben" was experienced during testing. In addition, the windows do not point in the direction of any card readers in the building, and the radiation will therefore not be able to affect them.

An interesting aspect of the values presented in the Week 47 portion of the tables 5.4 -

5.7 is that they have the same amplitude of received power (-80 dBm) on the spectrum analyzer as the baseline measurements from 2021, but they are not able to carry the same amount of flux density. This is because the measurements through the windows are recorded at a higher frequency (75-125MHz) than the baseline frequency (10-20MHz) when no Faraday cage was present.

Based on the guidelines on consumer electronics presented in [21, p. 12] and the ICNIRP guidelines, this is well within the 2 W/m^2 power density limit for frequencies up to 200MHz when all values for estimated power flux density have a denominator of pico-Watt per square meter.

It should be mentioned that the estimated values listed in tables 5.4 - 5.7 are not 100% equal between the tables. This is due to uncertainty about how the gain (dBi) for the antenna that has been used should be implemented for the logarithmic method. Despite the exclusion of the mentioned gain factor, the estimated values are similar enough to each other. After a discussion with EBC, the candidate has taken the decision that it will still give a representative image if the gain for the antenna is omitted in the logarithmic method. This has been done due to a lack of time and the desire to include more than a single method to provide the best possible basis for comparison. This also applies to the discussion of HV test results for weeks 24 (2021) and 33 (2022).

Chapter 6

Conclusions

Quality control measurements of shielding effectiveness for a tailor-fitted Faraday cage, as well as electric field and electromagnetic radiation measurements during live high voltage experiments, have been conducted in this thesis to compare and analyse the recorded values with theoretical calculations and regulations that dictate the required performance of a shielded structure.

As presented in the results chapter 5.1 and discussed in chapter 5.2, it is now concluded that the Faraday cage has a satisfactory shielding effectiveness, it includes an analogue viewing experience for observers, and the wishes of the Western Norway University of Applied Sciences have been met on as many levels as possible.

The card reader outside the "elkraft lab" emits a peak value above recorded values for corona phenomena and flashovers occurring inside the high-voltage test chamber during tests. This is shown in figure 5.12b of chapter 5.1.3, where test voltage is 75kVAC RMS and the shielded door was open.

Image in figure 5.12a shows that no leaked EM radiation is detected during testing with a sealed Faraday cage at 75kVAC RMS.

During HV tests with test voltage 380kVAC RMS, the results for 10-20MHz were mostly similar except for some increases in leaked electromagnetic radiation during flashover when compared to tests at 75kVAC rms. Measurements made at viewing distance in front of the windows at 75-125MHz registered leaked radiation values with peaks reaching as high as -80 dBm (equal to the peak signal strength of the card reader). The card reader peak value is close to the peak measured EM radiation without the Faraday cage present. The measured value is estimated to a power flux density of approximately 19900 pW/m^2 (avg.) measured at point M6. The estimated power flux density through the shielded windows is equal to approximately 290 pW/m^2 (avg.) measured at point MVin. Because of the higher measuring frequency in point MVin, the power flux density of the leaked EM radiation at this point is estimated to be significantly lower values than the

equivalent peak for the card reader in point M6.

Since it has been chosen to use windows to provide an analogue way of observing experiments, it is necessary to utilize a big portion of funding on shielded windows. This was in order to achieve acceptable shielding effectiveness for frequencies below 10MHz. The difficulties with obtaining higher SE values for these low frequencies is partially because of how thin the mesh is, compared to the steel walls of the enclosure. Thicker material provides better attenuation for magnetic fields, as mentioned in chapter 5.2.1.

As mentioned at the beginning of the discussion chapter, a cheaper alternative would have been entirely possible to achieve if the presented solutions were to be implemented in place of the chosen alternatives.

So in relation to my presented hypothesis:

Yes, it is possible to achieve a cheaper and still satisfactory solution for a shielded enclosure. And yes, a full-fledged Faraday cage is also necessary to provide a safe working environment for employees with offices close to the laboratory premises and to provide a safe teaching environment for the students who will participate in classes.

Chapter 7

Future work

For future work, it would be helpful to look at the following list in order to get a better understanding of the workings of designing and constructing a Faraday cage:

1. Acquire more exact values for the properties of materials being used in the shielded enclosure, either by measuring (requires investment in instruments) or by obtaining values from a reliable source, such as a manufacturer or sending samples to a metallurgy laboratory facility.

2. Measure the specific resistance of the steel plating being used in the shielded structure.

3. Acquire better values in order to better calculate the expected shielding performance of the enclosure.

4. Conduct measurements and obtain dampening values for all around each window frame for all of the frequencies in order to examine if the window is at fault for the sub-expected (but adequate) shielding performance of Single Entry frame 1.

5. Obtain a correct inclusion of the antenna gain (dBi) for the logarithmic conversion method (in chapter 4.4).

Bibliography

[1] V. F. Hermosillo Worley, "Design of the ohio state university high voltage laboratory," Ph.D. dissertation, The Ohio State University, 1987. [Online]. Available: http://rave.ohiolink.edu/etdc/view?acc_num=osu1126811509.

[2] J. Bridges, "An update on the circuit approach to calculate shielding effectiveness," *IEEE Transactions on Electromagnetic Compatibility*, vol. 30, no. 3, pp. 211–221, Aug. 1988, Conference Name: IEEE Transactions on Electromagnetic Compatibility, ISSN: 1558-187X. DOI: 10.1109/15.3299.

[3] M. N. O. Sadiku, *elements of electromagnetics*, 3rd ed. 2001.

[4] H. D. Young and R. A. Freedman, *University Physics with Modern Physics*, 14th ed., in collab. with A. L. Ford. Pearson, 2016, 1596 pp.

[5] Britannica.com. "Electromagnetic radiation — spectrum, examples, & types — britannica." (), [Online]. Available: https://www.britannica.com/science/electromagnetic-radiation (visited on 11/17/2022).

[6] UiB. "The electromagnetic spectrum," University of Bergen. (Sep. 23, 2022), [Online]. Available: https://www.uib.no/en/hms-portalen/75292/electromagnetic-spectrum (visited on 11/21/2022).

[7] U. of New South Wales Sydney. "dB: What is a decibel?" Physclips. (Nov. 6, 2010), [Online]. Available: https://www.animations.physics.unsw.edu.au/jw/dB.htm (visited on 12/16/2022).

[8] "Decibel — definition, formula, & facts — britannica." (), [Online]. Available: https://www.britannica.com/science/decibel (visited on 12/16/2022).

[9] AstrodyneTDI. "Conducted EMI vs. radiated EMI — what's the difference?" (Apr. 23, 2021), [Online]. Available: https://www.astrodynetdi.com/blog/conducted-emi-vs.-radiated-emi-whats-the-difference (visited on 04/27/2022).

[10] *Electromagnetic, adj.* In *OED Online*, Oxford University Press. [Online]. Available: https://www.oed.com/view/Entry/269884 (visited on 12/14/2022).

[11] T. Holtebekk and L. F. Sidselrud, *lyn*, in *Store norske leksikon*, Sep. 19, 2022. [Online]. Available: http://snl.no/lyn (visited on 10/10/2022).

[12] F. materielverk, "PART-3 INSTALLATION AND SHELL PROTECTION," p. 138, Apr. 25, 2005.

[13] CODATA, *Recommended values of the fundamental physical constants*, May 20, 2019. [Online]. Available: https://www.physics.nist.gov/cuu/pdf/wall_2018.pdf (visited on 11/07/2022).

[14] J. D. Kraus and K. R. Carver, *Electromagnetics international student edition*, 2D ed. New York: McGraw-Hill, 1981, 828 pp., Open Library ID: OL18910696M, ISBN: 0-07-085388-6.

[15] A. B. Eriksen, *Graphed function showing regions of theoretical shielding effectiveness calculated using circuit method*, Dec. 15, 2022.

[16] COWI, "HVL kronstad høyspent lab beskrivende del."

[17] NEK, *NEK400:2018 - Elektriske lavspenningsinstallasjoner*, 6th ed. Oslo: Norsk Elektroteknisk Komite, 2018, 508 pp.

[18] ICNIRP, "Guidelines for limiting exposure to electromagnetic fields (100 kHz to 300 GHz)," *Health Physics*, vol. 118, no. 5, pp. 483–524, May 2020, ISSN: 1538-5159, 0017-9078. DOI: 10.1097/HP.0000000000001210. [Online]. Available: https://journals.lww.com/10.1097/HP.0000000000001210 (visited on 11/29/2022).

[19] E. C. Brantzeg, *DSA og ICNIRP.pptx*, Nov. 22, 2022.

[20] DSA. "Om oss," DSA. (Sep. 23, 2020), [Online]. Available: https://dsa.no/om-oss (visited on 11/30/2022).

[21] DSA, P. og teletilsynet, and S. strålevern. "Radiofrekvente felt i våre omgivelser: Målinger i frekvensområdet 80mhz - 3ghz." (Jun. 2011), [Online]. Available: https://dsa.no/publikasjoner/_/attachment/inline/fe3a0b55-71da-40a3-9a6e-0f240b028da4:a80390486270a2b630f7df61795f39652f2e2823/StralevernRapport_06-2011.pdf (visited on 11/27/2022).

[22] E. C. Brantzeg, *Dempingskrav faradaybur*, E-mail, Oct. 24, 2022.

[23] LOVDATA. "Forskrift om elektriske lavspenningsanlegg - lovdata." (Mar. 22, 2022), [Online]. Available: https://lovdata.no/dokument/SF/forskrift/1998-11-06-1060#KAPITTEL_6 (visited on 12/13/2022).

[24] NEK, *NEK440:2015 - Stasjonsanlegg over 1kV*. Oslo: Norsk Elektroteknisk Komite, Sep. 1, 2015, 184 pp.

[25] NEK, *Forskrift om elektriske forsyningsanlegg med veiledning*, 2nd ed. no#: Norsk Elektroteknisk Komite, Nov. 2006, 100 pp., ISBN: 82-91974-16-0. [Online]. Available: http://urn.nb.no/URN:NBN:no-nb_digibok_2014061205052.

[26] E. C. Brantzeg, *Beskrivelse vei til grunn*, E-mail, Oct. 27, 2022.

[27] K. Buitron, "Designing for a low resistance earth interface (grounding)," p. 16, Oct. 2007.

[28] S. Sidler. "Does aluminum rust?" The Craftsman Blog. (Dec. 17, 2018), [Online]. Available: https://thecraftsmanblog.com/does-aluminum-rust/ (visited on 11/04/2022).

[29] E. Bardal, *Korrosjon og korrosjonsvern*, 2. utg. Trondheim: Tapir, 1994, 337 pp., Accession Number: 999429611884702202 Publication Title: Norbok Source: NO-OsNB, ISBN: 978-82-519-1173-3. [Online]. Available: https://urn.nb.no/URN:NBN:no-nb_digibok_2008010300047 (visited on 11/04/2022).

[30] K. S. Lim, N. Yahaya, S. R. Othman, S. Fariza, Norhazilan, and N. Noor, "The relationship between soil resistivity and corrosion growth in tropical region," *The journal of corrosion science and engineering*, vol. 16, pp. 1–11, Feb. 2, 2013.

[31] T. Moberg, *VS: Jord HVL*, E-mail, May 20, 2022.

[32] A. B. Eriksen, *Overview of HV laboratory at western norway university of applied sciences, campus kronstad*, Dec. 16, 2022.

[33] MatWeb.com. "ASTM a525 galvanized steel." (), [Online]. Available: https://www.matweb.com/search/DataSheet.aspx?MatGUID=abbf07b7f93a4c358a0ddd194f5c18be&ckck=1 (visited on 11/15/2022).

[34] A. Askvik, A. Svensson, M. Hantveit, and T. Fischer, "Høyspenningslaboratoriet 2016 13helk," Bacheloroppgave, Høgskolen i Bergen, May 30, 2016, 92 pp.

[35] Lovdata. "Forskrift om endring i forskrift om tiltaksverdier og grenseverdier for fysiske og kjemiske faktorer i arbeidsmiljøet samt smitterisikogrupper for biologiske faktorer (forskrift om tiltaks- og grensev... - lovdata," Lovdata. (Jan. 7, 2021), [Online]. Available: https://lovdata.no/dokument/LTI/forskrift/2021-06-28-2248 (visited on 11/11/2022).

[36] E. C. Brantzeg, *Til master oppgaven — underlag skjermrom komponenter*, E-mail, Jun. 12, 2022.

[37] E. C. Brantzeg, "Testrapport2 sluttrapport høyspentlaboratorie HVL campus kronstad," EB Consulting AS, Sep. 12, 2022.

[38] IEEE, "IEEE standard method for measuring the effectiveness of electromagnetic shielding enclosures," *IEEE Std 299-2006 (Revision of IEEE Std 299-1997)*, pp. 1–52, Feb. 2007, Conference Name: IEEE Std 299-2006 (Revision of IEEE Std 299-1997). DOI: 10.1109/IEEESTD.2007.323387.

[39] E. C. Brantzeg, "Testrapport3 UTK hsplab HVL uke 47'22_8.12.12.pdf," EB Consulting AS, Aug. 12, 2022.

[40] R.
bibinitperiod Schwarz. "R and s HE300 active directional antenna (r and s HE300uk upgrade kit) manual." (2014), [Online]. Available: http://www.av.it.pt/Medidas/Data/Manuais%20&%20Tutoriais/63%20&%20-Handheld%20hSpetrum%20Analyser/Software%20&%20Documentation/documents/Manuals/HE300_Manual.pdf (visited on 12/02/2022).

[41] Rohde\&Schwarz. "HE300_2_img05_lightbox_landscape.jpg (JPEG image, 618 × 330 pixels)." (), [Online]. Available: https://cdn.rohde-schwarz.com/pws/product/h_1/he300_2/HE300_2_img05_lightbox_landscape.jpg (visited on 11/18/2022).

[42] "Spectrum-analyzer-ms2720t-front.png (PNG image, 420 × 310 pixels)," https://www.anritsu.com gb/test-measurement/products/ms2720t. (), [Online]. Available: https://dl.cdn-anritsu.com/images/products/tm-ms2720t/spectrum-analyzer-ms2720t-front.png?h=310&w=420&la=en-GB (visited on 11/18/2022).

[43] R. bibinitperiod Schwarz, *Field strength and power estimator*. [Online]. Available: https://www.eeweb.com/wp-content/uploads/articles-app-notes-files-field-strength-and-power-estimator-1340741009.pdf.

[44] EverythingRF. "What is an antenna factor? - everything RF." (), [Online]. Available: https://www.everythingrf.com/community/what-is-an-antenna-factor (visited on 12/02/2022).

[45] AaroniaAG. "Typical conversion formulas." (), [Online]. Available: https://www.aaronia.com/fileadmin/media-archive/conversion_formulas.pdf (visited on 12/02/2022).

[46] A. H. Systems. "A. h. systems - typical conversions formulas," TYPICAL CONVERSION FORMULAS. (), [Online]. Available: https://www.ahsystems.com/EMC-formulas-equations/typical-conversion-formulas.pdf.

[47] neonzeon. "Answer to "conversion from dBm to volt/ meter"," Electrical Engineering Stack Exchange. (Dec. 14, 2016), [Online]. Available: https://electronics.stackexchange.com/a/275071 (visited on 12/02/2022).

[48] A. H. Systems. "Antenna factor and gain calculations." (), [Online]. Available: https://www.ahsystems.com/EMC-formulas-equations/Antenna-Factor-Gain-calculation.php (visited on 12/08/2022).

[49] E. C. Brantzeg, "Testrapport1 måling av EMI i nytt skjermrom i høyspent lab campus kronstad HVL," EB Consulting AS, Jun. 13, 2022.

Chapter A

Measuring results

This chapter of the appendix contains the measuring results and is corrected for adjustment in gain value. Because of the size of each table and the amount of data, each table is given its own page in order to retain the readability of the tables.

A.1 Windows

Table A.1: Measuring results: real dampening of screened observing windows, south-east wall. Original solution implemented. Measurements from May 2022.

		Dampening [dB]					
		Screened Windows, original solution - measuring points (corrected)					
Corr.	Frequencies	Vi1_center	Vi1_mid v.edge	Vi2_center	Vi2_mid v.edge	Vi3_center	Vi3_mid v.edge
0	10kHz	2	4	1	5	2	8
0	156kHz	9	7	6	9	8	13
0	1MHz	22	15	17	20	25	25
0	10MHz	38	25	34	37	43	43
0	52MHz	56	58	73	78	82	
0	65MHz	36	40	48	51	55	
0	81MHz	57	47	58	69	69	
0	100MHz	43	38	41	49	52	
-7	130MHz	42	25	51	36	36	
0	170MHz	42	41	42	36	43	
0	209MHz	36	32	36	36	39	
0	260MHz	41	30	37	54	50	
0	327MHz	38	37	46	55	45	
0	415MHz	46	32	48	46	51	
0	523MHz	50	31	48	50	56	

Table A.1 continued from previous page (May 2022)

Corr.	Frequencies	Vi1_center	Vi1_mid v.edge	Vi2_center	Vi2_mid v.edge	Vi3_center	Vi3_mid v.edge
0	661MHz	50	28	43	33	47	
-2	830MHz	52	33	56	38	48	
-3	915MHz	54	32	56	44	64	
-2	1GHz	55	46	56	44	54	
-3	1.29GHz	55	50	56	62	58	
-4	1.86GHz	51	57	50	46	46	
-6	2.1GHz	55	51	44	59	48	
-3	2.45GHz	62	55	60	51	53	
-1	3.29GHz	68	59	57	62	54	
-2	4.19GHz	70	62	66	68	63	
-8	5.8GHz	60	81	55	72	58	
-14	6.6GHz	57	75	66	81	64	
-15	8.4GHz	63	80	66	76	63	
-20	10.495GHz	68	85	63	73	80	
-37	13.22GHz	83	78	78	79	83	
-60	18GHz	60	58	60	60	60	

Table A.2: Measured dampening of currently implemented solution for screened windows, correction factor applied. Measurements from August 2022.

		Dampening [dB]														
		Screened Windows, implemented solution - measuring points (corrected)														
		Window 1					Window 2					Window 3				
Corr.	Freq.	Mid	Top	Bot.	Rig.	Left	Mid	Top	Bot.	Rig.	Left	Mid	Top	Bot.	Rig.	Left
0	10kHz	7	10	7	5	6	7	7	6	6	5	7	7	7	5	6
0	156kHz	14	15	16	10	10	10	9	9	10	9	17	18	18	10	16
0	1MHz	27	27	29	20	16	17	18	15	16	15	30	32	31	15	31
0	10MHz	45	46	49	40	30	31	36	27	30	26	46	50	46	26	51
0	52MHz	59					48					69				
0	65MHz	51					36					43				
0	81MHz	56					48					60				
0	100MHz	57					38					44				
-7	130MHz	38					49					29				
0	170MHz	42					59					51				
0	209MHz	64					39					65				
0	260MHz	57					44					51				
0	327MHz	60					49					57				
0	415MHz	79					62					54				
0	523MHz	57					51					62				
0	661MHz	53					56					47				
-2	830MHz	60					60					55				
-3	915MHz	68					64					58				
-2	1GHz	65					58					63				
-3	1.29GHz	68					48					68				
-4	1.86GHz	53					62					62				
-6	2.1GHz	63					51					62				
-3	2.45GHz	66					58					71				
-1	3.29GHz	68					61					69				
-2	4.19GHz	66					66					68				
-8	5.8GHz	57					55					58				
-14	6.6GHz	60					54					62				
-15	8.4GHz	65					64					61				
-20	10.495GHz	75					68					80				
-37	13.22GHz	78					77					83				
-60	18GHz	60					60					60				

A.2 Surfaces

Table A.3: Measured dampening of surfaces in screened room, the correction factor is applied. Measurements from May 2022.

		Dampening [dB]														
		Measuring points, Screened surfaces (corrected)														
		Walls										Roof			Floor	
Corr.	Frequencies	V1	V2	V3	V4	V5	V6	V7	V8	V9	V15	T1	T2	T3	G3	G1
0	10kHz	75	63	67	74	70	67	36	24	60	53	58	75	72	43	77
0	156kHz	78	73	79	84	81	74	45	28	71	66	67	86	77	47	82
0	1MHz	95	84	90	97	90	84	58	34	82	78	77	95	85	55	94
0	10MHz	110	94	109	108	111	93	77	47	93	94	92	110	117	68	107
0	52MHz	91	95	97	75	84	73	69	83	89	100	78	88	89	92	87
0	65MHz	69	72	76	68	68	70	57	41	36	76	63	76	63	73	65
0	81MHz	58	50	58	64	64	79	66	87	54	65	72	92	61	90	92
0	100MHz	72	63	75	87	68	72	60	61	60	64	73	85	60	73	67
-7	140MHz	62	71	67	69	55	53	31	40	43	63	74	75	68	58	58
0	170MHz	59	70	68	74	63	52	54	34	39	63	62	55	68	53	54
0	209MHz	57	72	71	70	61	54	51	48	45	84	70	72	75	72	74
0	260MHz	66	66	75	81	66	57	56	52	64	65	76	70	66	58	70
0	327MHz	64	90	77	65	75	53	62	53	63	70	70	66	58	60	81
0	415MHz	64	71	69	96	75	54	60	50	61	80	73	84	67	65	73
0	523MHz	61	72	78	76	74	85	51	56	64	68	72	91	66	82	84
0	661MHz	105	80	81	81	80	61	55	55	65	75	71	85	60	71	80
-2	830MHz	72	75	68	93	56	66	49	65	64	67	46	79	55	74	77
-3	915MHz	64	74	67	81	52	64	59	55	69	64	28	83	81	73	94
-2	1GHz	68	60	62	81	61	68	60	55	63	61	44	81	59	69	91
-3	1.29GHz	60	75	77	79	79	53	59	52	67	75	64	72	62	82	88
-4	1.86GHz	61	69	71	72	71	67	57	66	61	69	75	84	71	79	88
-6	2.1GHz	60	71	69	79	66	64	57	60	62	65	66	69	78	90	89
-3	2.45GHz	68	63	78	71	71	59	50	52	53	67	67	75	75	84	93
-1	3.29GHz	74	56	75	71	68	69	63	64	62	81	75	79	71	93	94
-2	4.19GHz	78	51	66	76	59	81	68	69	53	69	83	78	93	96	100
-8	5.8GHz	64	54	75	76	61	67	82	70	61	83	82	87	85	112	112
-14	6.6GHz	85	56	80	67	75	81	71	65	67	87	81	86	81	106	106
-15	8.4GHz	65	55	76	75	55	65	69	83	52	90	80	76	90	105	105
-20	10.495GHz	53	61	72	70	57	68	80	79	63	72	70	85	80	100	100
-37	13.22GHz	70	58	75	73	64	83	71	83	57	83	68	68	68	83	83
-60	18GHz	60	60	58	50	60	57	60	60	53	60	45	45	45	60	60

A.3 Door

Table A.4: Measured dampening of screened door entrance to screened room, correction factor applied. Measurements from August 2022.

		Dampening [dB]							
		Measuring points, Screened door (corrected)							
Corr.	Freq.	D1	D2	D3	D4	D5	D6	D7	D8
0	10kHz	30	32	36	27	25	9	15	25
0	156kHz	42	47	45	37	29	15	28	36
0	1MHz	51	54	55	49	40	26	38	48
0	10MHz	66	75	76	67	58	45	58	65
0	52MHz	85	78	84	75	62	56	67	70
0	65MHz	74	77	70	59	61	62	72	56
0	81MHz	72	81	71	71	63	55	64	73
0	100MHz	65	68	58	59	43	47	58	55
-7	130MHz	53	65	69	56	43	53	46	45
0	170MHz	55	56	53	64	50	52	50	55
0	209MHz	65	62	60	56	50	51	44	48
0	260MHz	54	67	61	58	52	44	41	50
0	327MHz	61	60	68	65	45	49	40	54
0	415MHz	59	69	64	68	54	53	45	60
0	523MHz	61	79	69	68	58	55	53	66
0	661MHz	63	61	65	62	55	55	54	65
-2	830MHz	68	72	65	74	50	62	57	75
-3	915MHz	56	93	75	85	62	66	64	71
-2	1GHz	78	70	77	69	64	67	73	71
-3	1.29GHz	62	69	65	55	61	64	62	75
-4	1.86GHz	65	67	75	69	81	72	78	66
-6	2.1GHz	50	61	58	62	70	68	65	66
-3	2.45GHz	50	59	59	72	63	68	61	70
-1	3.29GHz	62	72	68	65	69	67	64	71
-2	4.19GHz	62	61	71	70	65	68	69	70
-8	5.8GHz	60	68	65	75	71	67	87	82
-14	6.6GHz	46	65	63	72	81	70	73	76

Table A.4 continued from previous page (August 2022)

Corr.	Freq.	D1	D2	D3	D4	D5	D6	D7	D8
-15	8.4GHz	55	72	78	69	81	74	77	77
-20	10.495GHz	54	75	78	79	90	75	75	78
-37	13.22GHz	55	69	71	83	83	73	68	83
-60	18GHz	40	60	61	61	60	60	60	60

Table A.5: Measured dampening of screened door entrance to screened room, 12th of May 2022. Correction factor applied. The secondary gasket was not delivered with the door, obsolete values. Included for discussion purposes. The fact of missing gasket was discovered during the measuring of the first point, D7.

Dampening [dB]	
Door, no secondary gasket. Corr. val.	
Frequency	D7
10kHz	22
156kHz	35
1MHz	45
10MHz	55
52MHz	51
65MHz	31
81MHz	43
100MHz	35
130MHz	24
170MHz	44
209MHz	32
260MHz	27
327MHz	28
415MHz	40
523MHz	38
661MHz	42
830MHz	56
915MHz	52
1GHz	57
1.29GHz	60
1.86GHz	61

Table A.5 continued from previous page (May 2022)

Frequency	D7
2.1GHz	57
2.45GHz	65
3.29GHz	72
4.19GHz	54
5.8GHz	68
6.6GHz	68
8.4GHz	66
10.495GHz	62
13.22GHz	61
18GHz	48

A.4 Single Entry frames, Access hatch and Wave traps

Table A.6: Measured dampening of screened cage openings from May 2022, correction factor applied.

		Dampening [dB]						
		Measuring points Single entry and Wave trap (corrected)						
Corr.	Frequencies	SE 1	SE 2	BF1/BF2	BF3	BF4	BF5	Access hatch
0	10kHz	29	43	57	36	30	24	82
0	156kHz	35	59	69	42	38	29	85
0	1MHz	47	71	84	55	50	38	98
0	10MHz	47	85	104	66	62	51	98
0	52MHz	72	87	100	100	75	76	85
0	65MHz	56	80	70	75	47	50	68
0	81MHz	77	80	62	61	61	74	66
0	100MHz	63	98	60	75	47	56	66
-7	140MHz	42	70	65	69	37	46	64
0	170MHz	34	77	67	70	31	33	52
0	209MHz	46	68	73	72	41	45	73
0	260MHz	44	67	77	64	37	57	66
0	327MHz	46	73	75	54	53	52	60
0	415MHz	35	75	73	64	45	64	72
0	523MHz	44	90	77	62	58	53	68
0	661MHz	47	90	77	62	58	53	57
-2	830MHz	36	75	74	68	47	58	59
-3	915MHz	36	85	72	71	42	57	64
-2	1GHz	51	78	69	68	50	56	56
-3	1.29GHz	54	80	67	67	56	53	68
-4	1.86GHz	48	73	71	63	76	47	61
-6	2.1GHz	54	68	66	61	64	56	54
-3	2.45GHz	56	70	62	82	55	51	52
-1	3.29GHz	62	72	69	71	56	47	62
-2	4.19GHz	73	75	69	63	53	61	57
-8	5.8GHz	57	67	68	82	48	53	80
-14	6.6GHz	62	83	62	70	42	49	69

Table A.6 continued from previous page (May 2022)

Corr.	Frequencies	SE 1	SE 2	BF1/BF2	BF3	BF4	BF5	Access hatch
-15	8.4GHz	42	64	59	71	54	45	62
-20	10.495GHz	41	68	69	73	32	54	71
-37	13.22GHz	47	83	62	68	57	50	83
-60	18GHz	31	58	45	60	50	45	60

Table A.7: Measured dampening of screened cage openings from August 2022, correction factor applied.

		Dampening [dB]						
		Measuring points Single entry and Wave trap (corrected)						
Corr.	Frequencies	SE 1	SE 2	BF1/BF2	BF3	BF4	BF5	Access hatch
0	10kHz	32	46	57	36	40	32	82
0	156kHz	35	59	69	42	49	32	85
0	1MHz	47	71	84	55	64	38	98
0	10MHz	47	85	104	66	77	51	98
0	52MHz	72	87	100	100	75	76	85
0	65MHz	56	80	70	75	47	50	68
0	81MHz	77	80	62	61	61	74	66
0	100MHz	63	98	60	75	47	56	66
-7	140MHz	42	70	65	69	37	46	64
0	170MHz	34	77	67	70	31	33	52
0	209MHz	46	68	73	72	41	45	73
0	260MHz	44	67	77	64	37	57	66
0	327MHz	46	73	75	54	53	52	60
0	415MHz	35	75	73	64	45	64	72
0	523MHz	44	90	77	62	58	53	68
0	661MHz	47	90	77	62	58	53	57
-2	830MHz	36	75	74	68	47	58	59
-3	915MHz	36	85	72	71	42	57	64
-2	1GHz	51	78	69	68	50	56	56
-3	1.29GHz	54	80	67	67	56	53	68
-4	1.86GHz	48	73	71	63	76	47	61
-6	2.1GHz	54	68	66	61	64	56	54

Table A.7 continued from previous page (August 2022)

Corr.	Frequencies	SE 1	SE 2	BF1/BF2	BF3	BF4	BF5	Access hatch
-3	2.45GHz	56	70	62	82	55	51	52
-1	3.29GHz	62	72	69	71	56	47	62
-2	4.19GHz	73	75	69	63	53	61	57
-8	5.8GHz	57	67	68	82	48	53	80
-14	6.6GHz	62	83	62	70	42	49	69
-15	8.4GHz	42	64	59	71	54	45	62
-20	10.495GHz	41	68	69	73	32	54	71
-37	13.22GHz	47	83	62	68	57	50	83
-60	18GHz	31	58	45	60	50	45	60

Chapter B

Method: Measured values converted from dBm to $\mathbf{Wm^{-2}}$

Tables presented here must be viewed in context with the equations linked in the respective tables, they are also presented in chapter 4.4. The values in each table of this appendix must be viewed in conjunction with equations in chapter 4.4.

Tables B.1 and B.2 contain calculations based on the logarithmic method.

Tables B.3 and B.4 contain calculations based on the numeric method.

Table B.1: Measured field strength during Corona passing through the shielded Faraday cage while the door was open and closed. Converted using the logarithmic method.

Shielded Door	Freq. f [MHz]	AF (Tab. 4.2)	Received power [dBm]	V - Eq. (4.1a) $[dB\mu V]$	$E_{(log,V)}$ - Eq. (4.1b) $[dB\mu V/m]$	$E_{(num)}$ - Eq. (4.1c) $[\mu V/m]$ (10^{-6})	S - Eq. (4.1d) $[pW/m^2]$ (10^{-12})
Week 47, 2022:							
Closed	10 - 20	40 - 42	-125	-18	22 - 24	12,589 - 15,848	0,4203 - 0,6662
Closed	10 - 20	40 - 42	-120	-13	27 - 29	22,387 - 28,183	1,3294 - 2,1069
Open	10 - 20	40 - 42	-120	-13	27 - 29	22,387 - 28,183	1,3294 - 2,1069
Open	10 - 20	40 - 42	-115	-8	32 - 34	39,810 - 50,118	4,2039 - 6,6628
Closed	75 - 125	22 - 24	-85	22	44 - 46	158,48 - 199,52	66,6283 - 105,599
Week 33, 2022:							
Closed	10 - 20	40 - 42	-125	-18	22 - 24	12,589 - 15,848	0,4203 - 0,6662
Open	10 - 20	40 - 42	-120	-13	27 - 29	22,387 - 28,183	1,3294 - 2,1069
Open	10 - 20	40 - 42	-115	-8	32 - 34	39,810 - 50,118	4,2039 - 6,6628
Week 24, 2021:							
Open	10 - 20	40 - 42	-110	-3	37 - 39	70,794 - 89,125	13,2941 - 21,0697
Open	10 - 20	40 - 42	-100	7	47 - 49	223,872 - 281,838	132,941 - 210,697

Table B.2: Measured field strength during Flashover passing through the shielded Faraday cage while the door was open and closed. Converted using the logarithmic method.

Shielded Door	Freq. f [MHz]	AF (Tab. 4.2)	Received power [dBm]	V - Eq. (4.1a) $[dB\mu V]$	$E_{(log,V)}$ - Eq. (4.1b) $[dB\mu V/m]$	$E_{(num)}$ - Eq. (4.1c) $[\mu V/m]$ (10^{-6})	S - Eq. (4.1d) $[pW/m^2]$ (10^{-12})
Week 47, 2022:							
Closed	10 - 20	40 - 42	-120	-13	27 - 29	28,1838 - 22,3872	1,3294 - 2,1069
Open	10 - 20	40 - 42	-115	-8	32 - 34	50,1187 - 39,8107	4,2039 - 6,6628
Open	10 - 20	40 - 42	-110	-3	37 - 39	89,1251 - 70,7946	13,2941 - 21,0697
Closed	75 - 125	22 - 24	-80	27	49 - 51	354,813 - 281,838	210,697 - 333,932
Week 33, 2022:							
Closed	10 - 20	40 - 42	-125	-18	22 - 24	12,5893 - 15,8489	0,4203 - 0,6662
Closed	10 - 20	40 - 42	-120	-13	27 - 29	22,3872 - 28,1838	1,3294 - 2,1069
Open	10 - 20	40 - 42	-115	-8	32 - 34	39,8107 - 50,1187	4,2039 - 6,6628
Open	10 - 20	40 - 42	-110	-3	37 - 39	70,7946 - 89,1251	13,2941 - 21,0697
Week 24, 2021:							
Open	10 - 20	40 - 42	-90	17	57 - 59	707,946 - 891,251	1329,41 - 2106,97
Open	10 - 20	40 - 42	-80	27	67 - 69	2238,721 - 2818,383	13294,1 - 21069,7

Table B.3: Measured field strength during Corona passing through the shielded Faraday cage while the door was open and closed. Converted using the numeric method.

Shielded Door	Freq. f [MHz]	Gain - Eq. (4.2) G_n	AF - Eq. (4.3) K_a	Received power [dBm]	Received power [W] (4.5a)	U_r - Eq. (4.5b) $[\mu V]$ (10^{-6})	E - Eq. (4.5c) $[\mu V/m]$ (10^{-6})	S - Eq. (4.5d) $[pW/m^2]$ (10^{-12})
Week 47, 2022:								
(M6)Closed	10 - 20	6,30957E-06 - 31,6228E-06	115,398 - 129,172	-125	3,162E-16	0,1257	14,5106 - 16,2426	0,5585 - 0,6997
(M6)Closed	10 - 20	6,30957E-06 - 31,6228E-06	115,398 - 129,172	-120	1E-15	0,2236	25,8038 - 28,8838	1,7661 - 2,2129
(M6)Open	10 - 20	6,30957E-06 - 31,6228E-06	115,398 - 129,172	-120	1E-15	0,2236	25,8038 - 28,8838	1,7661 - 2,2129
(M6)Open	10 - 20	6,30957E-06 - 31,6228E-06	115,398 - 129,172	-115	3,162E-15	0,3976	45,8864 - 51,3635	5,5850 - 6,9978
(MVin)Closed	75 - 125	0,022387211 - 0,1	12,825 - 16,264	-85	3,162E-12	12,5743	161,274 - 204,511	68,9902 - 110,94
Week 33, 2022:								
(M6)Closed	10 - 20	6,30957E-06 - 31,6228E-06	115,398 - 129,172	-125	3,16228E-16	0,125743	14,5106 - 16,2426	0,5585 - 0,6997
(M6)Open	10 - 20	6,30957E-06 - 31,6228E-06	115,398 - 129,172	-120	1E-15	0,223607	25,8038 - 28,8838	1,7661 - 2,2129
(M6)Open	10 - 20	6,30957E-06 - 31,6228E-06	115,398 - 129,172	-115	3,16228E-15	0,397635	45,8864 - 51,3635	5,5850 - 6,9978
Week 24, 2021:								
(M6)Open	10 - 20	6,3095E-06 - 31,6228E-06	115,398 - 129,172	-110	1E-14	0,707107	81,5989 - 91,3386	17,6615 - 22,1293
(M6)Open	10 - 20	6,3095E-06 - 31,6228E-06	115,398 - 129,172	-100	1E-13	2,23607	258,038 - 288,838	176,615 - 221,293

Table B.4: Measured field strength during Flashover passing through the shielded Faraday cage while the door was open and closed. Converted using the numeric method.

Shielded Door	Freq. f [MHz]	Gain - Eq. (4.2) G_n	AF - Eq. (4.3) K_a	Received power [dBm]	Received power [W] (4.5a)	U_r - Eq. (4.5b) $[\mu V]$ (10^{-6})	E - Eq. (4.5c) $[\mu V/m]$ (10^{-6})	S - Eq. (4.5d) $[pW/m^2]$ (10^{-12})
Week 47, 2022:								
(M6)Closed	10 - 20	6,3095E-06 - 31,62E-06	115,398 - 129,172	-120	1E-15	0,223607	25,8038 - 28.8838	1,76615 - 2,21293
(M6)Open	10 - 20	6,3095E-06 - 31,62E-06	115,398 - 129,172	-115	3,162E-15	0,397635	45,8864 - 51,3635	5,58505 - 6,99789
(M6)Open	10 - 20	6,3095E-06 - 31,62E-06	115,398 - 129,172	-110	1E-14	0,707107	81,5989 - 91,3386	17,6615 - 22,1293
(MVin)Closed	75 - 125	0,022387211 - 0,1	12,8256 - 16,2641	-80	1E-11	22,3607	286,79 - 363,677	218,166 - 350,824
Week 33, 2022:								
(M6)Closed	10 - 20	6,3095E-06 - 31,62E-06	115,398 - 129,172	-125	3,162E-16	0,125743	14,5106 - 16,2426	0,558505 - 0,699789
(M6)Closed	10 - 20	6,3095E-06 - 31,62E-06	115,398 - 129,172	-120	1E-15	0,223607	25,8038 - 28,8838	1,76615 - 2,21293
(M6)Open	10 - 20	6,3095E-06 - 31,62E-06	115,398 - 129,172	-115	3,162E-15	0,397635	45,8864 - 51,3635	5,58505 - 6,99789
(M6)Open	10 - 20	6,3095E-06 - 31,62E-06	115,398 - 129,172	-110	1E-14	0,707107	81,5989 - 91,3386	17,6615 - 221,293
Week 24, 2021:								
(M6)Open	10 - 20	6,3095E-06 - 31,62E-06	115,398 - 129,172	-90	1E-12	7,07107	815,989 - 913,386	1766,15 - 2212,93
(M6)Open	10 - 20	6,3095E-06 - 31,62E-06	115,398 - 129,172	-80	1E-11	22,3607	2580,384 - 2888,38	17661,5 - 22129,3

Chapter C

Detail Images

C.1 Images of the shielded room.

The location of the test points has been edited into the images to give a better impression of where the measurements were made. The points are in approximate proximity to their respective yellow ellipses.

Figure C.1: Image of the surfaces on the north- and west facing walls. Photo: Daniel Asle Vingen Endal.

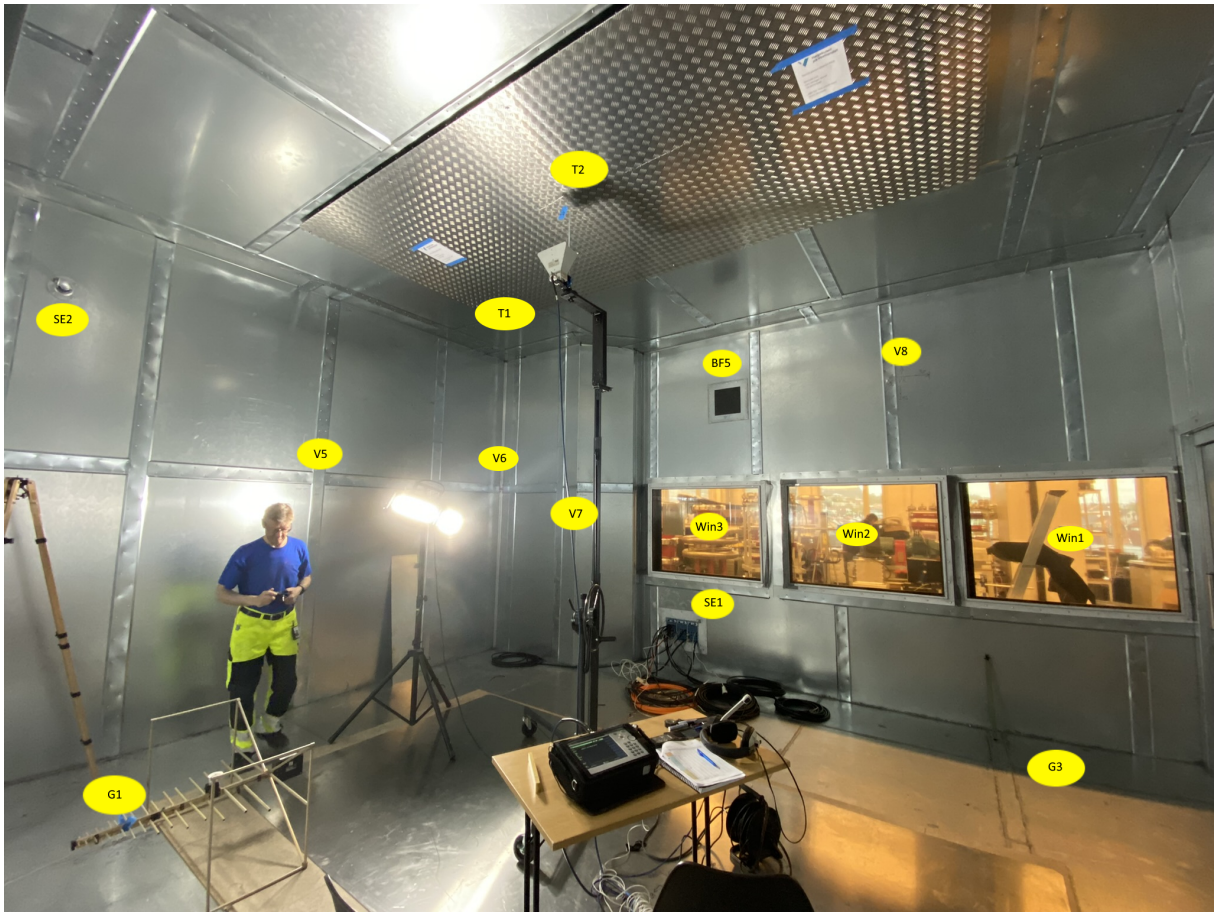

Figure C.2: Image of the surfaces on the south- and east facing walls. Bilog antenna in lower left hand corner, reciever/Anritsu spectrum analyzer and headphones for communication on table. Horn antenna mounted on fixture for high frequency measuring of dampening on point in roof. Picture taken may 10th 2022, mounting solution for the windows in the picture is the first attempted solution that was improved upon. Photo: Daniel Asle Vingen Endal.

Figure C.3: Single entry for the NOVAC fire suppression system. Photo: Daniel Asle Vingen Endal.

Figure C.4: Improved windows, close-up view of rubber/foam gaskets connecting laminated mesh to faraday cage. Photo: Daniel Asle Vingen Endal.

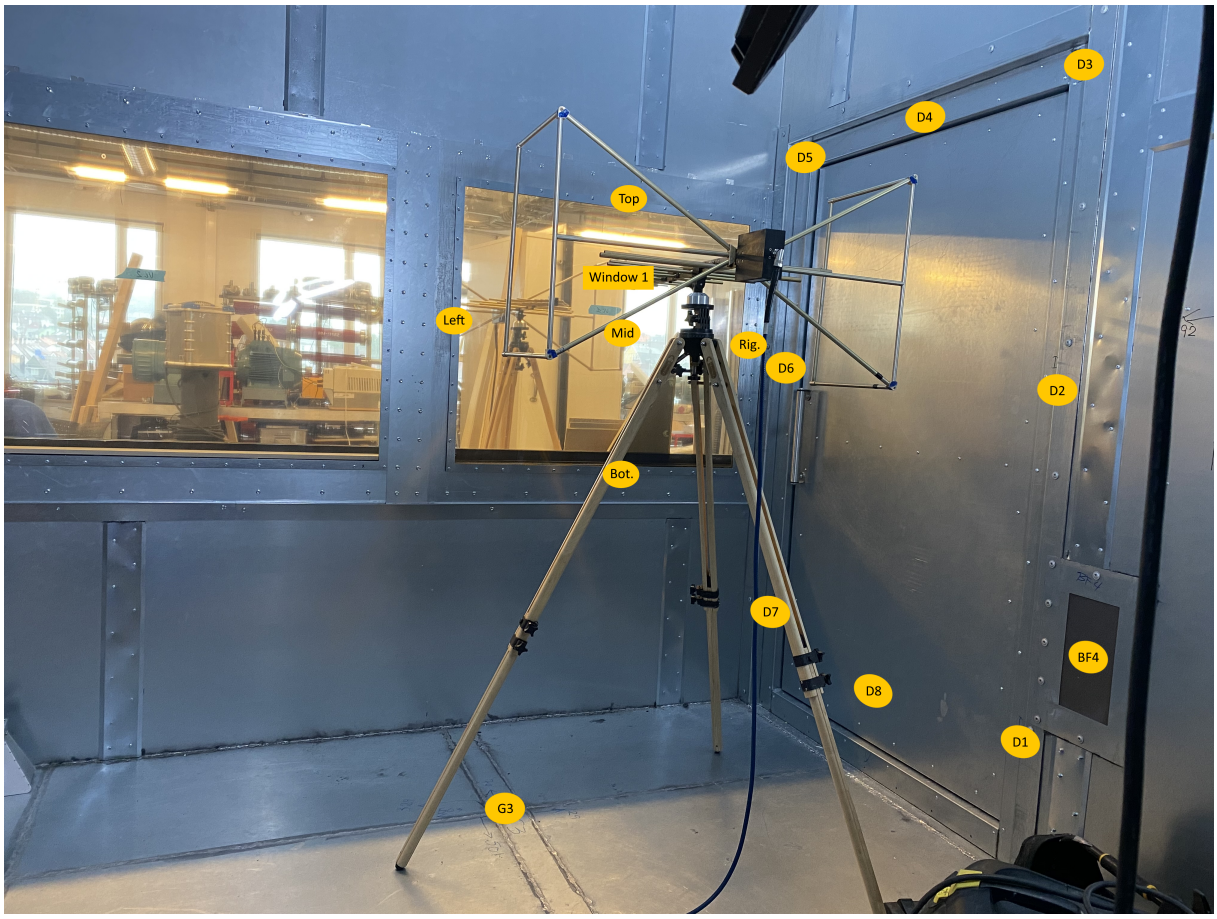

Figure C.5: Location of test points on the shielded door and window number 1.

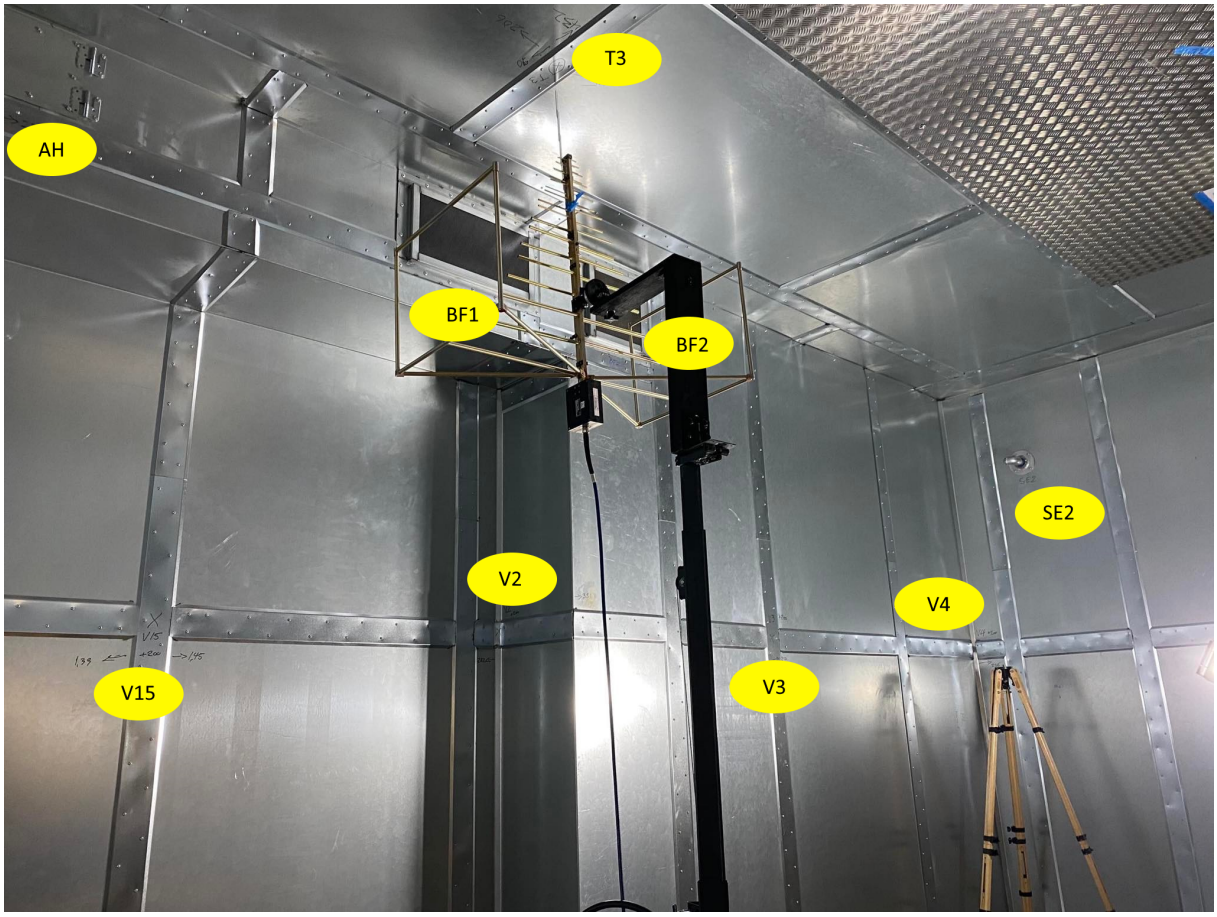

Figure C.6: Location of test points on north wall of shielded enclosure. Photo: Daniel Asle Vingen Endal.

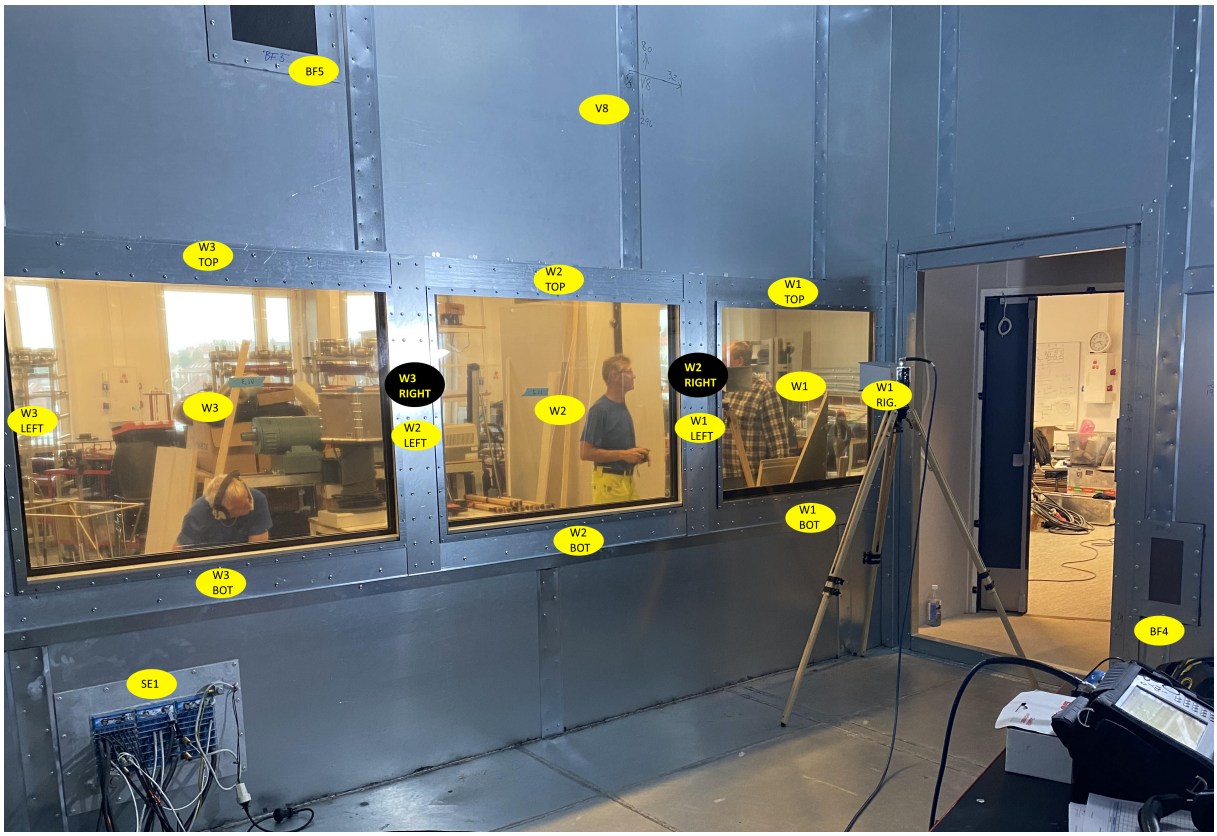

Figure C.7: Location of test points on north wall of shielded enclosure. Photo: Daniel Asle Vingen Endal.

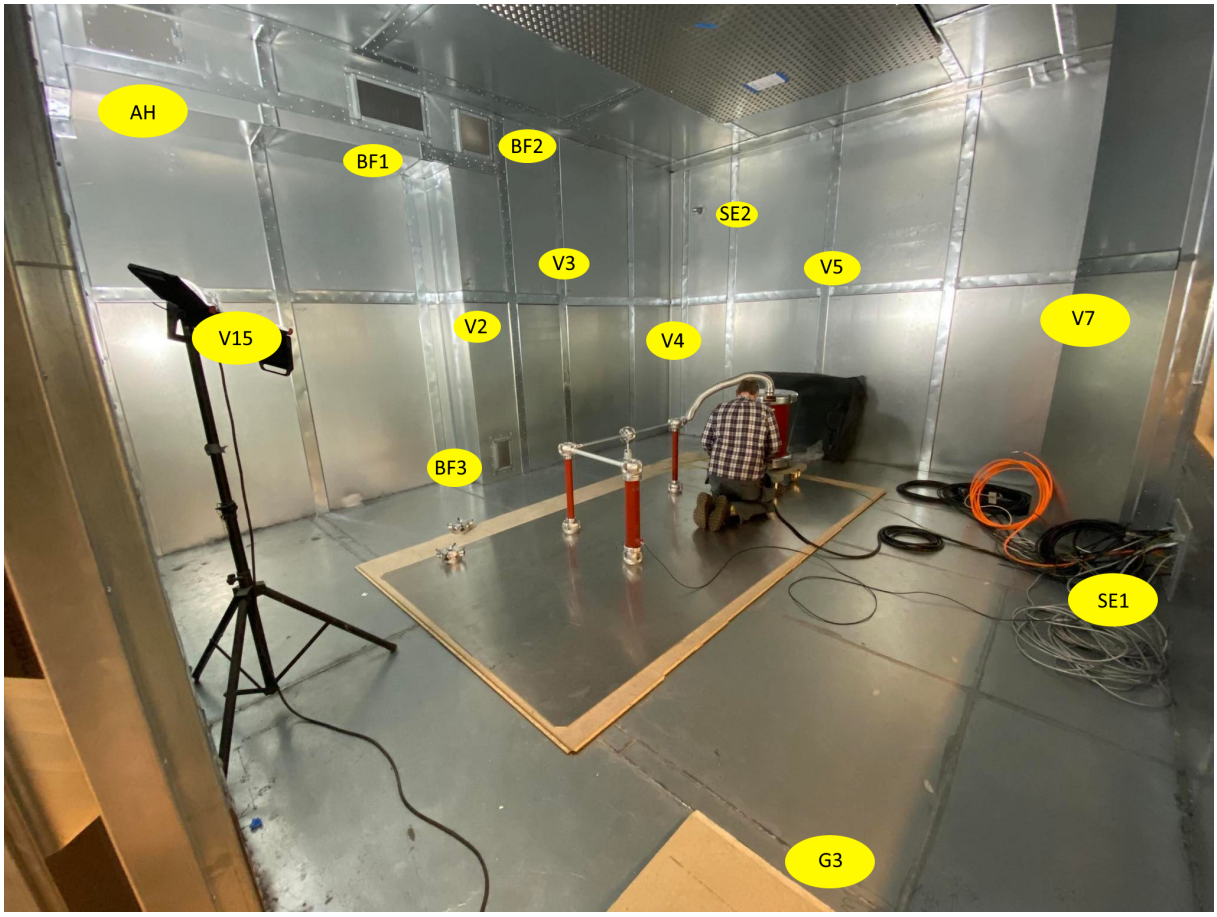

Figure C.8: Location of test points on the north and east walls of shielded enclosure. Photo: Daniel Asle Vingen Endal.

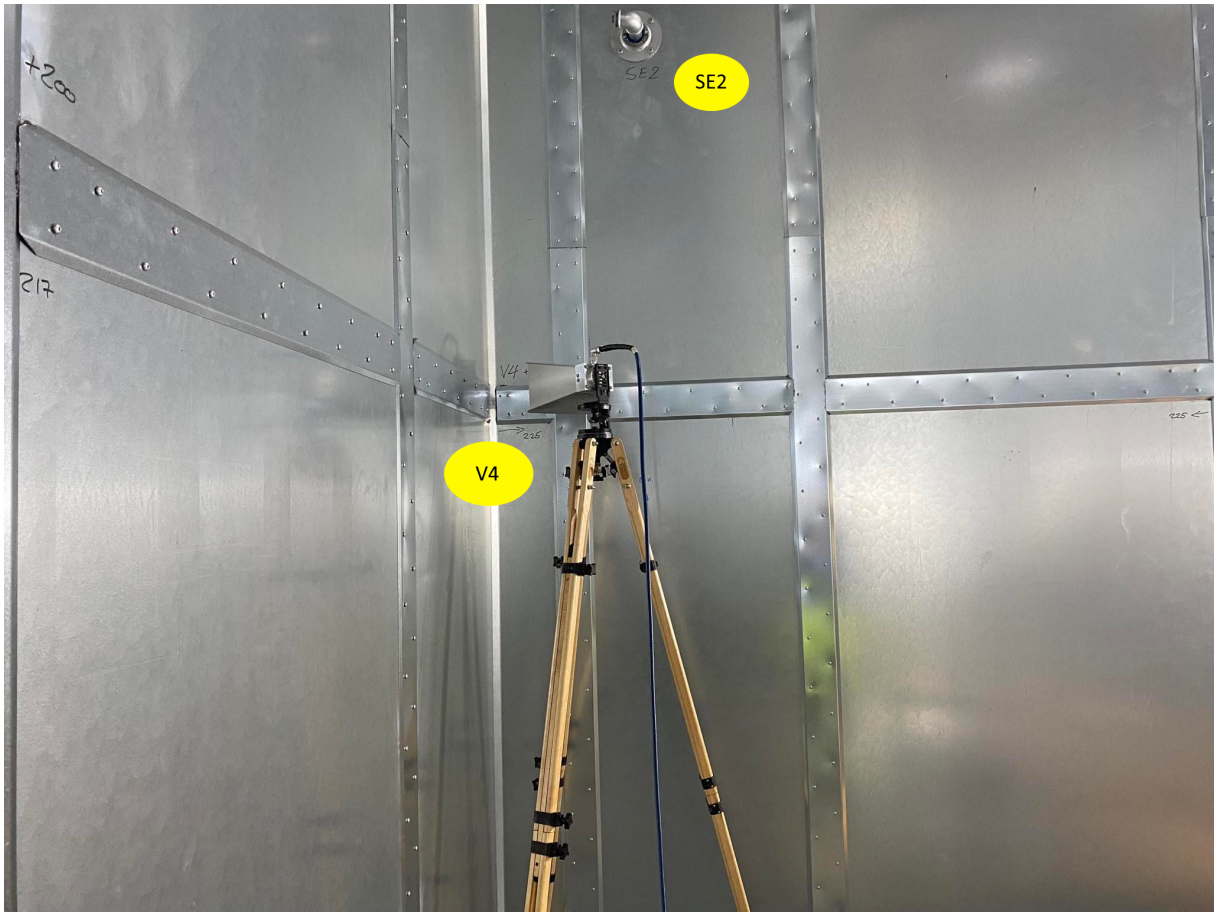

Figure C.9: Location of test points V4 and SE2 on east wall of shielded enclosure. Photo: Daniel Asle Vingen Endal.

Chapter D

Documents from manufacturer

1. Summary of tests

The given result is based on a shared risk principle with respect to the measurement uncertainty.

Conclusion

The test object mentioned in this report is measured according to IEEE 299.1:2013 Chapter 7.2 .

Measured minimum shielding effectiveness can be found in the table below. For detailed results see graph in Section 4.

Frequency range	Shielding effectiveness [dB]
9 kHz – 200 MHz	85
200 MHz – 1000 MHz	71
1 GHz – 2 GHz	84
2 GHz – 4 GHz	51
4 GHz – 10 GHz	42

The test results are limited by the screening effectiveness of the test fixture (i.e. the nested reverberation chamber).

The test results relate only to the object tested.

Figure D.1: Summary of measurements for the Single Entry frames from Roxtec International AB, courtesy of EB Consulting AS [36].

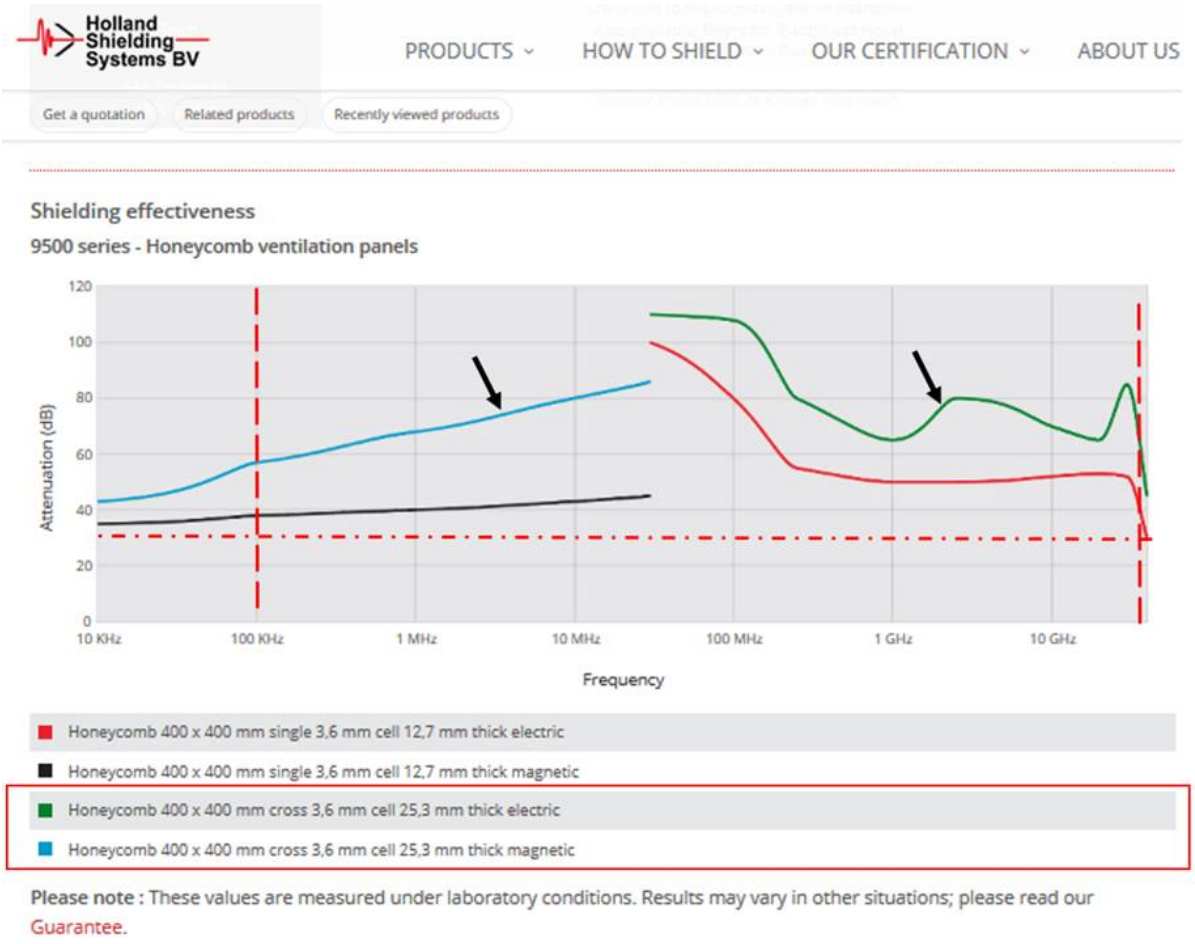

Figure D.2: Shielding effectiveness measurements of the Holland Shielding Systems Honeycomb wave traps conducted in a laboratory indicating the performance during optimal conditions, courtesy of EB Consulting AS [36].

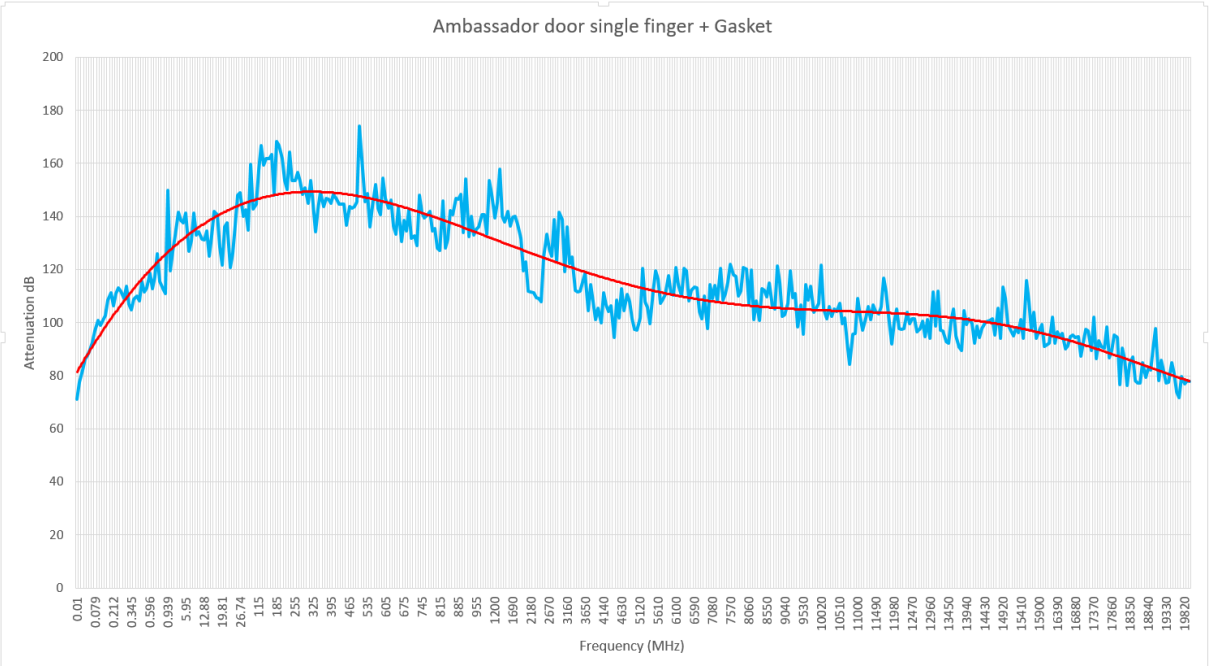

Figure D.3: Shielding effectiveness measurements of the Holland Shielding Systems shielded door conducted in a laboratory indicating the performance during optimal conditions, courtesy of EB Consulting AS [36].

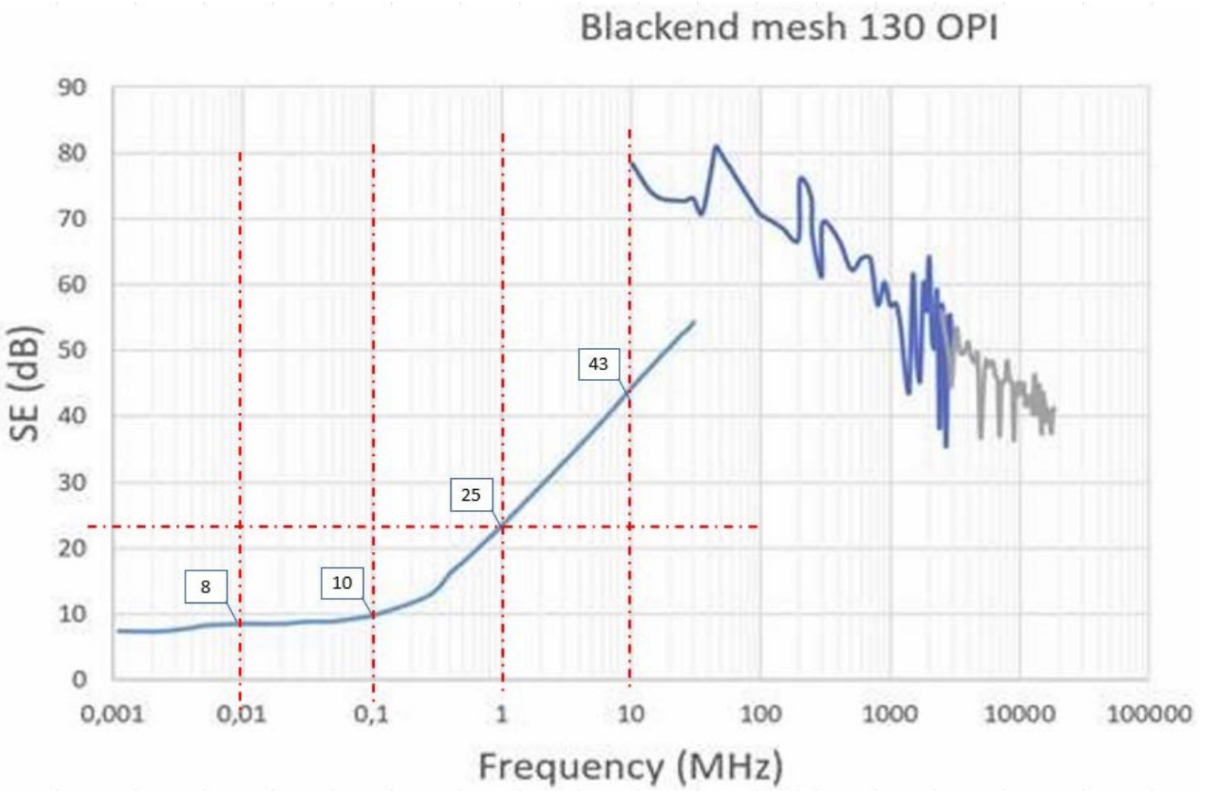

Figure D.4: Manufacturers specification of dampening in improved windows during ideal conditions, obtained in a laboratory. Courtesy of EB Consulting AS [37, p. 43].

Chapter E

Raw measuring data

This appendix contains the raw data obtained during the weeks of testing and measuring the attenuation of the screened structure in the high-voltage laboratory at HVL campus Kronstad. Correction values are then applied to each measurement in order to produce the data in appendix A. With the amount of datapoints making up this database, it is necessary to dedicate a new page to each table, in order to ensure the readability of each table. Data is provided curtesy of Espen Brantzeg from EB Consulting AS.

E.1 Windows

Table E.1: Raw measuring results: Dampening of screened observing windows, south wall. Original solution implemented.

		Dampening [dB]					
		Screened Windows, original solution - measuring points (raw data)					
Corr.	Frequencies	Vi1_center	Vi1_mid v.edge	Vi2_center	Vi2_mid v.edge	Vi3_center	Vi3 mid v.edge
0	10kHz	2	4	1	5	2	8
0	156kHz	9	7	6	9	8	13
0	1MHz	22	15	17	20	25	25
0	10MHz	38	25	34	37	43	43
0	52MHz	56	58	73	78	82	
0	65MHz	36	40	48	51	55	
0	81MHz	57	47	58	69	69	
0	100MHz	43	38	41	49	52	
-7	130MHz	49	32	58	43	43	
0	170MHz	42	41	42	36	43	
0	209MHz	36	32	36	36	39	
0	260MHz	41	30	37	54	50	
0	327MHz	38	37	46	55	45	
0	415MHz	46	32	48	46	51	
0	523MHz	50	31	48	50	56	
0	661MHz	50	28	43	33	47	
-2	830MHz	54	35	58	40	50	
-3	915MHz	57	35	59	47	67	
-2	1GHz	57	48	58	46	56	
-3	1.29GHz	58	53	59	65	61	
-4	1.86GHz	55	61	54	50	50	
-6	2.1GHz	61	57	50	65	54	
-3	2.45GHz	65	58	63	54	57	
-1	3.29GHz	69	60	58	63	55	
-2	4.19GHz	72	64	68	70	65	
-8	5.8GHz	68	89	63	80	66	
-14	6.6GHz	71	89	80	95	78	
-15	8.4GHz	78	95	81	91	78	
-20	10.495GHz	88	105	83	93	100	
-37	13.22GHz	120	115	115	116	120	
-60	18GHz	120	118	120	120	120	

Table E.2: Measured dampening of currently implemented solution for screened windows, correction factor not applied.

		Dampening [dB]														
		Screened Windows, implemented solution - measuring points (raw data)														
		Window 1					Window 2					Window 3				
Corr.	Frequencies	Center	Top	Bottom	Right	Left	Center	Top	Bottom	Right	Left	Center	Top	Bottom	Right	Left
0	10kHz	7	10	7	5	6	7	7	6	6	5	7	7	7	5	6
0	156kHz	14	15	16	10	10	10	9	9	10	9	17	18	18	10	16
0	1MHz	27	27	29	20	16	17	18	15	16	15	30	32	31	15	31
0	10MHz	45	46	49	40	30	31	36	27	30	26	46	50	46	26	51
0	52MHz	59					48					69				
0	65MHz	51					36					43				
0	81MHz	56					48					60				
0	100MHz	57					38					44				
-7	130MHz	45					56					36				
0	170MHz	42					59					51				
0	209MHz	64					39					65				
0	260MHz	57					44					51				
0	327MHz	60					49					57				
0	415MHz	79					62					54				
0	523MHz	57					51					62				
0	661MHz	53					56					47				
-2	830MHz	62					62					57				
-3	915MHz	71					67					61				
-2	1GHz	67					60					65				
-3	1.29GHz	71					51					71				
-4	1.86GHz	57					66					66				
-6	2.1GHz	69					57					68				
-3	2.45GHz	69					61					74				
-1	3.29GHz	69					62					70				
-2	4.19GHz	68					68					70				
-8	5.8GHz	65					63					66				
-14	6.6GHz	74					68					76				
-15	8.4GHz	80					79					76				
-20	10.495GHz	95					88					100				
-37	13.22GHz	115					114					120				
-60	18GHz	120					120					120				

E.2 Surfaces

Table E.3: Measured dampening of surfaces in screened room, correction factor is not applied.

		Dampening [dB]														
		Measuring points, Screened surfaces (raw data)														
		Walls (V1-V15)										Roof (T1-T3)			Floor (G1 & G3)	
Corr.	Frequencies	V1	V2	V3	V4	V5	V6	V7	V8	V9	V15	T1	T2	T3	G3	G1
0	10kHz	75	63	67	74	70	67	36	24	60	53	58	75	72	43	77
0	156kHz	78	73	79	84	81	74	45	28	71	66	67	86	77	47	82
0	1MHz	95	84	90	97	90	84	58	34	82	78	77	95	85	55	94
0	10MHz	110	94	109	108	111	93	77	47	93	94	92	110	117	68	107
0	52MHz	91	95	97	75	84	73	69	83	89	100	78	88	89	92	87
0	65MHz	69	72	76	68	68	70	57	41	36	76	63	76	63	73	65
0	81MHz	58	50	58	64	64	79	66	87	54	65	72	92	61	90	92
0	100MHz	72	63	75	87	68	72	60	61	60	64	73	85	60	73	67
-7	140MHz	69	78	74	76	62	60	38	47	50	70	81	82	75	65	65
0	170MHz	59	70	68	74	63	52	54	34	39	63	62	55	68	53	54
0	209MHz	57	72	71	70	61	54	51	48	45	84	70	72	75	72	74
0	260MHz	66	66	75	81	66	57	56	52	64	65	76	70	66	58	70
0	327MHz	64	90	77	65	75	53	62	53	63	70	70	66	58	60	81
0	415MHz	64	71	69	96	75	54	60	50	61	80	73	84	67	65	73
0	523MHz	61	72	78	76	74	85	51	56	64	68	72	91	66	82	84
0	661MHz	105	80	81	81	80	61	55	55	65	75	71	85	60	71	80
-2	830MHz	74	77	70	95	58	68	51	67	66	69	48	81	57	76	79
-3	915MHz	67	77	70	84	55	67	62	58	72	67	31	86	84	76	97
-2	1GHz	70	62	64	83	63	70	62	57	65	63	46	83	61	71	93
-3	1.29GHz	63	78	80	82	82	56	62	55	70	78	67	75	65	85	91
-4	1.86GHz	65	73	75	76	75	71	61	70	65	73	79	88	75	83	92
-6	2.1GHz	66	77	75	85	72	70	63	66	68	71	72	75	84	96	95
-3	2.45GHz	71	66	81	74	74	62	53	55	56	70	70	78	78	87	96
-1	3.29GHz	75	57	76	72	69	70	64	65	63	82	76	80	72	94	95
-2	4.19GHz	80	53	68	78	61	83	70	71	55	71	85	80	95	98	102
-8	5.8GHz	72	62	83	84	69	75	90	78	69	91	90	95	93	120	120
-14	6.6GHz	99	70	94	81	89	95	85	79	81	101	95	100	95	120	120
-15	8.4GHz	80	70	91	90	70	80	84	98	67	105	95	91	105	120	120
-20	10.495GHz	73	81	92	90	77	88	100	99	83	92	90	105	100	120	120
-37	13.22GHz	107	95	112	110	101	120	108	120	94	120	105	105	105	120	120
-60	18GHz	120	120	118	110	120	117	120	120	113	120	105	105	105	120	120

E.3 Door

Table E.4: Measured dampening of screened door entrance to screened room, correction factor not applied.

		Dampening [dB] (raw)							
		Measuring points, Screened door							
Corr.	Frequencies	D1	D2	D3	D4	D5	D6	D7	D8
0	10kHz	30	32	36	27	25	9	15	25
0	156kHz	42	47	45	37	29	15	28	36
0	1MHz	51	54	55	49	40	26	38	48
0	10MHz	66	75	76	67	58	45	58	65
0	52MHz	85	78	84	75	62	56	67	70
0	65MHz	74	77	70	59	61	62	72	56
0	81MHz	72	81	71	71	63	55	64	73
0	100MHz	65	68	58	59	43	47	58	55
-7	130MHz	60	72	76	63	50	60	53	52
0	170MHz	55	56	53	64	50	52	50	55
0	209MHz	65	62	60	56	50	51	44	48
0	260MHz	54	67	61	58	52	44	41	50
0	327MHz	61	60	68	65	45	49	40	54
0	415MHz	59	69	64	68	54	53	45	60
0	523MHz	61	79	69	68	58	55	53	66
0	661MHz	63	61	65	62	55	55	54	65
-2	830MHz	70	74	67	76	52	64	59	77
-3	915MHz	59	96	78	88	65	69	67	74
-2	1GHz	80	72	79	71	66	69	75	73
-3	1.29GHz	65	72	68	58	64	67	65	78
-4	1.86GHz	69	71	79	73	85	76	82	70
-6	2.1GHz	56	67	64	68	76	74	71	72
-3	2.45GHz	53	62	62	75	66	71	64	73
-1	3.29GHz	63	73	69	66	70	68	65	72
-2	4.19GHz	64	63	73	72	67	70	71	72
-8	5.8GHz	68	76	73	83	79	75	95	90
-14	6.6GHz	60	79	77	86	95	84	87	90
-15	8.4GHz	70	87	93	84	96	89	92	92
-20	10.495GHz	74	95	98	99	110	95	95	98
-37	13.22GHz	92	106	108	120	120	110	105	120
-60	18GHz	95	120	121	121	120	120	120	120

E.4 Single Entry frames and Wavetraps

Table E.5: Measured dampening of single entry frames (SE) and wavetraps (BF) in screened room.

		Dampening [dB] (raw)						
		Measuring points Single entry and Wavetrap						
Corr.	Frequencies	SE 1	SE 2	BF1/BF2	BF3	BF4	BF5	Access hatch
0	10kHz	29	46	57	36	40	24	82
0	156kHz	35	59	69	42	49	29	85
0	1MHz	47	71	84	55	64	38	98
0	10MHz	47	85	104	66	77	51	98
0	52MHz	72	87	100	100	75	76	85
0	65MHz	56	80	70	75	47	50	68
0	81MHz	77	80	62	61	61	74	66
0	100MHz	63	98	60	75	47	56	66
-7	120MHz	49	77	72	76	44	53	71
0	150MHz	34	77	67	70	31	33	52
0	209MHz	46	68	73	72	41	45	73
0	260MHz	44	67	77	64	37	57	66
0	327MHz	46	73	75	54	53	52	60
0	415MHz	35	75	73	64	45	64	72
0	523MHz	44	90	77	62	58	53	68
0	661MHz	47	90	77	62	58	53	57
-2	830MHz	38	77	76	70	49	60	61
-3	915MHz	39	88	75	74	45	60	67
-2	1GHz	53	80	71	70	52	58	58
-3	1.29GHz	57	83	70	70	59	56	71
-4	1.86GHz	52	77	75	67	80	51	65
-6	2.1GHz	60	74	72	67	70	62	60
-3	2.45GHz	59	73	65	85	58	54	55
-1	3.29GHz	63	73	70	72	57	48	63
-2	4.19GHz	75	77	71	65	55	63	59
-8	5.8GHz	65	75	76	90	56	61	88
-14	6.6GHz	76	97	76	84	56	63	83
-15	8.4GHz	57	79	74	86	69	60	77
-20	10.495GHz	61	88	89	93	52	74	91
-37	13.22GHz	84	120	99	105	94	87	120
-60	18GHz	91	118	105	120	110	105	120